Systematic Review of Wound Dressings: A Movement from the Past to the Present

Pouriya Norooz Kermanshahi[*], Graça Maria Barbosa Soares[b]

Centre for Textile Science and Technology (2C2T), University of Minho, Campus Azurém, 4800-058 Guimarães, Portugal

Abstract

This systematic review aims at investigating different wound dressings commonly used for the healing process and skin repair. Five databases, namely SCOPUS, Web of Science, Medline, Google Scholar, and Cochrane Database of Systematic Reviews, up to 2020, were scanned for papers specific to the topic of concern. The blinded randomized controlled trials, in vivo and in vitro studies comparing common wound dressings, including traditional, natural/biological, and artificial ones were studied in the present review. Finally, the researchers selected 22 studies. From which the data related to the clinical features of wound dressings and their advantages and disadvantages) were derived. The review of literature suggests that many treatment combinations are utilized as wound dressings based on the wound type and hospital guidelines. Nevertheless, there are conflicting views about the most appropriate choice. The findings of the reviewed articles indicate that hydrogels are the most common wound dressing used for wounds and burns due to high thermal/mechanical stability and low water evaporation. However, it is suggested to apply hybrid hydrogel membranes to overcome the low mechanical strength of a single component.

Keywords: Medical textiles, Hydrogel, Skin, Wound, Wound dressing.

---

[*]* Corresponding author. Tel:.
   E-mail address: poria.kermanshahi@gmail.com;ld8110@alunos.uminho.pt

1. Introduction

Skin is the widest organ of the human body and plays several significant roles. The main purpose of this multi-layered organ is to preserve the inner organs from the environment [1, 2]. It also acts as a shield against the entry of chemicals and microorganisms [3, 4] and forms an exterior shell against fluid and salt depletion resulting in the regulation of body temperature [5]. Histologically, skin is 1.5 mm thick and has three layers of epidermis, dermis, and the deepest layer of hypodermis [6]. Accordingly, a wound can be defined as an injury in any layers of skin that breaks the physical barrier, thus intervening in the normal structure of human body and physiology [7]. The wound may occur given to acute trauma, thermal trauma, genetic disorders, injuries, or surgical interventions [8].

Wounds can be classified based on their complexity, morphology, severity, thickness, level of contamination, and time elapsed since the trauma occurred. Acute wounds heal easily but chronic wounds, such as surgical incisions, need outside sutures or materials to assist the healing process. Other kinds of wounds, such as chemical, thermal, and electric burn wounds, require intense attention and can be life-threatening if left untreated. Therefore, a precise evaluation of the wound environment is necessary for its examination, diagnosis, management, and treatment. Accordingly, thorough and accurate assessment of wounds necessitate examining the extent and related features of the wound, host factors that impact the wound status, and environmental factors that influence the most favorable wound management [9, 10].

Wound healing involves a particular biological process that heavily relies on physiological parameters. When a wound healing process fails to help the skin properly, germs, such as bacteria and viruses, can easily invade our body freely [11]. Therefore, choosing the proper wound dressing material for a particular kind of wound necessitates a thorough understanding of the wound healing process which plays a crucial role in saving the patients' lives [12, 13]. In this regard, many studies have addressed a variety of physiological and biological stages involved in the wound healing process consisting of five sequential phases of hemostasis, inflammation, migration, proliferation, and maturation [14].

In the case of acute wounds and chronic non-healing wounds, the main goal is to heal the wound. Nevertheless, the optimum dressing material must facilitate wound healing, also, it must decrease the loss of electrolytes, fluid, and protein from the wound leading to less pain and infection [13, 15, 16].

This research aimed to address the efficacy of different wound dressings applied to different types of wounds. The findings of the present study may help emergency physicians to the best decision possible in terms of the required dressings.

2. Materials and Methods

This systematic review aimed to examine the classifications of wounds, proper wound dressings, and the advantages and disadvantages of commonly used dressings. In doing so, comprehensive research was performed to find the articles on the effectiveness of different types of wound dressings on the healing process of different types of wounds. Cochrane Handbook was used to design the research steps, namely question formation, inclusion criteria, search process, selection of studies, determination of article assessment criteria, extraction of information, and discussion [17]. Moreover, a protocol was specified prior to the beginning of the research.

2.1. Inclusion Criteria

This systematic review was carried out on the original studies only in the form of randomized controlled trials and *in vivo* and *in vitro* studies in which different types of wound healing were used on patients. Therefore, all parallel randomized, quasi-randomized, prospective observational, and retrospective studies were excluded from this research. The inclusion criteria consisted of 1) a clear description of the wound healing, 2) objective

findings and measurements, and 3) publication in the English language. However, the exclusion criteria were insufficient data, and publications in different languages. Moreover, the current review study does not include qualitative studies as well as editorial letters, case reports or case series, meta-analyses, consensus statements, and expert opinions.

2.2. Wound Dressing Types and Interventions

Both surface and deep wounds and burns were treated with drugs plus wound dressings, such as natural polymers, hydrogels, polysaccharides, sulphated polysaccharides, electrospun dextran, antibacterial chitosan–nanosilver film, chitosan film plus an antioxidant agent, chitosan–cellulose–silver nanoparticle composite films, chitosan–alginate polyelectrolyte complex membranes, chitosan film/gel plus fucoidan, biocompatible composite, sodium alginate–chitosan, alginates pectins, proteoglycans, keratin, collagen, silk fibroin, ciprofloxacin hydrochloride, poly-L-lactide, ciprofloxacin hydrochloride, polyethylene glycol, and gelatine sponges. In all studies, emergency physicians or care providers, such as wound healing practitioners, provided the required medical treatments. Wound dressings are used individually or in conjunction with other medications to treat wounds.

2.3. Data Collection

Five electronic databases, namely Web of Science, SCOPUS, Medline, Google Scholar, and Cochrane Database of Systematic Reviews, up to 2020, were scanned for papers specific to the topic of concern. The following keywords were used to search for related studies: "wound", "wound dressing", "hydrogel", "collagen", "skin damage", and "injury" in combination with "healing procedure", "physiological process", and "infection".

The first stage involved the evaluation of all titles and abstracts of the articles concerning the eligibility criteria. The next step included the retrieval of the full-text versions of the related studies and their evaluation The removal of the unrelated papers was accomplished by screening the titles of the articles. The remaining studies were carefully investigated. The data were objectively recorded through a standardized data form. The extracted data were then examined by two reviewers who selected the required data based on an agreement. The completion of data extraction took three months and the last search was performed on September 5, 2020. The recorded data included the used medications, type of wound, combination of wound healing plus drugs, recovery time, and painful procedure. Figure 1 describes the article selection process in a PRISMA flow diagram.

2.4. Properties of the Included Studies

The search process yielded 2,394 articles, out of which 1,831 were eliminated after initial assessment since they were irrelevant and redundant. Of the remaining 562 papers, 541 articles were not eligible; therefore, in total, 22 studies were nominated for the final analysis. The retrieved articles were then analyzed by two researchers who reached a consensus about the inclusion criteria. Those studies that had missing data were categorized as unclear. The included studies were performed on both animals and patients. The applied wound dressings were different depending on the studies, and in some cases, drugs were also used to enhance wound healing (Table 1).
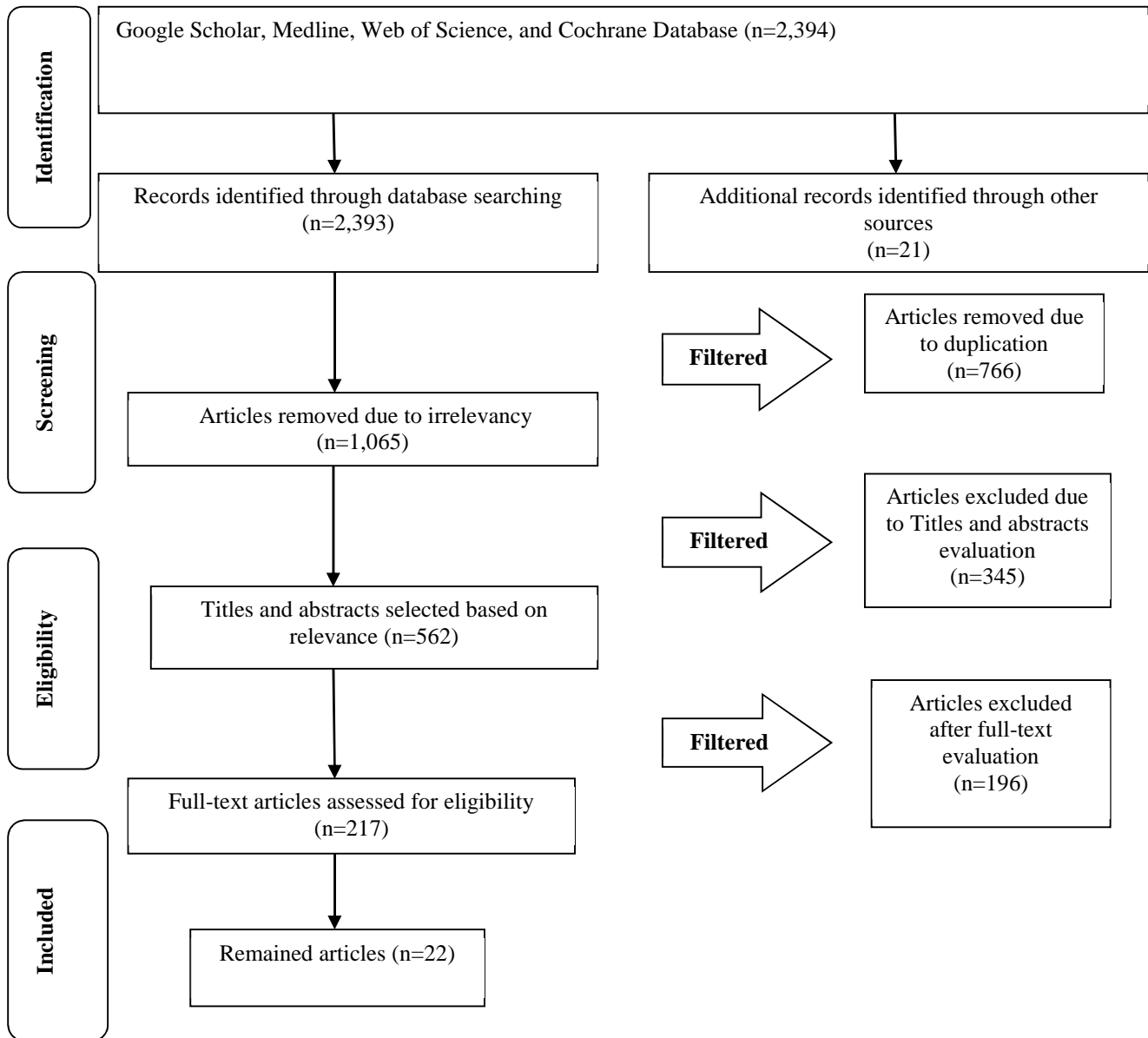
Figure 1. PRISMA flowchart representing the study selection process

Table 1. Characteristics of different research projects using various wound dressings

Type of wound	Wound dressing	Characteristics	Reference
Diabetic wound	bioactive compounds-loaded chitosan film	Moist wound environment Low the risk of dehydration Good antioxidant activity Proliferative effect	18
Skin inflammation	Hydrocortisone-loaded chitosan nanoparticles	Low severity of the pathological features of atopic dermatitis	19
Chronic wound	Activated charcoal silver dressings	Reduction of healing times Elimination of bacterial barriers	20
Osteomyelitis	Chitosan with gentamicin	Improvement of infection and anti-inflammatory	21
Second-degree burn wounds	Dendritic thioester hydrogel burn dressing	Prevention of bacterial infection On-demand dissolution for atraumatic removal	22
Second-degree burn wounds	Chitosan gel containing liposomes loaded with epidermal growth factor	High epithelization	23
Necrotic skin due to dermal burns	Hyaluronic acid sponge containing arginine and epidermal growth factor	Decreased size of the full-thickness skin defect Increased epithelization from the wound margin Moderate inflammation	24
Wound infection	Silver-containing wound dressings	Faster healing time	25
Keloids	Hyaluronic acid	Normalized keloid fibroblast characteristic features	26
Cutaneous wounds	Hydrogels with type I collagen	Faster wound healing	27
Surgery trauma	Polyvinyl alcohol–gelatin esterified hydrogel	Good potential to be hemo-compatible and moisture retentive	27
Excision wounds	Seed Husk of *Psyllium*	Remarkable antibacterial activity against both gram-positive and gram-negative selected bacteria Faster epithelialization and greater rates of wound contraction	28
Deep wounds	Collagen sponge	Shortened healing time Enhanced quality of the wound repair	29
Dermal burns	Fucoidan-chitosan films	Good potential to be a potential treatment system	23
Open wounds	Protein hydrogel	Faster wound healing of open wounds	12
Burn injury	Collagenous chitosan	Faster wound healing mechanism	30
Excisional splint wound	Aloe vera and curcumin loaded oxidized pectin–gelatin	Strong anti-inflammatory effect	31
Wound infection	Cyclodextrin-based hydrogels	Destroying bacterial cells preserving the gallic acid antibacterial activity	32
Partial- and full-thickness wounds	Poly(ethylene glycol)-protein hydrogels	Fast reepithelialisation	33

General wounds	Hydrogel dressing	Faster rate of closure and reepithelialisation	34
General wounds	PVA–clay nanocomposite hydrogels	Relatively good swelling Appreciated vapour transmission rate Excellent barrierity against microbe penetration and mechanical properties.	35
Infectious wounds	*Mentha pulegium* essential oil	Enhanced infected wound healing increase of antibacterial properties Decrease of inflammatory phase	36

3. 3. Wound Dressings Characteristics

Recently, many different materials are being used to produce wound dressings. Biopolymeric nanofibers have been studied to construct efficient wound dressings due to their properties of biocompatibility and eco-friendliness [30, 31, 37-40]. Polysaccharides, such as chitosan, chitin, hyaluronic acid, alginates, and cellulose, are the most studied biopolymers applied for wound treatment [41, 42].

Currently, with scientific and technological progress, more than 3000 types of dressings have been produced to improve the healing process. However, there is still no optimal product that cures chronic ulcers, including diabetes, pressure ulcers, and venous ulcers, which often are not fully healed [43]. It is expected that the global wound care market will involve more than USD 24.8 billion by 2024 from USD 19.8 billion in 2019, at a Compound Annual Growth Rate of 4.6% from 2019 to 2024 [9].

Wound dressing studies started with the ground-breaking study of Winter [44] who took the initial steps in designing the first wound dressing/film as a material that can keep the wound environment wet. In this regard, wound dressings were classified based on their wettability degrees in the eighties. Accordingly, dried wound dressings, such as woven cotton gauze lost their popularity, and hydrogels have been introduced as the best choice [45]. However, wound dressing selection depends on several factors, including wound site, surrounding skin, and exudate level. Therefore, depending on the type of wound (i.e., appearance, namely necrotic, sloughy, granulating, epithelializing [7]), the following characteristics should be present in an optimal wound dressing: the ability to a) preserve the moisture of the environment around the wound, b) enhance the transmission of good gases, c) eliminate unneeded exudates without reaching saturation on the outer surface of the wound, d) shield the wound from infections, contaminations, or micro-organisms, e) cease the desiccation of the wound, f) lessen the wound surface necrosis, g) trigger the growth factor, h) protect mechanically, i) be easily removed and changed, non-allergic, elastic, biocompatible, biodegradable, and non-toxic, j) decrease the pain of the wound and be cost-effective and commercially acceptable, and h) be easily sterilized [35].

4. 3.1. Traditional Wound Dressings

Wound dressings are commonly categorized as traditional, artificial, and natural/biological dressings [46]. Traditional wound dressings were introduced in the mid-1970s. Some problems, such as fast dehydration, bacterial growth, and difficult removal, led to the development of cotton gauze coated with Chitosan-Ag-ZnO nanocomposites [47]. However, such cotton gauzes expanded the capacity of swelling and enhanced antibacterial activity against *Escherichia coli* and *Staphylococcus aureus*.

5. 3.2. Natural/Biological Wound Dressings

Biological dressings are found to be an excellent treatment that can heal deep and chronic burns and wounds completely. This dressing is composed of collagen-type structures, such as lipids and elastin. Collagen and gelatin (the denatured form of collagen) are the most suitable natural macromolecules that can be used to produce wound dressings and biomaterials that are biomimetic to human skin. Collagen extraction in water-soluble, acid-neutral, or neutral forms is dependent on simple chemical or enzymatic hydrolysis [29]. Gelatin is a combination of collagen-derived peptides extracted from tissues via the same collagen techniques but are supplemented by heat treatment or acquired via acid or alkaline collagen. Collagen type I can be simply extracted from different mammalian connective tissues, including tendon, cornea, and skin [27]. Gelatin and collagen have the same properties and amino acid sequence repeats of Gly-X-Y, in which X and Y are mostly proline and hydroxyproline, respectively [31]. The main drawback of biological materials is the lack of donated skin for profound or extensive wounds, which leads to the need for new tissue donors [48]. Common natural wound dressings have two elements, gelatin or collagen and plant extracts or plant-based compounds [49]. The compounds responsible for the bioactivity of wound dressings are frequently from natural sources. Due to their nature, they are unstable under environmental conditions, and encapsulation strategies are needed to ensure their activity.

It is possible to use plant bioactive compounds in hydrogels, films, electrospun nanofiber matrices, and sponges. Likewise, micro particles and microspheres of gelatin or collagen are established as novel drug delivery systems. Sponge-like collagen and hyaluronic acid materials filled with epigallocatechin gallate were produced to treat chronic wounds. They had inhibitory activity against main wound enzymes, myeloperoxidase, and collagenase, as well as strong biocompatibility [26, 29]. Wound dressings composed of hyaluronic acid sponge with arginine and epidermal growth factor can reduce the extent of full-thickness skin defects, improve epithelization from the wound edge, and maintain moderate inflammation [24].

This type of wound healing presents multifunctional biomaterials induced dermal regeneration and exhibits anti-inflammatory properties. Collagen/chitosan scaffolds were filled with gelatin microspheres including ginsenoside Rg1, a natural compound isolated from *Panax notoginseng* [49]. The findings of different studies on chitosan-based wound dressings (loaded with fucoidan, liposomes, gentamicin, and hydrocortisone) indicated that chitosan can reduce healing time, promote epithelization, and improve antibacterial activity [19, 21-23, 50].

Bioactive compounds, including minerals, omega-3-fatty acids, probiotics, vitamins, polyphenols, and bioactive proteins or peptides, have been scrutinized for their possible usages in functional foods nutraceuticals and pharmaceuticals [26]. The antimicrobial activity of wound dressing is vital in preventing infection. There are many different natural compounds with antifungal and antibacterial activities. *Curcuma longa L.* (*Zingiberaceae* family) and its polyphenolic compound curcumin have been extensively investigated. This compound is widely used traditionally as an antimicrobial and it has low side effects. A combination of curcumin and other antimicrobial agents or silver can improve the quality of wound dressings and skin protection [20, 25, 50]. In fact, the wound healing process is faster due to the quickened epithelialization and greater rates of wound contraction [28].

There are several encapsulation strategies used to improve the bioactivity of wound dressings. Different structures, such as nanoparticles, nanospheres, or nanocapsules, can be used based on the production technique. Nanoparticles can be produced through various methods, among which the nanoprecipitation method is usually favoured due to its simplicity which leads to unimodal distribution with desirable reproducibility. Since some drugs, such as Ciprofloxacin, are water-soluble drugs, encapsulated nanoparticles were prepared by multiple emulsion solvent evaporation methods [52].

Recently, a lot of attention has been paid to lipid nanoparticles (LNPs). Nanostructured lipid carriers (NLCs) and solid lipid nanoparticles (SLNs) are two main types of Lipid-based nanoparticles [53].

The NLCs control drug release and enhance drug stability, safety, and bioavailability. Concerning drug encapsulation capacity and stability, lipid nanoparticles have advantages over the rest of the lipid-based nanocarriers (e.g., nano-emulsions) and nanovesicles (e.g., liposomes). Crystalline materials, like menthol, tend to be crystallized in a solid lipid structure and leak from it when it is stored. Therefore its amount in NLC is less, compared to SLN.[53] The exceedingly unordered lipid structured matrix of NLC increased drug stability and encapsulation. Their good release profiles led to their desirability in the nano pharmaceutical studies as well as other usages. They are also developed through various advanced techniques. It is possible to produce these systems and other lipid nanoparticles in the laboratory and on a large scale. Understanding the dynamics of LNPs on a molecular phase *in vivo* and *in vitro* requires further efforts [53].

Encapsulation in nanostructured lipid carriers can improve antibacterial properties. The required pharmacokinetic and pharmacodynamic characteristics can be designed through the encapsulation of the drugs in lipid vesicles. Liposomes as antibiotic carriers have some benefits: enhanced biodistribution and pharmacokinetics, low toxicity, target selectivity, and improved activity against extracellular pathogens. They are particularly used to overcome bacterial drug resistance[53] and enhance the treatment of infected wounds through prevention of bacterial growth, reduction of the inflammatory phase duration, and enhancement of the fibroblasts proliferation and collagen biosynthesis [36].

The food industry has shown interest in the nanofibers created by electrospinning due to their potential as vehicles for the encapsulation and controlled delivery or release of bioactive compounds [50]. Jiang et al., reported that coaxial electrospinning is a powerful method for one-step encapsulation of fragile, water-soluble bioactive agents, such as living organisms, DNA, and growth factors, into core-shell nanofibers [55]. The incorporation of bioactive oil in an encapsulation system can preserve these compounds (Figure 2).

Various methods used for preparing micro particles are: spray chilling, spray drying, fluidized bed, coacervation, extrusion, and interfacial polymerization. Some of the mentioned methods (e.g., spray drying and extrusion) depend on the preparation of emulsions before the encapsulation. Therefore, the production of the emulsion is essential for desirable encapsulation. Spray drying is one of the most used methods in the food industry [32].

Cyclodextrins (CDs) can also be used as a structuring material in the production of hydrogels. Functionalization using hydrogels, which can preserve the moist environment and increase the drug delivery capabilities of cotton, can overcome the limits of cellulosic wound dressings [32]. The hydrogel component preserves the moisture required for the healing process, and the cyclodextrin moiety can protect and modulate the release of bioactive molecules. Therefore, the conjugation of cyclodextrins with hydrogels can lead to the development of ideal wound-dressing material [56]. Pinho et al., obtained hydrogels with beta-cyclodextrin (b) or hydroxypropyl-beta-cyclodextrin (HPb) and hydroxypropyl methylcellulose by crosslinking with 1, 4-butanediol diglyceryl ether under mild conditions. The hydrogels were firm and transparent, with a desirable swelling capacity and gel-HPb had a more hydrophilic surface, in comparison to the gel-b. They reported that gel-b and gel-HPb combined with gallic acid have proved to be a practical choice for antibacterial wound dressing [57].
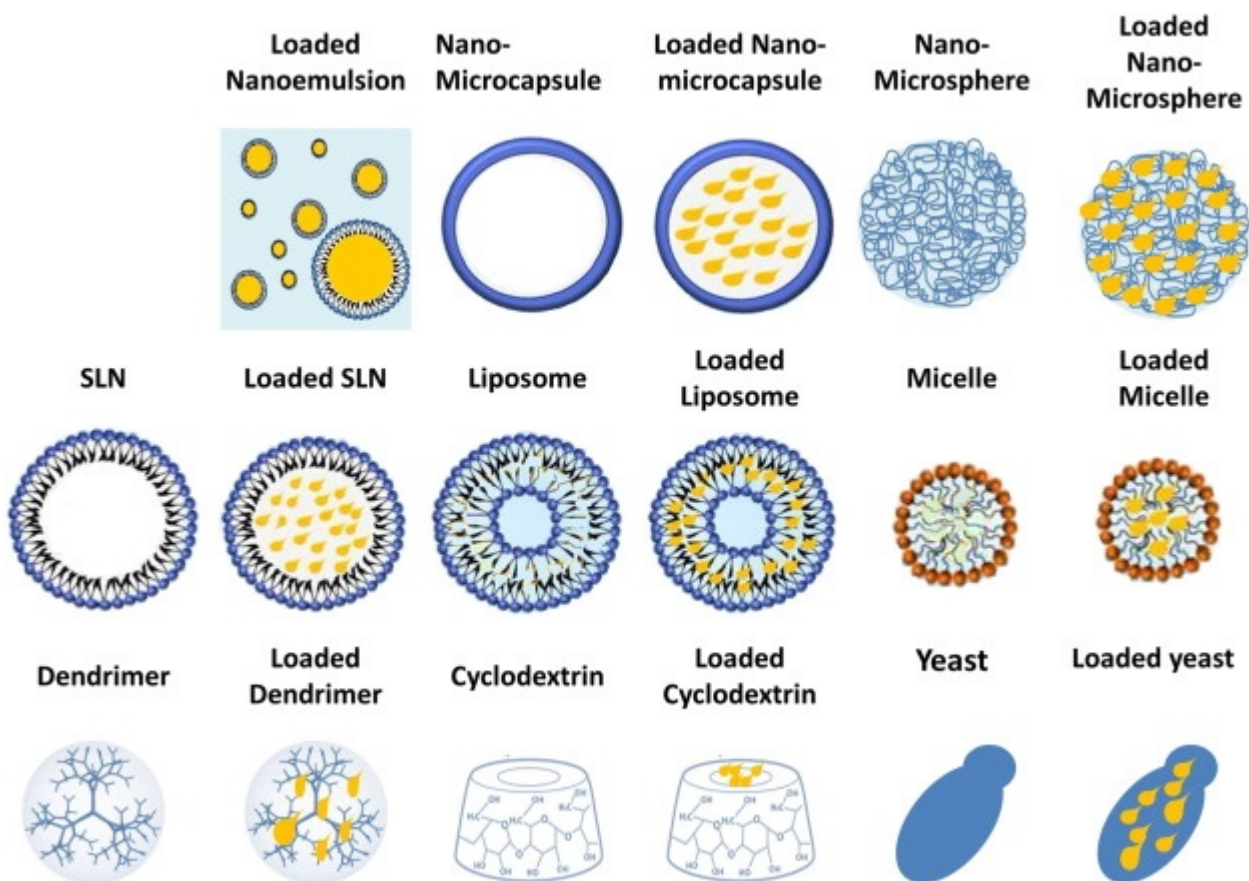
Figure 2. Different encapsulation structures for bioactive oils. The small drops inside structures represent bioactive oil in loaded systems [32]

It was also reported that the functionalization of cotton fibers with cyclodextrin-hydroxypropyl methyl cellulose-based hydrogel can improve cotton water uptake and surface characteristics and improve its function as a wound dressing. The best conditions were achieved, only the 1-step and pretreatment methodology created composites with stable cross-linking. They produced a composite material according to the cotton textile substrates functionalized with cyclodextrin-hydroxypropyl methyl cellulose-based hydrogel and controlled the drug delivery mechanism for developed composites by Fickian diffusion, according to the experimental data fitting to the Peppas-Sahlin model. Based on the findings, the produced composites can be used to prevent or treat chronic wounds [58, 59]. In another study, hydroxypropyl methylcellulose and 2-hydroxypropyl-beta-cyclodextrin hydrogel were developed and utilized as a delivery system that releases its content in a pH-dependent manner, controls the spread of microorganisms on the wounded area, and prohibits wound infection [60].

3.3. Artificial Wound Dressings

Synthetic materials, including non-biological materials and polymers not found in skin components, are used to make artificial dressings [48]. Synthetic dressings must be non-toxic, biodegradable, physically stable, and have a condition conducive to tissue repair. There has been a surge in demand for polymeric membrane products for wound dressings.

3.3.1. Semi-Permeable Film Dressings

This type of wound dressing consists of adherent and transparent polyurethane-type film which enhances the transference of CO_2, O_2, and water vapour from the wound and allows the adherence of the dressing to the skin [61]. This transparency feature of semi-permeable films provides the chance for assessing wound closure without the need to remove the wound dressing. Vapour transmission rates are within the range of 300-800 $g/m^2/24$ hours. The semi-permeable film dressings, impermeable to bacteria and liquids, contain autolytic debridement of eschar. The flexibility of this type of dressings makes them appropriately practical for shallow, superficial, and epithelializing wounds with low exudates. However, the available film dressings have different adhesive characteristics, extensibility, conformability, and vapor permeability [62]. Since adhesiveness of dressings can affect the epidermal layer of the skin, caution must be exercised when trying to remove film dressings

3.3.2. Semi-Permeable Foam Dressings

Foam dressings consist of hydrophilic and hydrophobic foam with adhesive borders [63]. The hydrophobic characteristics of the outer layer preserve the liquid; however, they enhance gaseous transference and water vapor. Silicone-based rubber foam (Silastic) easily forms to wound shape. Foam can absorb different amounts of wound drainage based on the thickness of the wound. Foam dressings are usually used as primary dressings for absorption and eliminate the need for secondary dressings due to their high absorption and moisture permeability of steam [64, 65]. Foam dressings have a major downside which necessitates frequent dressing; moreover, they are not ideal for dry wounds, dry cuts, and low exuding wounds since they require exudates for healing [64].

3.3.3. Hydrogels dressing

The hydrogel-based wound dressing is among the most favorable wound care materials and meets the requirements for dressing, including a) sensitive subcutaneous, (b) pain reduction through cooling, and (c) the possibility of active intervention in the wound healing process [33, 34, 65]. They promote healing faster than traditional gauze dressings [66].

Hydrogels, because of high level of water, porosity, and soft consistency, naturally simulate natural living tissues more closely than any artificial biological class [27, 67, 68]. If molecular collisions or secondary forces, including ions, hydrogel bonds, or hydrophobic forces have a major impact on the network formation, hydrogels are called as reversible or physical gels. Physical gels can be solubilized by altering the environmental circumstances, like temperature or pH, and the ionic strength of the solution. Chemical hydrogels are usually made using two various methods, namely three-dimensional polymerization, in which a hydrophobic monomer is polymerized in the presence of a multifunctional crosslinking agent or by direct cross-linking of water-soluble polymers.

Polymerization typically begins with free radical-generating compounds, including benzoyl peroxide, 2,2-azo-isobutyronitrile (AIBN), and ammonium peroxodisulphate, or using ultraviolet, gamma-ray, or electron beams [69]. Figure 3 illustrates this polymerization.

Hydrogels and hydrocolloids are developed as products to manage the moist wound healing process. Both produce autolytic debridement, which eases the removal of dead tissues [67]. Hagan (1992) suggests a transparent wound dressing as a thin film that has a non-adhesive central portion including hydrogel material that contained polypropylene glycol or polyethylene glycol and isophorone diisocyanate [70]. Due to the transparency of this product, it is possible to observe the wound healing process and it is also easy to remove [70].
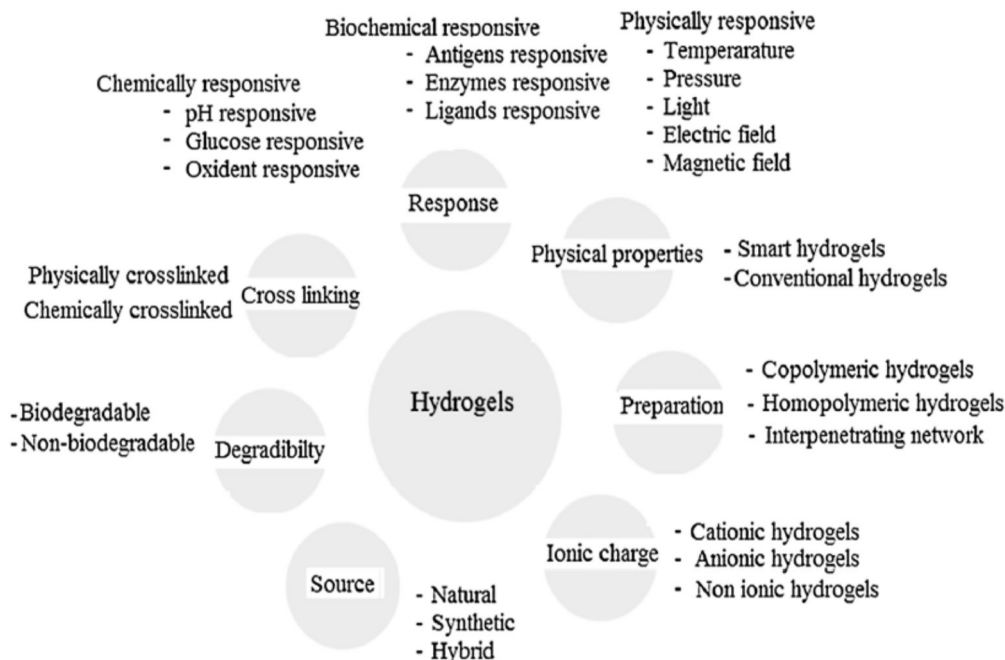

Figure 3. a) Synthesis of hydrogels by three-dimensional polymerization. b) Synthesis of hydrogels by cross-linking of ready-made water-soluble polymers [69]

3.3.3.1 Types of Hydrogels

Hydrogels are categorized based on their physical characteristics, such as preparation method, swelling, origin, ionic charges, degree of biological degradation, and observed nature of the crosslinking. In physical gels, the nature of the process is physical interaction. In a chemical process, the crosslinking of chemical covalent (simultaneous or subsequent polymerization) is used to produce chemical hydrogels. Physical hydrogels are reversible because of structural alterations, while chemical hydrogels are permanent and irreversible due to configured alterations. Double-network hydrogels are the other class of hydrogels. Double-network hydrogels are developed through combining physical and chemical cross-hydrogels by electrostatic interaction. In recent years, double-network hydrogels with high liquid absorption capacity in a wide range of pH have been used to overcome the shortcomings of using only chemical or physical hydrogels.

As can be seen in Figure 4, hydrogels can be classified according to their stimuli response as pH-responsive, temperature-responsive, glucose-responsive, protein-based, and antigen-responsive hydrogels [72].
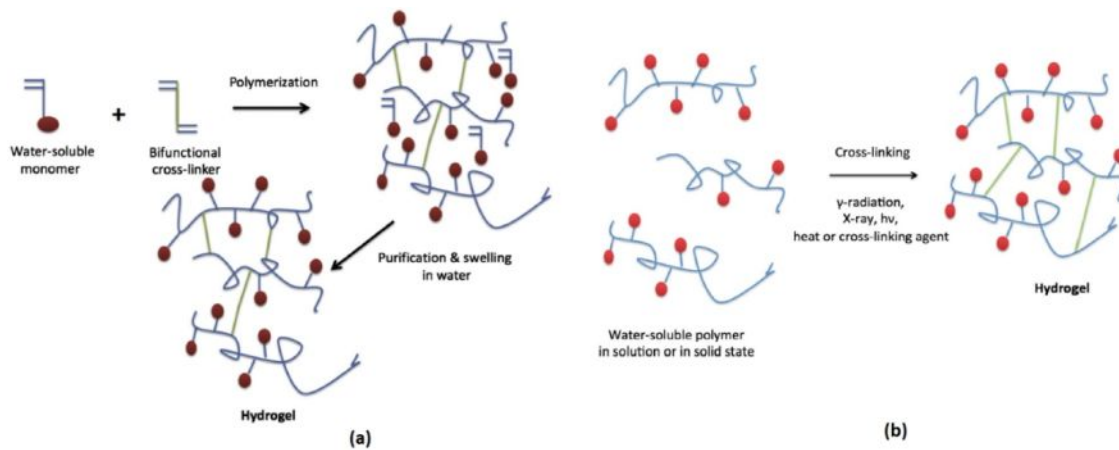

Figure 4. Classification of hydrogels based on the different properties [70]

3.3.4. Hydrocolloid Dressing

Hydrocolloid dressings are another type of interactive dressings which are commonly used. They are composed of two layers, the inner colloidal layer and the outer water impermeable layer. Hydrocolloid dressings are produced by combining gel-forming agents (carboxymethylcellulose, gelatin, and pectin) with other substances, like adhesives and elastomers [72]. Hydrocolloids can be penetrated by water vapor but not bacteria. They also allow debridement and absorption of wound exudates [73]. Hydrocolloid dressings can be properly used for mild to moderately exudating wounds, including traumatic wounds, minor burn wounds, pressure sores, and management of pediatric wounds. The main advantage of these dressings is that the patients do not suffer from the removal pain [74]. However, hydrocolloid dressings are commonly applied as a secondary dressing and they are not recommended for the management of highly exudating wounds or neuropathic ulcers [72].

6. 3.3.5. Alginate Dressing

Alginate dressings, mainly derived from seaweed, are highly absorbent and are used for moderate to large amounts of exudate. The fluid absorption of alginate is accompanied by sturdy hydrophilic gel formation that maintains the wound environment moisturized. Similar to hydrocolloid dressings, alginate dressings are used along with a secondary dressing to stay in place. It is not recommended to use alginate dressings for the management of severe wounds with exposed bone, third-degree burn wounds, and dry wounds [72]. Table 2 summarizes various polymeric dressing materials available in the global market and their brand names, their preferred usages, and the utilization percentages in wounds and burns care.

7. Table 2. List of polymeric wound dressing materials currently available in the global markets [66]

Dressing type	Commercial names	Description	Application	Global use (%)
Polymeric Films	Tegaderm	Films were synthesized from polyurethane or any other polymeric materials	–Superficial wounds	8
	Blister		– Laser wounds	
	Poly skin II		– Surgery defect sites	
	Silon-TSR		– Skin tears	
	Opsite, Aluderm			
Polymeric Foams	Flexzan	Foam dressings were produced by combination of hydrophilic foams and hydrophobic backing or semi-permeable with nonabsorbent membranes, such as polyoxyethylene glycol surrounded with polyurethane or silicone/ polyester	– Chronic wounds	5
	Biopatch		– Burns	
	Crafoams		– Mohs surgery and wounds	
	Biatain		– Laser resurfacing wounds	
	Cutinova			
	Reston			
	Lyofoam			
	Ivalon			
Polymeric Hydrogels	Cultinova Gel,	Hydrogels were made by the combination of crosslinked hydrophilic polymers, such as polyethylene oxide, polyvinyl pyrrolidone, polyvinyl alcohol	–Chemotherapy peels	44
	Biolex, TegaGel,		– Ulcers	
	Carrasyn, NuGel,		– Laser resurfacing	
	Skin Flexderm,		–Average thickness wounds	
	Exu Dry Dressing,		–Graft donor sites and artificial	
	CarraSorb, and GRX wound Gel		– Organs wounds	
Polymeric Alginates	AlgiSite	Alginate hydrogels were produced by the combination of chemical crosslinking of sodium alginate algae with Mg, Ca, or Zn salt solutions	– Thickness burns	20
	AlgiDerm		– Surgical wounds	
	Sorbsan		– High exudates wounds	
	Kaltostat		– Chronic ulcers	
	Omiderm			
Polymeric Hydrocolloids	Iodosorb	Hydrocolloides were synthesized by immobilization of iodine onto water-soluble modified starch based on cadexomeriodine beads; the gel was formed by iodine exchange between polymeric material and wound exudates. The second form is Dextranomer, where crosslinked dextran is grafted with polyethylene glycol	– Chronic ulcers	24
	(Cadexomer),		– Burns	
	Debrisan		– Average thickness wounds	
	(Dextranomer), and		– Donor graft sites	
	Sorbex, Duoderm			
	(Polymer blend)			

4. Conclusion

The awareness of the available wound dressings, their appropriate use, and their side effects is fundamental for wound management. The main concern of wound care practitioners in this field is to find a fast-acting medication that is both appropriate and safe and causes the lowest possible pain for the infected patients. Over 3000 wound dressings have been introduced in the market for different types of wounds and burns. The present work provided a review of common trends and materials used for wound management to allow the development of a wound dressing that can tackle the main disadvantages of each type and accelerate the healing process of patients. Since conventional wound dressings usually do not show a suitable performance in the treatment, researchers had recently paid attention to nanoparticles and nanofibers due to their biocompatibility and eco-friendliness. Based on the results, there are still no one-fits-all wound dressings and even those fabricated using nanoparticles have their deficiencies and restrictions in use. For instance, nanofibers can enhance drug delivery while nanoemulsions can improve drug penetration to the wound. Accordingly, there is a need to conduct future studies on fabricating wound dressing that could fulfil the needs of patients the most. (

References

[1] R. D. Sontheimer, "Skin is not the largest organ", J. Invest. Dermatol., vol. 134, no. 2, pp. 581-582, 2014. doi: 10.1038/jid.2013.335

[2] A. Moeini, P. Pedram, P. Makvandi, M. Malinconico, and G. Gomez d'Ayala, "Wound healing and antimicrobial effect of active secondary metabolites in chitosan-based wound dressings: A review", Carbohydr. Polym., vol. 233, pp. 115839, 2020. doi: 10.1016/j.carbpol.2020.115839

[3] A. W. Chua, Y. C. Khoo, B. K. Tan, K. C. Tan, C. L. Foo, and S. J. Chong, "Skin tissue engineering advances in severe burns: Review and therapeutic applications", Burns. Trauma., vol. 4, no. 3, 2016. doi: 10.1186/s41038-016-0027-y

[4] T. C. Wikramanayake, O. Stojadinovic, and M. Tomic-Canic, "Epidermal Differentiation in Barrier Maintenance and Wound Healing", Adv. Wound. Care. (New Rochelle), vol. 3, no. 3, pp. 272-280. 2014. doi: 10.1089/wound.2013.0503

[5] R. Goyal, L. K. Macri, H. M. Kaplan, and J. Kohn, "Nanoparticles and nanofibers for topical drug delivery", J. Control. Release., vol. 240, pp. 77-92, 2016. doi: 10.1016/j.jconrel.2015.10.049

[6] E. A. Gantwerker, and D. B. Hom, "Skin: Histology and physiology of wound healing", Facial. Plast. Surg. Clin. North. Am., vol. 19, no. 3, pp. 441-53, 2011. doi: 10.1016/j.fsc.2011.06.009

[7] T. Abdelrahman, and H. Newton, "Wound dressings: principles and practice", Surgery (oxford), vol. 29, no. 10, pp. 491-495, 2011. doi: 10.1016/j.mpsur.2011.06.007

[8] S. MacNeil, "Progress and opportunities for tissue-engineered skin", Nature, vol. 445, no. 7130, pp. 874-880, 2007. doi: 10.1038/nature05664

[9] Wound care market by product (foams, hydrocolloids, alginates, antimicrobial dressings, assessment, NPWT devices, substitutes, sutures, staples, tapes), wound (surgical, trauma, diabetic ulcers, burns), end-user, region - Global Forecast to 2024 [database on the Internet]. 2019.

[10] J. M. Reinke, H. Sorg, "Wound repair and regeneration", Eur. Surg. Res., vol. 49, no. 1, pp. 35-43, 2012. doi: 10.1159/000339613

[11] S. Namgoong, and S. K. Han, "Status of wound management in Korea", Wound. Repair. Regen., vol. 26, Suppl 1, pp. S3-s8, 2018. doi: 10.1111/wrr.12576

[12] A. Manikandan, S. T. K. Raja, T. Thiruselvi, M. Vaishnavi, R. Siva, and A. Gnanamani, "Engineered protein hydrogel for open wound management in Canines", Wound. Med., vol. 22, pp. 32-36, 2018. doi: 10.1016/j.wndm.2018.07.001

[13] S. Sarabahi, "Recent advances in topical wound care", Indian J. Plast. Surg., vol. 45, no. 2, pp. 379-387, 2012. doi: 10.4103/0970-0358.101321

[14] P. Zahedi, I. Rezaeian, S. O. Ranaei-Siadat, S. H. Jafari, and P. Supaphol", A review on wound dressings with an emphasis on electrospun nanofibrous polymeric bandages", Polymers. Adv. Technol., vol. 21, no. 2, pp. 77-95, 2010. doi: 10.1002/pat.1625

[15] H. C. Korting, C. Schöllmann, and R. J. White, "Management of minor acute cutaneous wounds: importance of wound healing in a moist environment", J. Eur. Acad. Dermatol. Venereol., vol. 25, no. 2, pp. 130-137, 2011. doi: 10.1111/j.1468-3083.2010.03775.x

[16] R. S. Ambekar, and B. Kandasubramanian, "Advancements in nanofibers for wound dressing: A review", Eur. Polymer. J., vol. 117, pp. 304-336, 2019. doi: 10.1016/j.eurpolymj.2019.05.020

[17] J. P. Higgins, J. Thomas, J. Chandler, M. Cumpston, T. Li, M. J., "Cochrane handbook for systematic reviews of interventions: John Wiley & Sons, 2019.

[18] L. Colobatiu, A. Gavan, A. V. Potarniche, V. Rus, Z. Diaconeasa, A. Mocan, I. Tomuta, S. Mirel, and M. Mihaiu, "Evaluation of bioactive compounds-loaded chitosan films as a novel and potential diabetic wound dressing material. Reactive. Functional. Polymers., vol. 145, p. 104369, 2019. doi: 10.1016/j.reactfunctpolym.2019.104369

[19] Z. Hussain, H. Katas, M. C. Mohd Amin, E. Kumolosasi, and S. Sahudin, "Downregulation of immunological mediators in 2,4-dinitrofluorobenzene-induced atopic dermatitis-like skin lesions by hydrocortisone-loaded chitosan nanoparticles", Int. J. Nanomedicine, vol. 9, pp. 5143-5156, 2014. doi: 10.2147/ijn.s71543

[20] J. C. Kerihuel, "Effect of activated charcoal dressings on healing outcomes of chronic wounds" J. Wound. Care., vol. 19, no. 5, pp. 208-215, 2010. doi: 10.12968/jowc.2010.19.5.48047

[21] A. B. Stoian, I. Demetrescu, and D. Ionita, "Nanotubes and nano pores with chitosan construct on TiZr serving as drug reservoir" Colloids. Surf. B. Biointerfaces., vol. 185, p. 110535, 2020. doi: 10.1016/j.colsurfb.2019.110535

[22] M. D. Konieczynska, J. C. Villa-Camacho, C. Ghobril, M. Perez-Viloria, K. M. Tevis, W. A. Blessing, A. Nazarian, E. K. Rodriguez, and M.W. Grinstaff, "On-Demand Dissolution of a Dendritic Hydrogel-based Dressing for Second-Degree Burn Wounds through Thiol-Thioester Exchange Reaction" Angew. Chem. Int. Ed. Engl., vol. 55, no. 34, pp. 9984-9987, 2016. doi: 10.1002/anie.201604827

[23] Z. Değim, N. Çelebi, C. Alemdaroğlu, M. Deveci, S. Öztürk, and C. Özoğul, "Evaluation of chitosan gel containing liposome-loaded epidermal growth factor on burn wound healing" Int. Wound. J., vol. 8, no. 4, pp. 343-354, 2011. doi: 10.1111/j.1742-481X.2011.00795.x

[24] Y. Matsumoto, and Y. Kuroyanagi, "Development of a wound dressing composed of hyaluronic acid sponge containing arginine and epidermal growth factor" J. Biomater. Sci. Polym. Ed., vol. 21, no. 6-7, pp. 715-726, 2010. doi: 10.1163/156856209x435844

[25] M. N. Storm-Versloot, C. G. Vos, D. T. Ubbink, and H. Vermeulen, "Topical silver for preventing wound infection", Cochrane. Database. Syst. Rev. vol. 2010, no. 3, p. Cd006478, 2010. doi: 10.1002/14651858.CD006478.pub2

[26] P. Wen, M. H. Zong, R. J. Linhardt, K. Feng, and H. Wu, "Electrospinning: A novel nano-encapsulation approach for bioactive compounds", Trends. Food. Sci. Technol., vol. 70, pp. 56-68, 2017. doi: 10.1016/j.tifs.2017.10.009

[27] K. Pal, A. K. Banthia, and D. K. Majumdar, "Biomedical evaluation of polyvinyl alcohol-gelatin esterified hydrogel for wound dressing", J. Mater. Sci. Mater. Med., vol. 18, no. 9, pp. 1889-1894, 2007. doi: 10.1007/s10856-007-3061-2

[28] B. S. Patil, V. S. Mastiholimath, and A. R. Kulkarni, "Development and evaluation of psyllium seed husk polysaccharide based wound dressing films", Oriental. Pharm. Exper. Med., vol. 11, no. 2, pp. 123-129, 2011. doi: 10.1007/s13596-011-0012-8

[29] C. Jinno, N. Morimoto, R. Ito, M. Sakamoto, S. Ogino, T. Taira, and S. Suzuki, "A Comparison of Conventional Collagen Sponge and Collagen-Gelatin Sponge in Wound Healing" Biomed. Res. Int. vol. 2016, p. 4567146, 2016. doi: 10.1155/2016/4567146

[30] L. Sun, J. Han, Z. Liu, S. Wei, X. Su, and G. Zhang, "The facile fabrication of wound compatible anti-microbial nanoparticles encapsulated Collagenous Chitosan matrices for effective inhibition of poly-microbial infections and wound repairing in burn injury care: Exhaustive in vivo evaluations", J. Photochem. Photobiol. B, vol. 197, p. 111539, 2019. doi: 10.1016/j.jphotobiol.2019.111539

[31] M. Tummalapalli, M. Berthet, B. Verrier, B. L. Deopura, M. S. Alam, and B. Gupta, "Composite wound dressings of pectin and gelatin with aloe vera and curcumin as bioactive agents", Int. J. Biol. Macromol., vol. 82, pp. 104-113, 2016. doi: 10.1016/j.ijbiomac.2015.10.087

[32] E. Pinho, and G. Soares, "Functionalization of cotton cellulose for improved wound healing", J. Mater. Chem. B., vol. 6, no. 13, pp. 1887-1898, 2018. doi: 10.1039/c8tb00052b

[33] K. I. Shingel, L. Di Stabile, J. P. Marty, and M. P. Faure, "Inflammatory inert poly(ethylene glycol)--protein wound dressing improves healing responses in partial- and full-thickness wounds" Int. Wound. J., vol. 3, no. 4, pp. 332-342, 2006. doi: 10.1111/j.1742-481X.2006.00262.x

[34] N. Sahiner, S. Sagbas, M. Sahiner, C. Silan, N. Aktas, and M. Turk, "Biocompatible and biodegradable poly(Tannic Acid) hydrogel with antimicrobial and antioxidant properties" Int. J. Biol. Macromol., vol. 82, pp. 150-159, 2016. doi: 10.1016/j.ijbiomac.2015.10.057

[35] M. Kokabi, M. Sirousazar, and Z. M. Hassan, "PVA–clay nanocomposite hydrogels for wound dressing", Eur. Polymer. J., vol. 43, no. 3, pp. 773-781, 2007. doi: 10.1016/j.eurpolymj.2006.11.030

[36] K. Khezri, M. R. Farahpour, and S. M. Rad, "Efficacy of Mentha pulegium essential oil encapsulated into nanostructured lipid carriers as an in vitro antibacterial and infected wound healing agent" Colloids. Surf. A, vol. 589, p. 124414, 2020. doi: 10.1016/j.colsurfa.2020.124414

[37] A. C. Alavarse, F. W. de Oliveira Silva, J. T. Colque, V. M. da Silva, T. Prieto, E. C Venancio, and J. J. Bonvent, "Tetracycline hydrochloride-loaded electrospun nanofibers mats based on PVA and chitosan for wound dressing", Mater. Sci. Eng. C. Mater. Biol. Appl., vol. 77, pp. 271-281, 2017. doi: 10.1016/j.msec.2017.03.199

[38] S. Calamak, C. Erdoğdu, M. Ozalp, and K. Ulubayram, "Silk fibroin based antibacterial bionanotextiles as wound dressing materials", Mater. Sci. Eng. C Mater. Biol. Appl., vol. 43, pp. 11-20, 2014. doi: 10.1016/j.msec.2014.07.001

[39] G. D. Mogoşanu, and A. M. Grumezescu, "Natural and synthetic polymers for wounds and burns dressing" Int. J. Pharm., vol. 463, no. 2, pp. 127-136, 2014. doi: 10.1016/j.ijpharm.2013.12.015

[40]. Z. Zarei, M. Mirjalili, and P. Norooz Kermanshahi, "Optimization of Dendrimer Polyamidoamin Electrospun Nanofibers: Preparation and Properties", Iranian J of Biotech, vol. 20, no. 1, pp. 36-45, 2022.

[41] R. Jayakumar, M. Prabaharan, P. T. Sudheesh Kumar, S. V. Nair, and H. Tamura, "Biomaterials based on chitin and chitosan in wound dressing applications", Biotechnol. Adv., vol. 29, no. 3, pp. 322-337, 2011. doi: 10.1016/j.biotechadv.2011.01.005

[42] S. Homaeigohar, A. R. Boccaccini, "Antibacterial biohybrid nanofibers for wound dressings" Acta. Biomater., vol. 107, pp. 25-49, 2020. doi: 10.1016/j.actbio.2020.02.022

[43] S. Dhivya, V. V. Padma, and E Santhini, "Wound dressings - a review", Biomedicine (Taipei), vol. 5, no. 4, p. 22, 2015. doi: 10.7603/s40681-015-0022-9

[44] G. D. Winter Formation of the scab and the rate of epithelization of superficial wounds in the skin of the young domestic pig. Nature, vol. 193, pp. 293-294, 1962. doi: 10.1038/193293a0

[45] E. A. Kamoun, X. Chen, M. S. M. Eldin, and E. R. S. Kenawy, "Crosslinked poly (vinyl alcohol) hydrogels for wound dressing applications: A review of remarkably blended polymers", Arabian J. Chem., vol. 8, no. 1, pp. 1-14, 2015. doi: 10.1016/j.arabjc.2014.07.005

[46] T. S. Stashak, E. Farstvedt, Othic A. Update on wound dressings: Indications and best use. Clin Techniq Equine Pract 2004;3(2):148-63. doi: 10.1053/j.ctep.2004.08.006

[47] M. Abbasipour, M. Mirjalili, R. Khajavi, and M. M. Majidi, "Coated cotton gauze with Ag/ZnO/chitosan nanocomposite as a modern wound dressing", J. Eng. Fibers. Fabrics., vol. 9, no. 1, p. 155892501400900114, 2014. doi: 10.1177/155892501400900114

[48] V. C. van der Veen, M. B. van der Wal, M. C. van Leeuwen, M. M. Ulrich, and E. Middelkoop, "Biological background of dermal substitutes", Burns, vol. 36, no 3, pp. 305-321, 2010. doi: 10.1016/j.burns.2009.07.012

[49] A. Gaspar-Pintiliescu, A. M. Stanciuc, and O. Craciunescu, "Natural composite dressings based on collagen, gelatin and plant bioactive compounds for wound healing: A review", Int. J. Biol. Macromol., vol. 138, pp. 854-865, 2019. doi: 10.1016/j.ijbiomac.2019.07.155

[50] A. D. Sezer, F. Hatipoğlu, E. Cevher, Z. Oğurtan, A. L. Baş, and J. Akbuğa, "Chitosan film containing fucoidan as a wound dressing for dermal burn healing: preparation and in vitro/in vivo evaluation", AAPS PharmSciTech., 2007;8(2):Article 39. doi: 10.1208/pt0802039

[51] S. Z. Moghadamtousi, H. A. Kadir, P. Hassandarvish, H. Tajik, S. Abubakar, and K. Zandi, "A review on antibacterial, antiviral, and antifungal activity of curcumin" Biomed. Res. Int., vol. 2014, p. 186864, 2014. doi: 10.1155/2014/186864

[52] Y. I. Jeong, H. S. Na, D. H. Seo, D. G. Kim, H. C. Lee, M. K. Jang, S. K. Na, S. H. Roh, S. I. Kim, and J. W. Nah, "Ciprofloxacin-encapsulated poly(DL-lactide-co-glycolide) nanoparticles and its antibacterial activity", Int. J. Pharm., vol. 352, no. 1-2, pp. 317-23, 2008. doi: 10.1016/j.ijpharm.2007.11.001

[53] N. Naseri, H. Valizadeh, and P. Zakeri-Milani, "Solid Lipid Nanoparticles and Nanostructured Lipid Carriers: Structure, Preparation and Application", Adv. Pharm. Bull., vol. 5, no. 3, pp. 305-313, 2015. doi: 10.15171/apb.2015.043

[54] Z. Drulis-Kawa, and A. Dorotkiewicz-Jach, "Liposomes as delivery systems for antibiotics". Int. J. Pharm., vol. 387 no. 1-2, pp. 187-198, 2010. doi: 10.1016/j.ijpharm.2009.11.033

[55] H. Jiang, L. Wang, and K. Zhu, "Coaxial electrospinning for encapsulation and controlled release of fragile water-soluble bioactive agents", J. Control. Release., vol. 193, pp. 296-303, 2014. doi: 10.1016/j.jconrel.2014.04.025

[56] E. Pinho, M. Grootveld, G. Soares, and M. Henriques, "Cyclodextrin-based hydrogels toward improved wound dressings", Crit. Rev. Biotechnol., vol. 34, no. 4, pp. 328-337, 2014. doi: 10.3109/07388551.2013.794413

[57] E. Pinho, M. Henriques, and G. Soares, "Cyclodextrin/cellulose hydrogel with gallic acid to prevent wound infection", Cellulose, vol. 21 no. 6, pp. 4519-4530, 2014. doi: 10.1007/s10570-014-0439-4

[58] E. Pinho, and G. Soares, "Cotton-hydrogel composite for improved wound healing: synthesize optimization and physicochemical characterization—part 1", Polymers Adv. Technol., vol. 29, no. 12, pp. 3114-3124, 2018. doi: 10.1002/pat.4432

[59] E. Pinho, R. C. Calhelha, I. C. Ferreira, and G. Soares, "Cotton-hydrogel composite for improved wound healing: Antimicrobial activity and anti-inflammatory evaluation—Part 2", Polymers Adv. Technol., vol. 30, no. 4, pp. 863-871, 2019. doi: 10.1002/pat.4519

[60] E. Pinho, S. Machado, and G. Soares, "Smart Hydrogel for the pH-Selective Drug Delivery of Antimicrobial Compounds', Macromolecular Symposia., vol. 385, no. 1, p. 1800182, 2019. doi: 10.1002/masy.201800182

[61] V. Moshakis, M. J. Fordyce, J. D. Griffiths, and J. A. McKinna, "Tegadern versus gauze dressing in breast surgery", Br. J. Clin. Pract., vol. 38, no. 4, pp. 149-152, 1984.

[62] S. Thomas, P. Loveless, and N. Hay, "Comparative review of the properties of six semipermeable film dressings", Pharm. J., vol. 240, pp. 785-787, 1988.

[63] D. Morgan, "Wounds—What should a dressing formulary include", Hosp. Pharmacist. vol. 9, pp. 261-266, 2002 .

[64] Thomson T. Foam composite. Google Patents; 2006.

[65] P. Chaganti, I. Gordon, J. H. Chao, and S. Zehtabchi, "A systematic review of foam dressings for partial thickness burns", Am. J. Emerg. Med., vol. 37, no. 6, pp. 1184-1190, 2019. doi: 10.1016/j.ajem.2019.04.014

[66] E. A. Kamoun, E. S. Kenawy, and X. Chen, "A review on polymeric hydrogel membranes for wound dressing applications: PVA-based hydrogel dressings", J. Adv. Res., vol. 8, no. 3, pp. 217-233, 2017. doi: 10.1016/j.jare.2017.01.005

[67] T. Chen, Y. Chen, H. U. Rehman, Z. Chen, Z. Yang, M. Wang, H. Li, and H. Liu, "Ultratough, Self-Healing, and Tissue-Adhesive Hydrogel for Wound Dressing," ACS. Appl. Mater. Interfaces, vol. 10, no. 39, pp. 33523-33231, 2018. doi: 10.1021/acsami.8b10064

[68] E. Pinho, M. Grootveld, G. Soares, and M. Henriques, "Cyclodextrin-based hydrogels toward improved wound dressings," Crit. Rev. Biotechnol., vol. 34, no. 4, pp. 328-337, 2014. doi: 10.3109/07388551.2013.794413

69Caló E, Khutoryanskiy VV. Biomedical applications of hydrogels: A review of patents and commercial products. Eur Polymer J 2015;65:252-67. doi: 10.1016/j.eurpolymj.2014.11.024

[70] G. Hagan, United States Patent Washington, D.C.: United States Patent and Trademark Office; 1992.

[71] F. Ullah, M. B. H. Othman, F. Javed, Z. Ahmad, and H.M. Akil, "Classification, processing and application of hydrogels: A review", Materials Sci. Eng. C., vol. 57, pp. 414-133, 2015. doi: 10.1016/j.msec.2015.07.053

[72] J. S. Boateng, K. H. Matthews, H. N. Stevens, G. M. Eccleston, "Wound healing dressings and drug delivery systems: a review", J. Pharm. Sci., vol. 97, no.8, pp. 2892-923, 2008. doi: 10.1002/jps.21210

[73] K. Vowden, and P. Vowden, "Wound dressings: principles and practice", Surgery (Oxford), vol. 35, no. 9, pp. 489-94, 2017. doi: 10.1016/j.mpsur.2017.06.005

[74] S. Thomas," Hydrocolloids," J. Wound. Care., vol. 1 no. 2, pp, 27-30, 1992. doi: 10.12968/jowc.1992.1.2.27

Effect of Corona Treatment Time on Surface Morphology and Dyeability Properties of Cotton Fabric with Reactive Dye

Hamid. Akbarpour *

Department of Sewing and Garment Design Engineering,Amol Branch(Tohid), Technical and Vocational University, Mazandaran, Iran

Abstract

In this paper was investigated dyeability cotton fabric sample using surface modification to corona discharged method. At first. In accordance with the design of experiments. We exposed the samples to Corona conditions with power of 100 (w) and the main current was 4A applied, at 60 and 300 secs and then dyed with Reactive Yellow K-RN Dyes. Then, scanning electronic microscope(SEM) was used to determine the effects of this operation on the surface morphology and also, a reflective spectrophotometer was employed to evaluate K/S, %R and L* a* b* values. Experiments indicated that dye stability of the samples were good and but with increased time of Corona after washing it was decline. Also, results showed that greater time of Corona operation at a constant pressure, enhanced cracks and pores on the surface morphology of the samples. As, Fourier transform infrared (FTIR) spectroscopy test displayed the effects of the Corona operation on the determination of Surface changes as well as changes in the existing functional groups in fabric after being wash and finally, the optimal conditions of the experiment were determined using the statistical method of Central Composite Design. In fact, aim of this study was to investigate the dyeing properties of cotton fabric and surface morphology changes using corona operation and to obtain optimal dyeing conditions. The results obtained in this research illustrated that optimize condition of cotton fabric samples dyed with the Reactive Yelow3 dye for K/S1 and K/S2 at F-value respectively, equal to 29879.53 and 15940.10, and probe values greater than F is equal to < 0.0001.
Keywords: Cotton fabric, Corona discharge, Reactive Yellow KRN, FTIR, Reflective Spectrophotometer.

** Corresponding author. Tel:.
 E-mail address: hamidakbarpour578@gmail.com

1. Introduction

The Cotton fiber that is known as one of the natural fibers enjoys a very complex structure and chemical processes have a widespread utilization to modify the fibers' surfaces for increase of dyeability. Moreover, researchers have shown the extensive application of Corona discharge for modifying the fibers' surfaces. Results indicated simpler treatment and higher practicality than any other physico-chemical techniques due to the quick treatment of the samples under atmosphere pressure [1]. Furthermore, researchers have demonstrated suitability of the corona operation as one of the dry methods. Therefore, they identified the plasma operation as one of the efficient techniques to promote the surface properties employed for various kinds of textile reform [2]. Numerous investigations have been done on the surface modified process of cotton as well as other fibers with corona discharge treatment, including wool and polyester, the impact of the treated time, treated voltages and powers on the features of cotton fibers, and the surface modified processes [3-6]. This method improves the surface with changing the bulk properties in a dry system without chemicals and water. The attention has been paid to improve the wettability, friction, adhesion, reflection of light, water repellency, soil release, printing, dyeing and other finishing process of textile fibres and fabrics by using corona technology [7]. Nourbakhsh et all [8] investigated the newly proposed corona discharge treatment of the cotton fabric with Cu and ZnO nanoparticles (NPs) and demonstrated the enhanced adsorption of copper NPs through pre-treatment method of corona discharge as well as greater self-cleaning effect and anti-bacterial function of the copper NPs than the post-treatment. Moreover, ZnO NPs exhibited the greatest anti-bacterial and self-cleaning effects using the pre-treatment technique. It is notable that the use of the post-treatment declined photo-catalyst activities of the ZnO NPs. Brzeziński et.al [9] founded that modifying the PET fabrics with corona discharge increased the fibers' surface energy and wettability of the activated samples. Research also has shown that greater ratio of oxygen to carbon indicates the formation of multiple functional polar groups in the top fibre layer of the PET fabrics, which have been activated with corona discharge. Because of development of the fibers' specific surfaces and removal of the direct contact between the negative charges accumulated on the surfaces of the activated PET fabric as well as the utilized bonding agents, adhesive ability of the fabrics remarkably enhanced, which has been revealed by the significant enhancement in the delamination force. The aim of this study was to investigate the dyeing properties of cotton fabric and surface morphology changes using corona operation and to obtain optimal dyeing conditions.

2. Experimental

2.1. Materials and Methods

At first, before Corona treatment, we selected 48 gr of the bleached cotton fabric in sizes of 50 ×50 cm2 from BABAKAN Textile Company and then washed the fabric with hot water and LCF-123 Jintery Eco anionic detergent at 60 ºC for 15 min for removing contamination from the fabric; finally dried the fabric at 80 ºC in a dryer for 1 hour.

2.2. Corona discharge treatment

In this unit, the two sample of fabrics at sizes of 5×5 cm^2 were put at a vacuum and corona conditions for one min and the other 5 min. Corona conditions included a system power of 100 (w) and the main current was 4A applied. Figure 1 shows the schema of the above system.
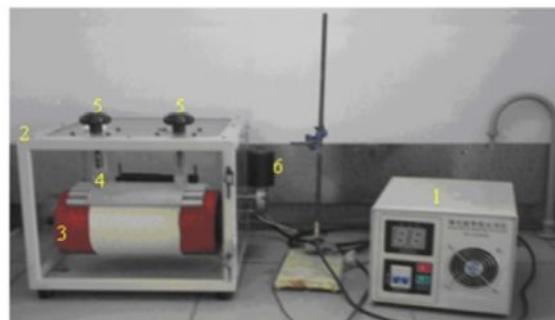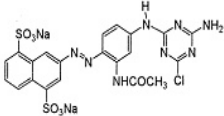
Fig.1. Equipment employed for performing the corona treatment. 1) Power supply, 2) Container Operation, 3) Roller, 4) Electrode spark production corona, 5) Electrode distance regulator screws up roller, and 6) Electro motor [2].

2.3. Dyeing process

At this step, sample was taken through 2 % of Reactive dye; that is, yellow K-RN (Reactive yellow 3) (Table.1). Tehran Dye Research Center was chosen to supply the Reactive dyes. The pre-determined L:R was 20:1 and therefore we examined the procured samples for evaluating the effects of Corona condition on determining Lab, light reflection rate (R %) as well as K/S and determining the fabrics' washing fastness.

Table .1. Molecular structure and properties of the reactive dye known as the reactive yellow K-RN [13,14]

Name of Color Index	Molecular Structure	Molecular Formula	Image of Molecular structure	Molecular Weight	Ligth fastness
C.I.Reactive Yellow 3, C.I.13245 Reactive Yekkow K-RN	Single Azo Class	$C_{21}H_{15}C_1N_8Na_2O_7S_2$		636,86	6 to 7

2.4. SEM

Pieces of experimented samples of 1×1 cm^2 size were cut and placed in the Sputter Coater machine for coating the samples with a gold layer. In the next step, we scanned the Corona-treated and untreated dyed samples for both samples with using of SEM instrument, model LEO440 made in England, for determining the effects of Corona condition on the fabrics' surface morphology.

2.5. Washing fastness of the samples

For this stage, we washed those samples with a weight of 5 g, which have been treated with Corona and dyed with the reactive dye at the exposure times of one and five minutes 5 times at 80 ºC in a soap bath consisting of 2 gr/L anionic soap and 4 gr/L sodium hydroxide (NaOH) with 40:1 ratio of bath mass on the fabric weight for 30min. Next, we dried the samples in a dryer for one hour and measured the Lab, % R rate as well as K/S of the washed samples with a reflective spectrophotometer machine for determining the fabrics' colour fastness.

2.6. Reflective spectro-photometer

As mentioned earlier, spectro-photometer ColourEye-7000A system with UV D65 standard light source and d/8º geometrical feature was employed for measuring the samples' Lab R % rate and K/S. In fact, the experiment was performed for determining the fabric's color fastness due to the exposure to nitrogen (N) gas cold plasma, prior to and following the washing process.

2.7. FTIR

All the samples were placed in the machine jaw for experimenting the entire level of the samples. After that, OMNIC software was employed for analyzing the samples and the experiment was operated in a machine known

as Thermo Nicollet 807 fabricated in America for proving reliability of the reflective spectrophotometer test in order to specify the fabric's color and washing fastness.

2.8. Experimental design

In this step, Central Composite Design (CCD) was utilized for the experimental plan with 2 variables [10]. These two variables included the percentage of Reactive dye and amount of irradiation time(sec). Findings revealed the variables range for irradiation time between 55.78 and 300sec) and percentage of Reactive dye (0.12–0.98%), through the trial version of the Design Expert 8.0.1.0 software provided from the Stat-Ease, Inc.(USA). Table (2) (runs 1–8) completely reports the design process of the samples of Cotton fabric with the dye percentage and the irradiation time. Results reflected the influence of the variables on the Y_1 (K/S) and Y_2 (R) outputs adjusted by the third-order polynominal function (Equation 1). Though we chose the samples for 3 series of time under radiation, softness of the range of changes was randomly chosen for ranges between 4 and 12 min of radiation in 8 distinct runs. Put differently, samples with four iterations were used to perform the laboratory experiments:

$$Y = b_0 + \sum b_i X_i + \sum b_{ij} X_i X_j + \sum c_i X_i^2 \qquad i \geq j \qquad\qquad \text{Eq. 1}$$
$$i,j = 1,2,3$$

Here, b_0 stands for an independent term according to the mean value of the experimental plan. B_i represents the regression coefficient, explaining the effects of variables on the linear form. b_{ij} is the regression coefficients of the interaction terms between the variables. C_i refers to the coefficients of the variables quadratic form.

Table 2. CCD for K/S and R of the fabric samples treated with Reactive dye at various irradiation times.

Run	Factor 1: A: Time treat (sec)	Factor 2: B: Reactive dye (%)	Response 1 K/S1	Response 2 K/S2	Response 3 R1	Response 4 R2
Control 1	60	0	Invisible	Invisible	Invisible	Invisible
Control 2	0	1	5.28	5.15	11.54	11.48
1	206.71	0.12	0.3	0.3	1.6	2.0
2	165.00	0.55	0.9	0.7	4.0	5.1
3	55.78	0.81	2.2	1.6	9.8	12.3
4	206.71	0.98	2.9	2.1	12.8	16.2
5	165.00	0.55	0.9	0.6	3.9	5.1
6	300.00	0.55	1.6	1.2	7.2	9.2
7	165.00	0.55	0.9	0.6	3.9	5.1
8	55.78	0.29	0.8	0.6	3.5	4.4

3. **Results and discussion**

With regard to Figure 4, Comparison of the curves of the raw sample dyed with reactive without Corona treatment with sample of dyed and Corona treated at time 1 and 5 min. The Corona conditions show that before washing rate of K/S decrease suddenly but after washing decrease gradually (a and c). Also, that before washing rate of %R decrease suddenly but after washing increase again (b and d). Table 3 indicated that comparison of

K/S, %R and CIELab between samples of untreated and treated with Corona before and after washing, respectively.

Table 3. Comparison of K/S, %R and CIELab between samples of untreated and treated with Corona before and after washing, respectively.

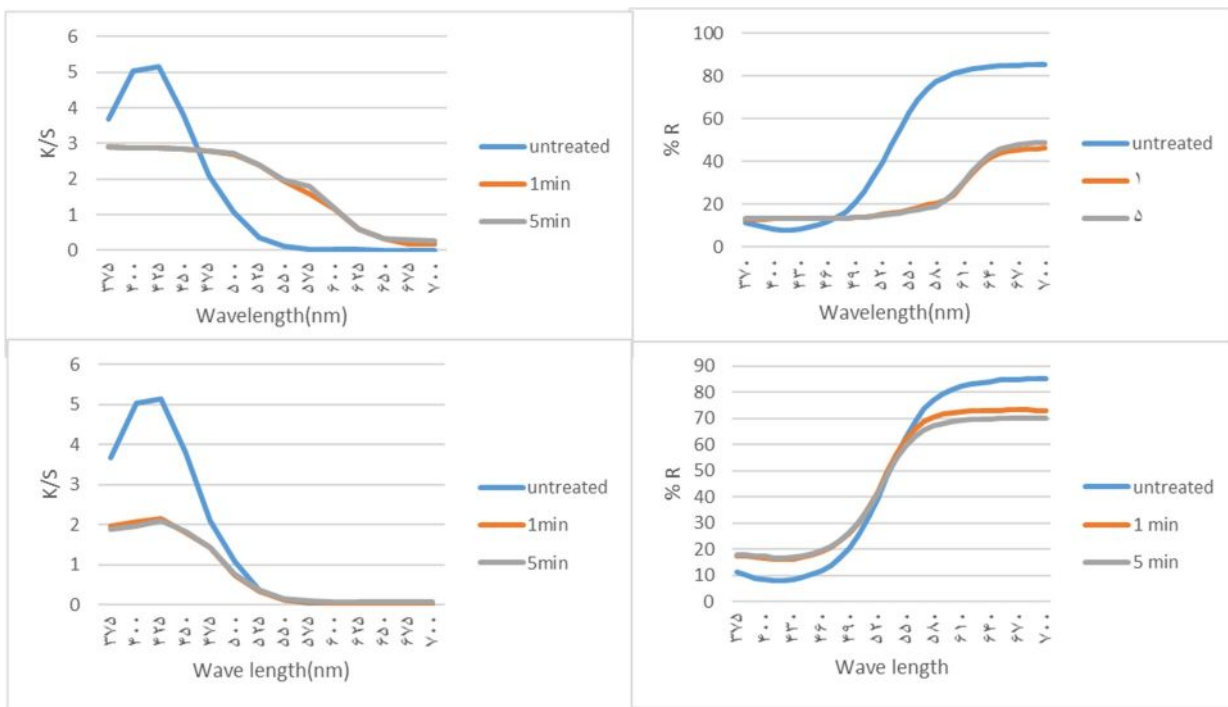| Sample	Untreated	Before washing		After washing	
Time of Corona		**1min**	**5min**	**1min**	**5min**
λ_{max}**(nm)**	425	375	375	425	425
K/S	5.28	2.92	2.9	2.16	2.1
%R	11.54	13.02	13.06	16.34	16.78
L*	80.51	49.27	49.45	79.47	78.34
a*	13.12	21.77	22.18	8.23	7.32
b*	67.59	9.96	10.32	48.93	46.23
c*	68.85	23.94	24.47	49.62	46.80
h○	79.01	24.59	24.95	80.45	81.00

Fig 4. Comparison of graphs between :
a)   Graph of K/S sample of untreated and treated with Corona before washing
b)   Graph of %R sample of untreated and treated with Corona before washing
c)   Graph of K/S sample of untreated and treated with Corona after washing
d)   Graph of %R sample of untreated and treated with Corona after washing

As shown in Table 4, the value of the adsorption coefficient to the diffusion (K/S) of the dye raw sample compared to the sample treated with corona (1 and 5 min) and dyed, shows a sudden decrease, which for both before and after Washing is observed to be almost identical, while for values of the reflectance spectrum (%R) this value shows a gradual increase over the dyed raw sample before and after washing. This indicates that the corona operation and degradation of the surface morphology of cotton fibers cause less dye adsorption due to the plasticizer phenomenon and low dye penetration into the fibers, while the color wash stability is improved due to the hydrogen and covalent bonds between reactive dye and cotton fibers. Scheme.1, indicated the mechanism of Corona discharge and dyeing with Reactive K-RN treatments on cotton fiber.
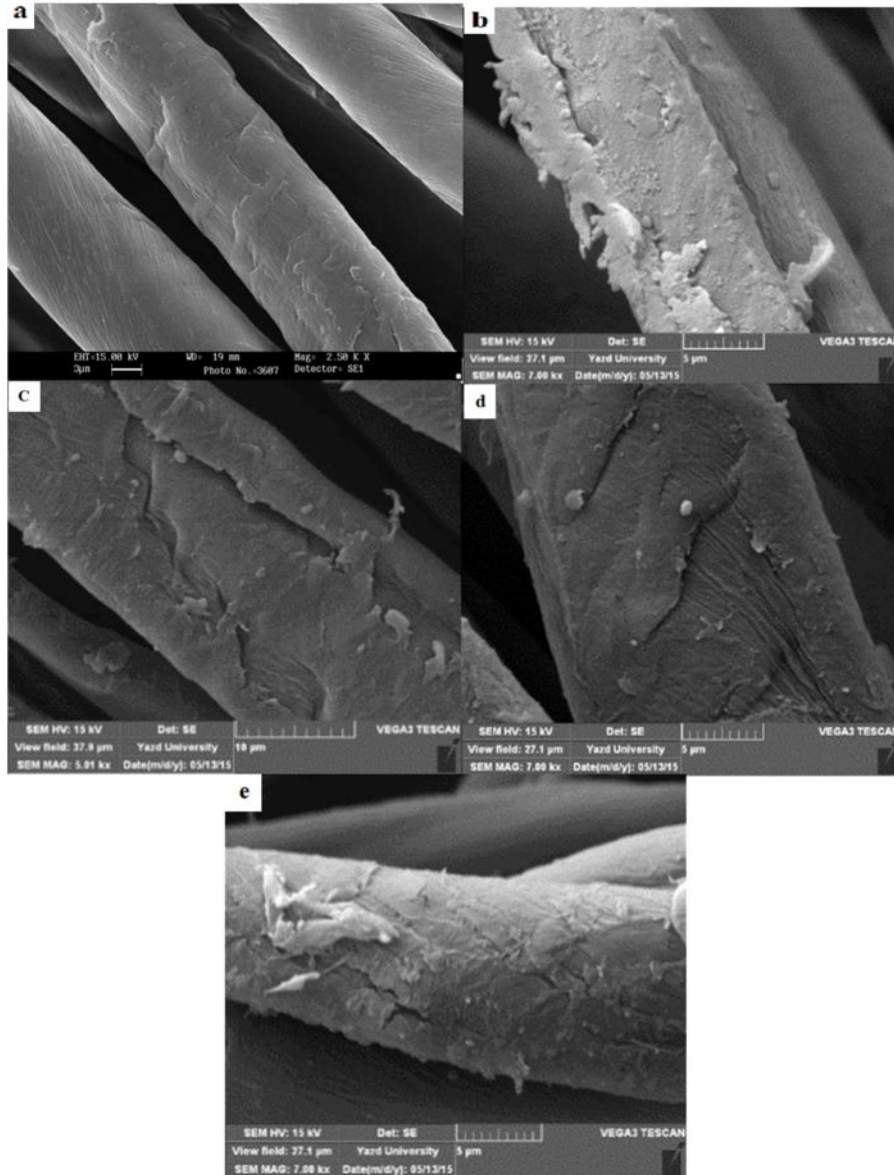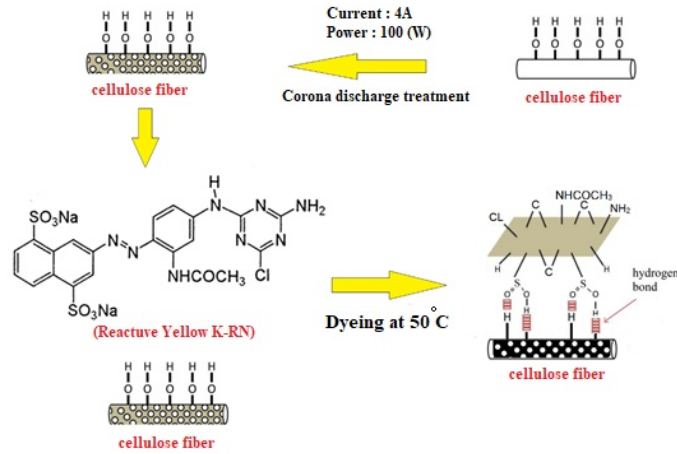

Fig 5. Image of SEM : a) Raw b) treated with corona at time 1 min, c) treated with corona at time five minutes, d) treated with corona at time 1 min and then dying e) treated with corona at time 5 min and then dying.

Fig.5, demonstrates SEM images obtained from the Raw samples' surfaces, which were treated with Corona at 1 and 5 min times through an electronic microscope, indicating differences in the surface morphology. As seen, if the samples are more exposed to the plasmatic condition, they would have more effects of destructive condition on them (b and c). The microscopic images of the fibers in figures (d) and (e) show well the uniform placement of the dye in the pores of the fibers created by the corona operation, and finally we see a smooth surface on the surface of the fibers, which is consistent with our previous results.

Scheme 1. The proposed mechanism of Corona discharge and dyeing with Reactive K-RN treatment on cotton fiber.
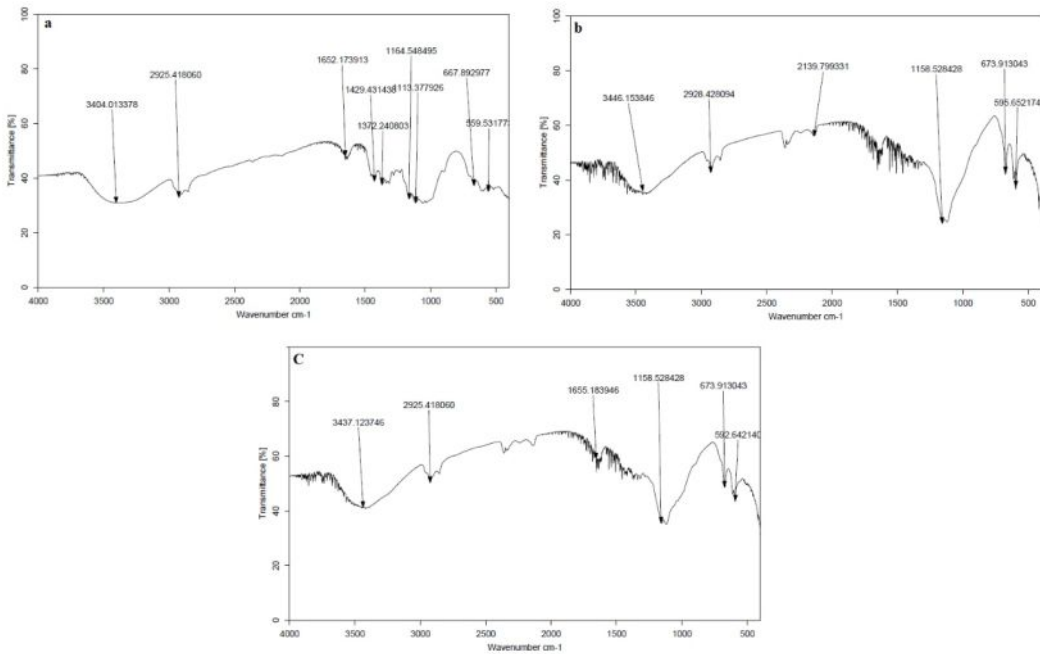

Fig 6. FTIR for : a) Raw   b) treated with corona at time 1 min and then dying
c) treated with corona at time 5 min and then dying

Studying Fig (6) as well as the peaks from the existing functional groups in the samples did not show any significant changes [14] so that CH stretching absorption in 3000 cm^{-1} 2850 cm^{-1} regions, ketone absorption in 1720 cm^{-1} region, and that of the sulphates in 3000 cm^{-1} and 2850 cm^{-1} regions are the same for each dyed sample of the treated and untreated samples with Corona. However, lower absorption was seen in 2350 cm^{-1} region on nitrile and in 650-720 cm^{-1} region of the stretching CH alkene or alcohol. With the enhanced operation time of Corona, peak also enhanced. Put differently, we found stronger absorption in 1150-1165 cm^{-1} region of sulphonic acid, indicating greater treatment time of Corona with increasing the peak. Hence, the fabrics dye fastness following the washing stage would be reasonable and for the taken samples. In fact, Corona condition was shown to not involve in the failed creation of washing fastness in the fabric in comparison with the untreated samples, reflecting minor effect of the operation on the K/S values and reflective spectrum.

3.1. Statistical *analysis*

Optimization of the application of the NPs reflected considerable involvement in the better function of the textile fabrics. In contrast to the conventional optimization, it is possible to consider statistical optimization interactions and processes between the variables to create a procedure response. In addition, RSM was demonstrated to be a strong statistical method to analyze numerous variables because it involves fewer crucial experimental trials as compared to the "one-factor-at-a-time" technique. On the one hand, RSM was considered as an efficient mathematical approach for optimizing the complex processes with the capability of producing an empirical pattern for evaluating correlations of several controlled experimental parameters with the observed results. On the other hand, RSM has a widespread utilization in various bio-chemical, nanochemical as well as chemical methods to examine the effect(s) of independent variables and optimize the process responses using proper values of the parameters [10–12]. It could be said that this study was performed according to RSM and CCD. Therefore, 8 experimental CCD runs were designed (see Table 2). We also addressed the evaluation of, the impact(s) of independent variables such as treat time and Reactive dye percentage on the response surface and showed %R and K/S features of the treated fabric samples. At the end, Equations (2), (3), (4), and (5) give actual factors of the K/S and %R of the fabric samples, which were treated with Corona treatment and Reactive dye:

K/S_1= +1.40565-0.012097 *Time treat*-1.31523 *Reactive Yellow 3*+0.001825 *Time treat* Reactive   Yellow 3* +0.000035 *Time treat*^{2}+3.50813 *Reactive Yellow 3*^{2} *Eq(2)*

K/S_2= +1.03158--0.008928 *Time treat*-0.965332 *Reactive Yellow 3*+0.001521*Time treat* Reactive Yellow 3* +0.000026*Time treat*^{2}+2.53548 *Reactive Yellow 3*^{2} *Eq(3)*

R_1= +6.27415-0.054369 *Time treat*-5.68116 *Reactive Yellow 3*+0.008027 *Time treat* Reactive Yellow 3*+0.000159 *Time treat*^{2} +15.56296 *Reactive Yellow 3*^{2} *Eq(4)*

R_2= +7.79478-0.067927 *Time treat*-6.87782 *Reactive Yellow 3*+0.011527 *Time treat* Reactive   Yellow 3*+0.000199 *Time treat*^{2} +19.22187 *Reactive Yellow 3*^{2} Eq(5)

Therefore, we employed the final statistical model for drawing the response surface (Equations 2–5), and in this way determined the relationship of each independent variable with K/S and %R of the fabric samples. Figures 7 and 8 represent the response surface of the samples of fabric.

Moreover, we applied Design-Expert software with the Corona time equal to 5 minutes or 300 sec for Reactive dye for obtaining optimum condition of the features of K/S and %R of the samples. In the next step, we used analysis of variance (ANOVA) for the process of data analysis in order to establish interaction of

independent variables with the responses. Then, this test was employed for analyzing results for evaluating K/S and %R of the mentioned samples (Tables 4, 5, 6, 7).

Results reflected significance of this new model of the fabric samples with the Reactive Yelow3 for K/S_1 and K/S_2 at F-value equal to 29879.53 and 15940.10, and prob values greater than F, < 0.0001, (Tables 4, 5). Consequently, the model of the treated fabric samples with the Reactive Yellow 3 for $\%R_1$ and $\%R_2$ was shown to be significant at F-value equal to **6.006×10^5** and **9.593×10^5** with the probability values more than F< 0.0001, respectively (Tables 6, 7).
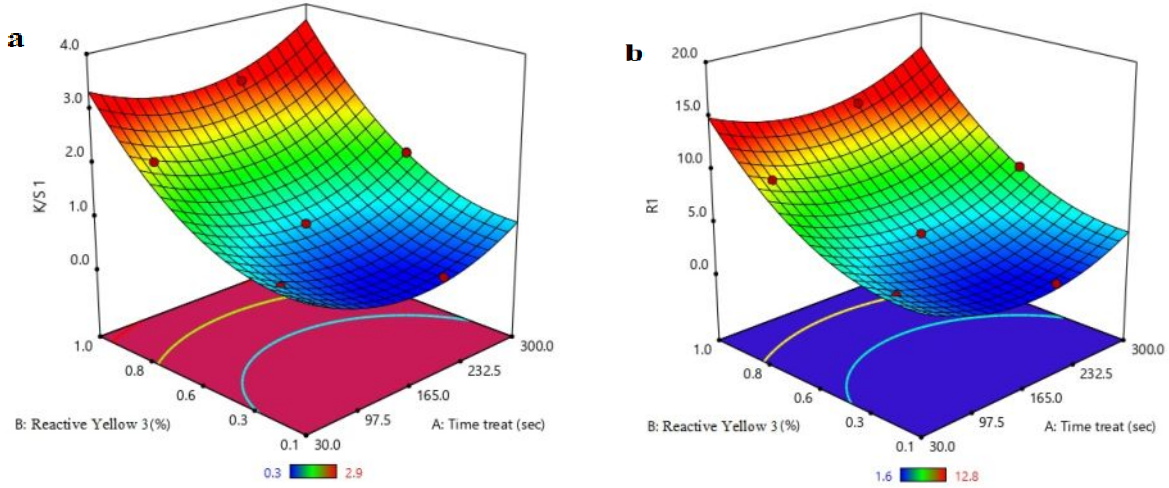

Figure 7. Response surface for a) K/S_1 and b) $\%R_1$ as the Corona time function and Reactive dye for the fabric samples.
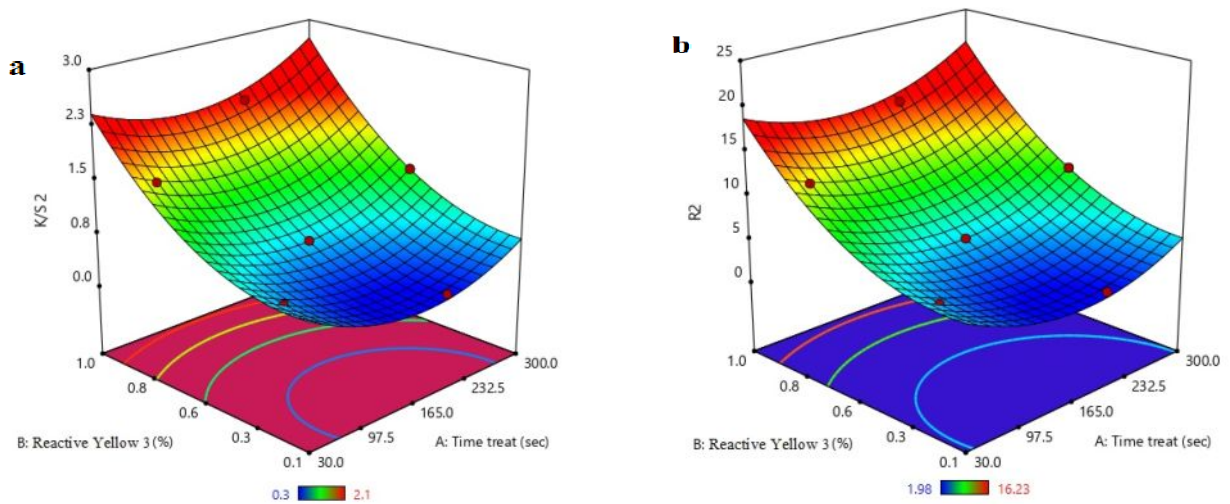

Figure 8. Response surface for a) K/S_2 and b) $\%R_2$ as the Corona time function and Reactive dye for the fabric samples.

Table 4. ANOVA result of K/S_1 for the fabric samples with Reactive yellow 3 at different Corona times

Source	Sum of Squares	df	Mean Square	F-value	p-value	prob > F
Model	4.98	5	0.9960	29879.53	< 0.0001	significant
A-Time treat	0.0136	1	0.0136	408.38	0.0024	
B-Cold dye	4.10	1	4.10	1.229×10^5	< 0.0001	
AB	0.0077	1	0.0077	230.49	0.0043	
A²	0.4428	1	0.4428	13284.57	< 0.0001	
B²	0.5406	1	0.5406	16218.81	< 0.0001	
Pure Error	0.0001	2	0.0000			
Cor Total	4.98	7				

Table 5. ANOVA Result of K/S_2 for the samples of fabric with Reactive yellow 3 at different Corona times

Source	Sum of Squares	df	Mean Square	F-value	p-value	prob > F
Model	2.66	5	0.5313	15940.10	< 0.0001	significant
A-Time treat	0.0125	1	0.0125	376.07	0.0026	
B-Cold dye	2.18	1	2.18	65377.40	< 0.0001	
AB	0.0053	1	0.0053	160.15	0.0062	
A²	0.2426	1	0.2426	7278.50	0.0001	
B²	0.2824	1	0.2824	8472.04	0.0001	
Pure Error	0.0001	2	0.0000			
Cor Total	2.66	7				

Table 6. ANOVA result of $\%R_1$ for samples of the fabric with Reactive yellow 3 at various Corona times.

Source	Sum of Squares	df	Mean Square	F-value	p-value	prob > F
Model	100.09	5	20.02	6.006×10^5	< 0.0001	significant
A-Time treat	0.2875	1	0.2875	8624.45	0.0001	
B-Cold dye	82.47	1	82.47	2.474×10^6	< 0.0001	
AB	0.1487	1	0.1487	4460.15	0.0002	
A²	9.00	1	9.00	2.699×10^5	< 0.0001	
B²	10.64	1	10.64	3.192×10^5	< 0.0001	
Pure Error	0.0001	2	0.0000			
Cor Total	100.09	7				

Table 7. ANOVA result of $\%R_2$ for samples of fabric with Reactive yellow 3 at various Corona times

Source	Sum of Squares	df	Mean Square	F-value	p-value	prob > F
Model	159.88	5	31.98	9.593×10^5	< 0.0001	significant
A-Time treat	0.7185	1	0.7185	21554.81	< 0.0001	
B-Cold dye	132.36	1	132.36	3.971×10^6	< 0.0001	
AB	0.3066	1	0.3066	9199.25	0.0001	
A²	14.05	1	14.05	4.214×10^5	< 0.0001	
B²	16.23	1	16.23	4.869×10^5	< 0.0001	
Pure Error	0.0001	2	0.0000			
Cor Total	159.88	7				

.

4. **Conclusion**

In this research and according to the design of experiments by the statistical software of the Central Composite Design(CCD), sample of the bleached cotton fabric was exposed to Corona condition at times of 60 and 300 sec and then dyed using Reactive yellow 3. Then, we examined the effect(s) of Corona on the degradation/destruction of the surface morphology and employed SEM to assess them. In the next step, reflective spectrophotometer machine was used to show the outputs resulting from Corona condition in determination of K/S, b*, a*, L* and R % rates. According to the results, those samples dyed with the reactive dyes had dye fastness, though washing fastness partly declined following the Corona operation that may be neglected because ATR-FTIR test proved it. Moreover, images from the Corona effect on the surface morphology with the use of SEM showed the enhanced destruction with the greater Corona treatment time. Also, Design-Expert software with a Corona time equal to 300 sec for Reactive Yellow 3 dye was employed for obtaining an optimum condition of the K/S features and %R of the fabric samples.

References

[1] Pibo Ma, Juan Huang, Genyang Cao, and Weilin Xu, Influence of Temperature on Corona Discharge Treatment of Cotton Fibers, Fibers and Polymers, Vol.11, No.6, 941-945(2010).

[2] M. Mirjalili1, S.Sharif Nasirian and L.Karimi, Effects of corona discharge treatment on some properties of wool fabrics, African Journal of Biotechnology Vol.10(83), pp.19436-19443, 21 December,(2011).

[3] W. Xu, X. Shen, X. Wang, and G. Ke, Sen'I Gakkaishi, 62,111 (2006).

[4] W. Xu and X. Liu, Eur. Polym. J., 39, 199 (2003).

[5] D. Sun and G. K. Stylios, J. Mater. Process. Tech., 173, 172 (2006).

[6] H. A. Karahan and E. Ozdogan, Fiber. Polym., 9, 21(2008).

[7] Peiman Valipour, Ramin Khajavi, Sahar Belaj , Shirin Nourbakhsh, PHYSICAL AND MECHANICAL PROPERTIES OF CORONA DISCHARGE TREATED POLYESTER FABRIC, XIIIth International Izmir Textile and Apparel Symposium April 2-5, (2014).

[8] Sh.Nourbakhsh, H.Sepehrnia and E.Akbari, Novel corona discharge treatment of cotton fabric with Cu and ZnO nanoparticles, The journal of textile institute Vol 111,(2020).

[9] Stefan Brzeziński, Stefan Połowiński, Dorota Kowalczyk, Iwona Karbownik, Grażyna Malinowska. Effect of the Corona Discharge Treatment of Polyester Fabrics on their Adhesive Properties, FIBRES & TEXTILES in Eastern Europe, Vol. 17, No. 4 (75) pp. 98-102(2009).

[10] Nazari, A., Montazer, M., Mirjalili, M., Nazari, S.: Polyester with durable uv protection properties through using nano TiO2 and polysiloxane softener optimized by RSM. J. Text. Inst. 104, 511–520 (2013).

[11] Zarrinabadi Ehsan, Abghari Ramin, Nazari Ali, Mirjalili Mohammad: Environmental effects of enhancement of mechanical and hydrophobic properties of polyester fabrics using silica/kaolinite/silver nanocomposite: a facile technique for synthesis and RSM optimization. Eurasia J Biosci 12, 1–14 (2018).

[12]H.Akbarpour, A.Rashidi, M.Mirjalili, A. Nazari, Comparison of the conductive properties of polyester/viscose fabric treated with Cu nanoparticle and MWCNTs; Journal of Nanostructure in Chemistry,(2019).

[13] Reactive yellow dye.www.worlddyevariety.com.

[14] H.Akbarpour, A.Rashidi, M.E Yazdanshenas and H.Tayebi; Effect of Nitrogen Gas Cold Plasma on Cotton Fabric Dyed with Reactive Dyes, Asian Journal of Chemistry; Vol. 25, No. 2, 695-700,(2013).

Development and Characterization of Graphene Oxide based Composite for Adsorptive Removal of Azo Reactive Dyes from Aqueous Media

Zahra Zareei[a*], Mohammadali Shirgholami[a], Saeid Jafari[a], Mohammad D. Ahmadabadi[a], Masoud Rohani-moghadam[b]

[a]Department of polymer engineering, Yazd branch, Islamic Azad University, Yazd, Iran
[b]Department of Chemistry, Faculty of Sciences, Vali-e-Asr University of Rafsanjan, Rafsanjan, Iran

Abstract

In this study, we tried to present an efficient method for removal of Reactive red 241 (RR241) from aqueous media, using a modified carbon composite with GO sheets. The prepared nanocomposites were then characterized by commonly identical techniques involving FESEM, BET, and FT-IR. In removal studies, various parameters affecting the adsorption process including pH, time, adsorbent dose, temperature as well as the amount of GO in the construction of composite were studied by response surface method. The optimum conditions for 100 mg/L dye removal was pH of 5.0, 75 minutes' time, and the adsorbent dose of 1.47 g/L containing 4.15 wt.% of GO. Also, under optimum conditions, the maximum, 96% removal, was achieved. Experiments showed that the adsorption was more consistent with the Langmuir equations, and the maximum adsorption under this model was 160 mg/g. The removal experiments showed that the amount of the adsorbent, GO content and pH had a significant effect on RR241 removal. BET analysis indicated that the addition of GO to the carbon composite structure improved the pore size, total pore volume, and effective surface area of the composite. Also, isotherms, kinetics, and thermodynamic studies of adsorption depicted that the Langmuir isotherm model, pseudo-second-order kinetic model, and self-adsorption are suitable models for RR241dye adsorption.
Keywords: Colorful Pollutants, Adsorption, Graphene Oxide, Composite.

---

* ∗ Corresponding author. Tel: +98-353187822
  E-mail address: z.zareei@iauyazd.ac.ir

1. Introduction

In today's world, color plays a vital role in cultivating human tastes and satisfying their aesthetic needs [1]. The use of dye in textile and decorative goods has been common since ancient times due to its beauty and effect on the human soul [2]. Many advances have been made in the field of dyeing and production of dyes for a long time. Today this industry has been able to offer the most desirable dyed goods to the market in various shades by using the latest dyeing techniques and different types of dyes [3]. In the dyeing process, four factors play major roles: dyes, goods, auxiliary chemicals, and machines [4]. Dyes used in the dyeing process are classified in two ways, one is based on chemical structure, and the other based on the type of application. In chemical class, dyes are classified into pigments, acidic dyes, azo dyes, anthraquinone dyes, vat dyes, indigo dyes, triaryl carbonium dyes, polymethine dyes, metallic dyes, Nitro and nitroso dyes and miscellaneous dyes [5]. Azo dyes are a group of reactive dyes that make up about 70-60% of all dyes used in various industries. These dyes are generally covalently bonded with textile fibers such as cotton. Due to their low degradability and widespread use, they have influenced conventional wastewater treatment in the textile industry in recent decades [6]. Today, the discharge of effluents from textile industries into natural waters has created serious problems. These color compounds are toxic to aquatic life [7]. They are visible in amounts less than one milligram per liter and cause unpleasant environmental scenery. It has also been shown that some azo dyes or compounds resulting from the degradation of color compounds are toxic, mutagenic, carcinogenic, and contain resistant compounds [8]. Therefore, it is very necessary for textile industries to have wastewater treatment before discharging effluents to the environment. Treatment of colored wastewater is relatively difficult by conventional biological and physicochemical processes due to the structure of the chemical complex of these dyes, especially azo dyes [9].

So far, various methods such as ion exchange [10], chemical precipitation [11], reverse osmosis [12], membrane technologies [13], coagulation [14], electrochemical purification [15], which have problems such as the need for continuous recovery, preliminary treatment, extremely high cost, biological sludge, and strict operating conditions. Coagulation, photolysis, and advanced oxidation are among the methods which have some disadvantages. High cost and time-consuming, low efficiency, high energy consumption and the need for reactive materials are some disadvantages of these methods. Among the various available methods, adsorption is one of the most effective processes for the removal that is both environmentally friendly and easy to operate [16]. The adsorption process has been suggested as an extensible process due to the low cost of design and operation, non-production of hazardous byproducts and the design simplicity to remove organic and inorganic compounds [17-18]. Over recent years, applications of graphene oxide (GO) in various fields have attracted the attention of scientists. GO is one of the graphene derivatives widely used as a potential superior adsorbent. Its excellent properties and the ability to control its properties through chemical functionalization have caused researchers to pay particular attention to it [19-20]. GO is a layer of graphite with numerous groups containing oxygen. GO, as a two-dimensional carbon allotrope has a lattice-like planar structure [21]. GO shows strange physical properties that have never been observed before at the nanoscale. High Young's modulus (about 1000 GPa), high fracture resistance (130 GPa), good heat conductivity (5000 W/mK), special surface area (2600 m2g-1), and amazing transfer phenomena such as the quantum Hall effect, the ability to absorb some metal ions and soil pollutants, and the catalytic properties are remarkable properties of GO [22]. A large number of oxygen-containing groups, such as epoxy, hydroxyl, and carboxyl groups at the plane structure of GO can be bonded with metal ions. In addition, the high surface of GO gives it a high adsorption capacity similar to that of carbon nanotubes [23]. The main limitation of the application of the GO is its separation from the solution after the adsorption process and the turbidity of the material in the sample [24]. Therefore, creating conditions for separation, optimum use of graphene, and transparent effluent production is an inevitable necessity. To overcome this limitation, several researchers have suggested modifying or merging it with other materials. Bhattacharyya et al. prepared a nanocomposite consisting of activated carbon graphene oxide as the adsorbent of methylene blue dye from the solution [25]. Martins et al. proposed a mixture of high superficial area carbon-

based nanomaterial strategy to improve the removal of basic blue 26 (BB26) by blending porous carbon nitride (CN) and graphene oxide (GO). The CN/GO nanocomposite's ability to remove the BB26 dye was 21 times higher than those reported in the literature, indicating CN/GO composites as potential filtering materials for basic dyes [26]. In another study, Cao et al. reported a novel GO/PNIPAM composite system that had been rationally designed for the removal of organic dyes from polluted water in a new mechanism- an extraction-like mechanism. The system gives a phase transition to produce a solution phase and a gel phase at temperatures above the lower critical solution temperature (LCST) of PNIPAM. During this phase the GO sheets are fully transferred into the gel phase. [27]. Rostamian et al. have proposed an eco-friendly adsorbent based on poly (glycerol sebacate) (PGS), including PGS-graphene oxide nanoparticles (GO), PGS-graft-chitosan(CS), and PGS–CS–GO nanocomposites as efficient dye adsorbents for the wastewater treatment procedure [28].

This study aimed at of this study was to synthesizing a GO-based carbon composite (GO-CC) as a suitable and environmentally friendly adsorbent for the removal of Reactive red 241 (RR241) dye from aqueous solutions. The effect of various variables such as solution pH, contact time, amount of GO on carbon composite, and amount of carbon composite as adsorbent on removal efficiency was investigated. Statistical modeling and optimization of removal conditions were performed using response surface methodology (RSM). The reason for using statistical modeling of RSM were benefits such as simplicity, reduction in the number of samples tested, comprehensive study of the simultaneous effect of variables on response, reduction of time, manpower, and cost. In addition, the kinetic and equilibrium data of adsorption with pseudo-first and pseudo-second kinetic models and Freundlich and Langmuir isotherm models were investigated.

2. Experimental

2.1. Chemicals

GO powder (Sigma-Aldrich, USA) and graphite powder (Merck, Germany) were used to prepare the carbon composite. The carbon composite was fabricated via sol gel using potassium trimethoxy silane (90% purity, Merck), methanol (99% purity, Merck), and hydrochloric acid (37% aqueous solution, Sigma-Aldrich). The removal experiments were performed on Reactive red 241 (RR 241,98% purity, Sigma-Aldrich) in a batch reactor. Its chemical structure is illustrated in Scheme 1.
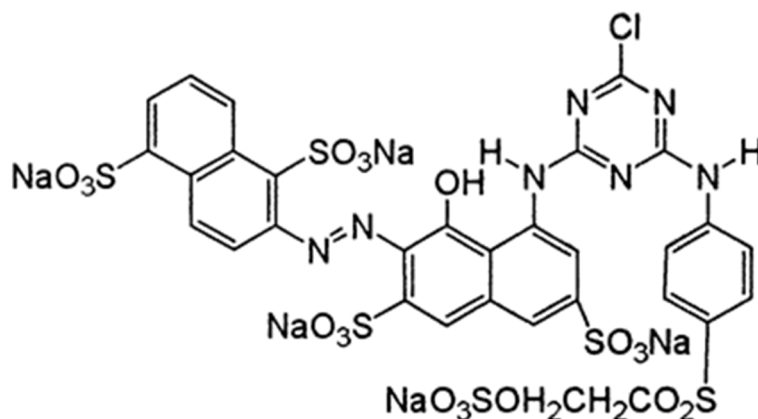
Scheme 1- Chemical structure of Reactive Red 241.

The pH of the aqueous solutions was adjusted using a 0.1 M phosphate buffer consisting of phosphoric acid (85% purity, Sigma-Aldrich) and sodium hydroxide (purity of 98%, Sigma-Aldrich), and an Autolab model 827

pH meter was used to measure it. A Fartest magnetic stirrer (Model HPMA 700, Farzaneh Arman Ltd.) was used to disperse the adsorbent in aqueous solutions during the test. The carbon nanocomposites were separated from aqueous samples by an Eppendorf 5810 Centrifuge device (MiniSpin, Germany). The concentration of RR241 in aqueous solutions was determined using the Cary 100 UV-Vis spectrophotometers (Agilent USA).

2.2. Preparation of the adsorbent

The adsorbent used to remove the RR241 from aqueous solutions was a carbon-composite, which contained GO platelets, prepared by sol-gel method at ambient temperature. The fabrication way for this composite is derived from Esfandiary et al., which is briefly described below. To prepare the sol (4 mL), first 3 mL of methanol was mixed with 600 μL of deionized water, and then 100 μL of potassium trimethoxy silane was added to the mixture. The gelation process of the resulting mixture (siloxane condensation polymerization) began with the reduction of the solution pH to the range of 5.0-6.0. The process was accelerated by the addition of a few drops of hydrochloric acid. After the formation of three-dimensional polymer gels containing repeating SiO_2 units, the sol color changed from transparent to milky.In the next step, 41.0 mg of GO powder was mixed with 1.0 g of graphite powder. Then, the sol-gel mixture prepared in the previous step was added to the carbon mass and gently homogenized with the spatula to produce a carbon paste. The resulting carbon paste was placed in a preheated oven at 60 °C for one hour. The composite powder was kept in desiccator until its subsequent usage in the adsorption experiments.

2.3. Adsorption tests

RR241 adsorption experiments were conducted in a batch reactor to investigate the effect of various variables such as the weight percentage of GO in the prepared composite, solution pH, the adsorbent dosage (i.e. amount of the composite) and reaction time on the dye removal efficiency using the GO-modified carbon composite by the models presented in Design of Expert (DOE) software. In the optimum conditions, 147 mg of the adsorbent containing 4.15 wt. % of GO was added to 100 mL of the buffer phosphate (0.1 M) containing 100 mg/L of RR241 with the pH of 5.0 for 75 min. After completion of the planned adsorption time, the composite was separated from the aqueous solution by centrifugation and the residual concentration of RR241 in the solution was measured using the uv-vis spectrophotometer. Finally, the dye removal efficiency (Re (%)) and the adsorbent adsorption capacity (qe) were calculated using Equations 1 and 2, respectively.

$$Re \ (\%) = \frac{C_0 - C_e}{C_0} \times 100 \qquad \text{(Eq. 1)}$$

$$q = \frac{(C_0 - C_e)v}{m} \qquad \text{(Eq. 2)}$$

In these equations, C0 and Ce are initial and final concentrations of RR241 in mg/L, respectively, and V and m are solution volume (L) and the adsorbent absorbed mass in grams, respectively.

2.4. Determination of isoelectric point of the prepared composite

The pH of the isoelectric point of the prepared carbon composite was estimated by adding 1.0 g of GO-modified carbon composite to bottles containing 50 mL of 0.1 M potassium nitrate, the pH of which was adjusted at a certain value in the range of 2.0–12.0 using the hydrochloric acid and sodium hydroxide. The mixture was agitated by the magnetic stirrer for 48 h. Then, the final pH of the solution was measured using an 827 Autolab pH meter. The final pH was plotted against the initial pH and a line was also drawn where final pH = initial pH. The intersection point of the final pH-initial pH curve and a line where pH= initial pH was introduced as the pH of the isoelectric point.

2.5. Design of the studies and optimization of dye removal

This study investigated the effect of pH, adsorption time, amount of GO used for fabrication of the carbon composite and amount of the carbon composite used for the RR241 removal, using Design of Expert (DOE) software. Sample size and a number of tests were calculated by response surface method (RSM) using central composite design (CCD). The efficiency of the dye removal was selected as the response in the design of experiments, as shown in Table 1.

Table 1 Experimental range and levels of the independent variables

Parameters	Unit	Symbol	Levels				
			α-	-1	0	1	α
pH	-	X_1	2	4.25	6.5	8.75	11
Time	min	X_2	20	45	70	95	120
GO content	Wt. %	X_3	0.1	1.325	2.55	3.775	5
Adsorbent (GO-CC)	g/L	X_4	0. 1	0.575	1.05	1.575	2

After performing the tests and entering the response values in the software, the optimal model was selected. For data analysis, analysis of variance (ANOVA) was used. lack of fit data (Lack of fit), p value, F-value and R^2 were determined. In analysis of the results, F-value is an index to evaluate the significance of the model. The larger the numerical value, the more significant the model is, and p-value less than 0.05 is approved by model. The response variable was presented as a function of independent variables in the form of the polynomial regression model shown in Equation 3.

$$Y = b_0 + \sum_{i=1}^{n}(b_i X_i) + \sum_{i=1}^{n}\sum_{j=1}^{n}(b_{ij} X_i X_j) + \sum_{i=1}^{n}(b_{ii} X_i^2) \quad \text{(Eq. 3)}$$

In the above equation, Y is the response variable, b0 is the intercept, bi is the regression coefficient calculated from the values obtained from Y and Xi of the levels encoded by the independent variables, the XiXj and Xi2 parts comprise the interaction terms (interaction effect) and the quadratic effect, respectively.

2.6. Studies of the adsorption kinetics and isotherm

In order to study the kinetic behavior of dye adsorption on the proposed carbon composite, solutions with specific concentration of RR241 were prepared at pH = 5.0 and then 147 mg of GO-CC containing 4.15 wt. % of GO was added to them. At intervals of 5-120 min, the residual concentration of RR241 was measured (according to the procedure discussed before).

The equilibrium adsorption behavior of RR241 on the synthesized composite was also fitted to the Langmuir and Freundlich isotherms models. For this experiment, solutions with initial concentrations of 30, 50, 80, 100, 120, and 150 mg/L of the RR241 were prepared at pH = 5.0 and after adding 147 mg of the carbon composite containing 4.15 wt% of GO to them, the solutions were placed on a magnetic stirrer for 75 minutes (equilibrium time). The residual dye concentration in the solution was also determined using spectrophotometry. Langmuir and Freundlich isotherm models were used to analyze the data. The pseudo-first-order and pseudo-second-order kinetics were used to study the kinetics of the adsorption process. The rate constants of adsorption and the isotherms' constants were extracted to interpret the results, capacity, type, and energy of the adsorption process.

2.7. Structural characterization of the adsorbent

The morphology and surface porosity of the prepared carbon composites were studied using a Mira3 XMU model field emission scanning electron microscope (Tescan, Japan). Fourier transform infrared spectrometer (FTIR, Burker Alpha) was used to study the structural groups between composite and dye molecules. In this technique, the resolution of 2 cm-1 is used in the wavelength range of 4000-400 cm-1. The samples were completely powdered using KBr method and were prepared as discs by compression method. The textural properties of the prepared composite including porosity, average volume and pore size were explored with the aid of N2 adsorption/desorption isotherms using a Belsorp analyzer (BEL Japan Inc.) at 77 K. The specific surface area of the composites was also calculated using the Brunauer–Emmett–Teller (BET) method.

3. Results and Discussion

3.1. Characteristics of the suggested carbon composite as adsorbent

3.1.1. Morphology

FESEM images demonstrating the morphologies of the carbon composite before and after the modification with GO are shown in Fig 1 a-b, respectively. As shown in Figure 1, wrinkled GO sheets are present in the carbon composite (b), causing the surface area of the adsorbent, which interacts with the surrounding environment, especially, with the contaminant molecules in the solution, to be increased. This will be shown to be verified by examining the textural properties of both composites. This structure will be very effective in the process of adsorption of dyes from aqueous solutions.
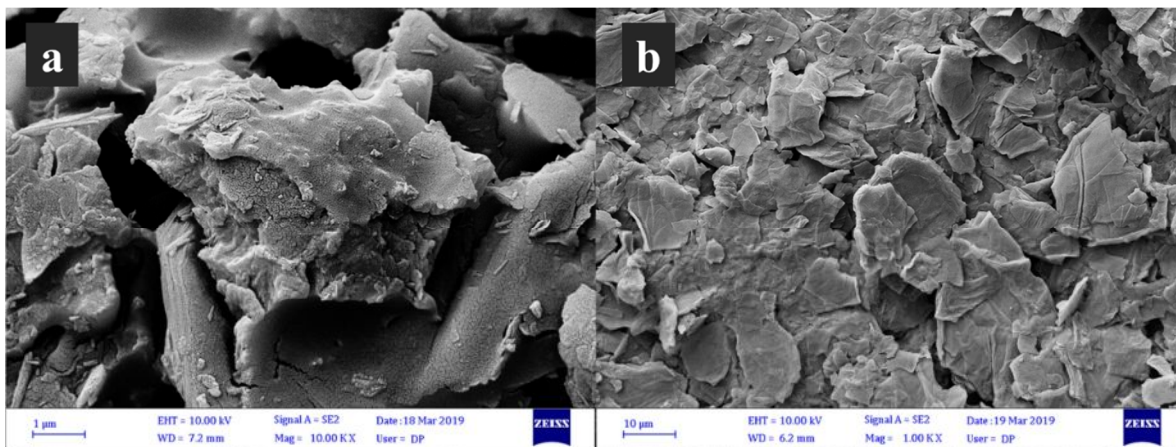

Figure 1. FESEM Images of the carbon composite a) before and b) after the modification with GO.

3.1.2. Potential at isoelectric point

The pH at the isoelectric point of an adsorbent is the point at which the number of positive and negative charges on the surface of the adsorbent are equal. In other words, the pH of the charge on the adsorbent surface is zero, referred to as the adsorbent isoelectric point or pHpzc. At pHs below pHpzc the adsorbent surface has a positive charge and at pHs above pHpzc the adsorbent has a negative charge. To determine this point, curve of the final pH of the solution containing the carbon composite is plotted against the initial pH of the solution, and the pHpzc is determined based on intersection of the curve with the line where final pH = initial pH, see

Figure 2. As shows the intersection point of the two plots is located at 5.7, indicating that the isoelectric point of the proposed adsorbent is 5.7, which is introduced as the potential at the isoelectric point.
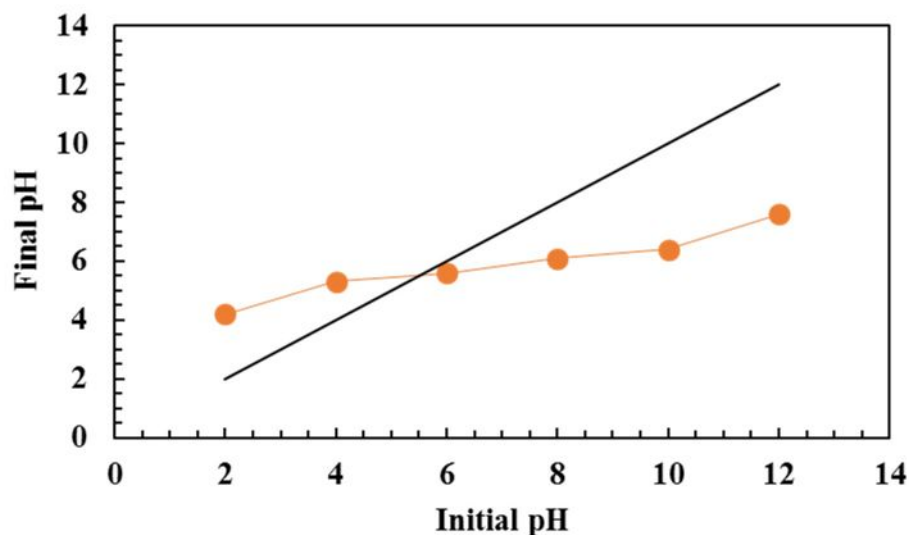

Figure 2. Diagram showing determination of potential at isoelectric point of the proposed adsorbent.

3.1.3. Textural characteristics

Textural characteristics including surface area, pore volume, and average pore size of GO-CC were determined by the BET method and were extracted from nitrogen adsorption-desorption isotherm diagrams (Fig. 3). For better comparison, the graphs of carbon composites without GO (CC) are also presented in the figure. The diagram shows that the presence of GO sheets in the carbon composite's structure amplifies the volumetric pressure of nitrogen gas adsorbed in the relative area of 0.7 to 0.9 with a steep upward slope compared to the unmodified sample. This sudden increase could be due to the capillary density inside the structure of GO-CC.

In addition, the calculations result of specific surface area, pore sizes, and average pore volume using BET are summarized in Table 2. The data in the table show that the texture characteristics of GO-CC are significantly higher than those (CC). The specific surface area and pore diameter of the GO-CC are 7.285 m2/g and 18.156 nm, respectively. However, the values for CC are 1.92 m2/g and 9.67 nm, respectively. The pore volume of GO-CC is about 2.5 times greater than CC. Increasing the pore volume and opening the pore diameter help improve the absorption efficiency of dye molecules on the nanocomposite surface and effectively remove them from aqueous solutions.

The results indicate that the integration of GO sheets with the activated carbon (graphite) and sol-gel process has caused the surface area, overall pore volume, and average composite pore size to be significantly increased. This may point out that the composite surface is more porous. In this way, it can be expected that the nano sheets can be easily separated from the solution by the formation of a porous and bulky composite through the stabilization of GO sheets in the composite matrix.
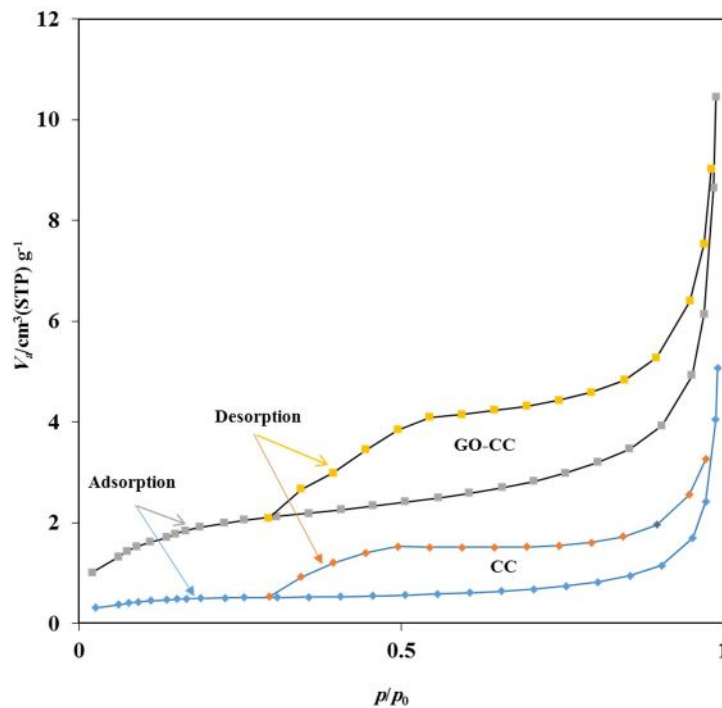
Figure 3. Nitrogen adsorption/desorption plot at 77.4 K for CC and GO-CC.

Table 2 Textural properties obtained by N_2 adsorption/desorption studies.

Parameters	Technique	CC	GO-CC
BET surface area (m2/g)	BET a	1.92	7.825
Pore volume (cm³/g)	BJH adsorption [b]	0.007	0.017
Pore diameter (nm)	BJH adsorption	9.671	18.156

a Computed in the P/P_0 range of 0.05–0.50.
b BJH (Barrett Joyner Halenda) cumulative adsorption pore volume for pores having diameter in range of 0 and 50.0 Å.

3.1.4. FTIR Study

Figure 4 displays the FTIR spectra of GO-CC in the wavenumber range of the 4000-400 cm⁻¹ before (curve A) and after absorption of RR241 (curve B), respectively. As can be seen, the functional groups present on GO-CC surface include OH groups with their characteristic absorption band at 3406 cm⁻¹ and stretching of epoxy group (C–O–C) showing absorption peak at 1151 cm⁻¹ [37,38].

In spectra B, which is related to the composite after contact with the dye, in addition to the characteristic peaks of the intact composite, new peaks have emerged that are likely correspond to RR241 functional groups. These peaks occurred at 1768 cm⁻¹ belonging to stretching of C=O group, 1598 cm⁻¹ for bending of N-H bond, 1498 cm⁻¹ for stretching of N-O bond, 1417 cm⁻¹ related to stretching of C-C bond in the aromatic ring, 1338 cm⁻¹ for stretching of C-N and 771 cm⁻¹ belonging to C-Cl group pertinent to the phenyl ring. The presence of

these peaks confirms the presence of azo dye on the surface of the carbon composite matrix after contact with the dye solution.
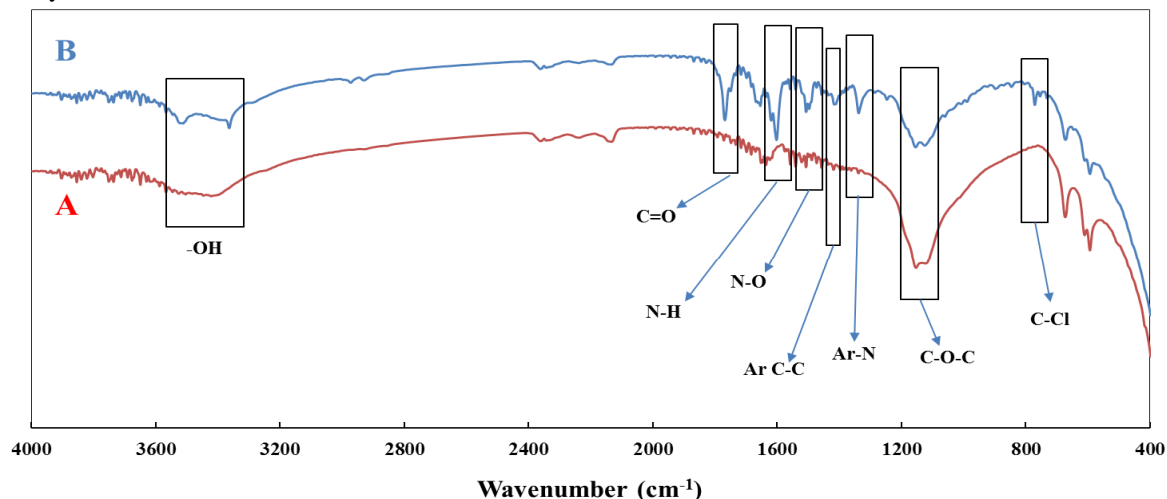

Figure 4- FTIR spectrums for GO-CC before (A) and After (B) adsorption of RR241.

3.2. Efficiency of GO-CC in RR241 dye removal

The efficiency of the GO-modified carbon composite in the removal of RR241 azo dye from its aqueous solutions was assessed by the central composite design route as a proper subset of RSM. The effects of pH, adsorption time, GO content in the composite and the adsorbent dose were investigated. The tests designed to optimize the removal conditions along with their responses are given in Table 3.

3.2.1. Statistical Findings

A quadratic model was achieved by prediction of the efficiency of RR241 removal using the response surface statistical method and Equation 6, which shows the empirical relationship between the selected variables and removal efficiency.

Re (%) = -118.446 + 29.6 X_1+ 1.09 X_2 +25.28 X_3 + 50.91 X_4 +1.90 X_3X_4 -2.12X_1^2 -4.37X_3^2 -

19.74X_4^2 (Eq . 6)

According to the results of the normal Probability of Internally Studentized Residuals (Figure 5), the model covers satisfactorily the ANOVA data. The residual values indicate the normal distribution of the operational variables near the mean values. Therefore, the regression model can be used to predict the removal efficiency of RR241 in the adsorption process. Figure 6 also shows the agreement between the experimental and the predicted values.

Table 3. Operational parameters and efficacy of dye removal after different runs.

| Run	X_1: pH	X_2: Time (min)	X_3: GO content (%wt)	X_4: Adsorbent (GO-CC) (g/L)	Y: Re (%)
1	6.5	70	2.55	1.05	82.75
2	4.25	45	1.325	0.575	49.88
3	6.5	120	2.55	1.05	70.55
4	8.75	45	1.325	0.575	60.42
5	8.75	45	3.775	0.575	61.46
6	6.5	70	2.55	0.1	62.66
7	6.5	70	2.55	1.05	87.98
8	6.5	70	2.55	2	64.93
9	4.25	95	1.325	1.525	62.07
10	8.75	95	3.775	1.525	70.89
11	8.75	95	1.325	1.525	72.80
12	4.25	95	1.325	0.575	55.18
13	8.75	95	3.775	0.575	62.14
14	4.25	45	3.775	1.525	67.98
15	6.5	20	2.55	1.05	61.85
16	8.75	45	1.325	1.525	63.22
17	11	70	2.55	1.05	36.52
18	4.25	45	3.775	0.575	52.84
19	6.5	70	0.1	1.05	49.26
20	4.25	45	1.325	1.525	62.56
21	6.5	70	5	1.05	61.46
22	6.5	70	2.55	1.05	88.09
23	8.75	45	3.775	1.525	77.31
24	4.25	95	3.775	1.525	68.65
25	2	70	2.55	1.05	40.57
26	8.75	95	1.325	0.575	62.62
27	6.5	70	2.55	1.05	96.10
28	6.5	70	2.55	1.05	80.42
29	4.25	95	3.775	0.575	58.10
30	6.5	70	2.55	1.05	82.5
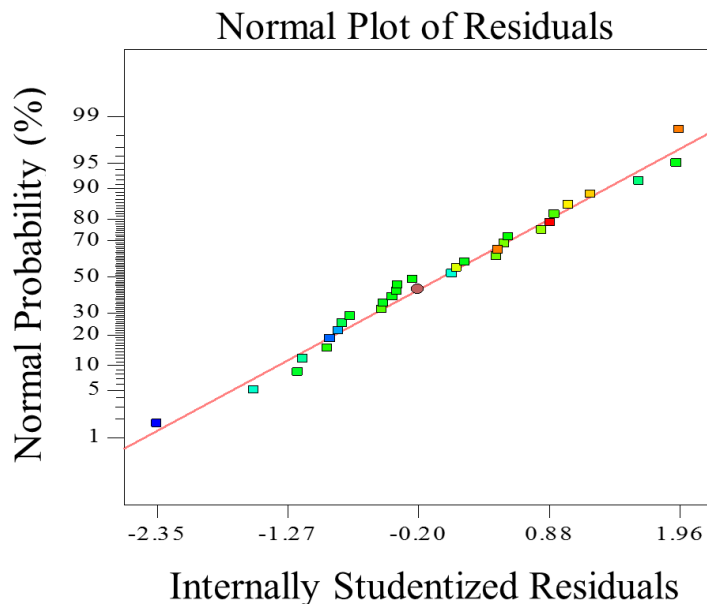
Figure 5. Normal probability distribution for residues of the RR241 removal by GO-CC.
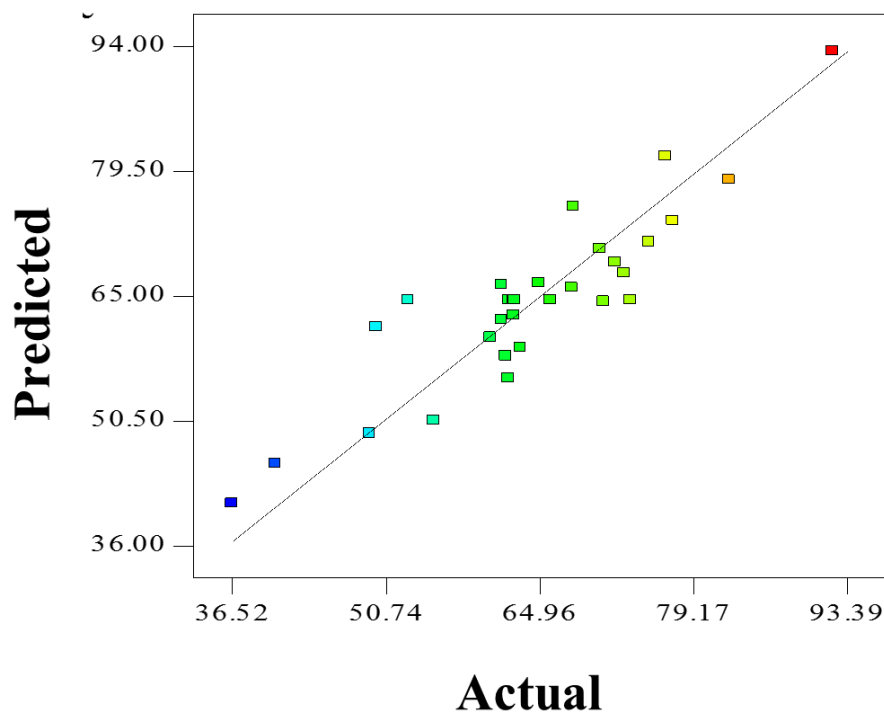

Figure 6. Relationship between experimental and predicted data (by RSM) of removal the RR241

using GO-CC.

The validity of the presented model was assessed by ANOVA (Table 4). Analysis of variance obtained from RSM for the adsorption process of RR241 by the proposed composite adsorbent shows that the parameters, pH (X_1), adsorption time (X_2), GO content in the composite (X_3), and the amount of adsorbent (X_4) as well as the interaction effect of pH and the adsorbent (X_1X_4), GO content and adsorbent (X_3X_4), X_1^2, X_3^2, and X_4^2 had significant effects on the removal efficiency.

The predicted R-value of 0.89 has reasonable conformity with the adjusted R^2 (0.932). Adeq adjusted measures noise, desirable values of which are more than 4. In this study, it was 9.61, which indicates a sufficient signal. Hence, this quadratic model can be used as a suitable spatial model for designing and optimizing the operational parameters.

Table 4. Analysis of variance of the data obtained from RSM for the adsorption process of RR241 dye by the composite adsorbent.

Source	Sum of Squares	df	Mean Square	F Value	p-value Prob > F	
Model	4725.29	14	337.52	5.098	< 0.0001	Significant
X1-pH	561.68	1	561.68	6.81	0.1980	
X2-time	524.12	1	524.12	6.02	0.3276	
X3-GO ratio	601.63	1	601.63	7.65	0.1241	
X4-absorbent	793.70	1	793.70	11.69	< 0.0001	
X1X2	476.83	1	476.83	5.29	0.8664	
X1X3	477.08	1	477.08	5.34	0.8548	
X1X4	479.14	1	479.14	5.77	0.7841	
X2X3	492.22	1	492.22	5.35	0.5612	
X2X4	481.81	1	481.81	5.13	0.7194	
X3X4	495.08	1	495.08	5.41	0.5300	
X1^2	3655.98	1	3655.98	71.89	< 0.0001	
X2^2	882.82	1	882.82	13.56	0.0104	
X3^2	1657.27	1	1657.27	29.85	< 0.0001	
X4^2	1019.69	1	1019.6	16.44	< 0.0001	
Residual	713.24	15	47.54			
Lack of Fit	549.4694	10	54.94694	1.67	0.2956	not significant
Pure Error	163.771	5	32.7542			
Cor Total	5438.536	29				

3.2.2. Effect of the variables on azo dye removal

The data presented in Table 4 and equation 4 indicate that amount of the carbon composite (X_4) had the most effect on the removal process (coefficient of 50.91 and F value of 11.69) and adsorption time (X_2) had the least effect compared to the other parameters (coefficient of 1.09 and F value of 6.02). The effects of independent variables on azo dye removal efficiency are illustrated in 3D plots of the response surface in Figure 7. In these diagrams, each factor except those involved in plots is fixed at a given value.

Figure 7a shows the effect of the amount of carbon composite as adsorbent, and pH of the solution on removal efficiency, while the time and GO content of the composite were assumed to be constant at 66 min and 4.0 wt%,

respectively. As the 3D plots show, the best efficiency was obtained at pH of 6.5 and the efficiency diminishes at a pH above and below it. The removal efficiency improves by increasing the amount of the composite adsorbent to the optimum amounts by increasing the amount of adsorbent from 0.1 g/L to 1.5 g /L, the removal efficiency amplifies from 30% to more than 80%.

The pH of solution is one of the contributing factors in the adsorption processes. Due to the presence of negative and positive species (OH⁻ and H⁺) in the solution, pH changes can affect the adsorbent surface charge, the degree of ionization of various pollutants, the dissociation of functional groups on the active sites of the adsorbent and the structure of the dye molecule. Indeed, the solution pH affects the chemistry of the aquatic environment and the adsorbent surface groups.

The pHpzc of the adsorbent (GO-CC) was obtained to be 5.7 (see section 3.1.2); this means that the adsorbent surface is negatively charged at higher pH values, and at pH values below 5.7 the adsorbent surface charge is positive. Consequently, it is expected that at pH values below 5.7, the removal rate is upward, since in this range the opposite charges reach their maximum value and electrostatic attraction occurs between the adsorbent surface and dye molecules.

According to the findings of this study, amount of the carbon composite (or adsorbent dose) was the most contributing factor affecting removal efficiency. The effect of adsorbent mass is one of the most critical issues on the adsorption processes. According to the obtained results, removal efficiency improves with increasing adsorbent dose at constant concentration of RR241 dye. It can be stated that at a constant concentration of dye, as the adsorbent dose increases, the ratio of active sites present on the adsorbent surface to the number of RR241 molecules grows, resulting in enhancement of the removal efficiency. Whereas at low adsorbent amounts, the ratio of active sites to the adsorbed material molecules is low and consequently, the adsorption efficiency is little. But the interesting point is that by increasing the adsorbent dose beyond its optimum value, the adsorption capacity decreases from its maximum value. As the total number of active sites available at the adsorbent is proportional to the adsorbent dose, all active sites available on the adsorbent are not fully utilized in this condition, thus reducing the absorption capacity. This phenomenon can be attributed to the use of the available surface in the unsaturated form of the adsorbent.

The effects of time and the GO content of the carbon composite on the removal efficiency are shown in Figure 7b using a 3D graph of the response surface. As the graph shows, the removal efficieny increases with the elevation of GO content in the carbon composite matrix, so the removal efficiency increases from 30% to more than 78 % when the GO grows from 0.1 wt% to 3.8 wt%. If the GO content is kept in the same range and the time reaches 80 minutes, the removal efficiency is 84%.

An important issue when applying the adsorption system is to provide an effective contact time under certain conditions. However, in this study, based on the analysis of variance; time had the least effect on the proposed model.

For the concentration of 1.0 mM of the RR241, the adsorption process reaches equilibrium at 80 minutes and then exhibits a relatively constant trend. The effect of the contact time can be interpreted as the enhancement of the probability of collision of the contaminant molecules with the adsorbent surface by expansion of the contact time, and, as a result, the removal efficiency rises, and the amount of the dye residue in the solution diminishes.

Chemical properties as well as the high contact surface area (in other words, the surface-to-volume ratio) of GO has made this organic compound a suitable option for the removal of toxic, metallic species and pharmaceutical compounds. Ideally, GO has a completely two-dimensional structure, which is a monolayer nanostructure of carbon atoms bonded by covalent bonds, so that forms a perfectly flat honeycomb network [38]. In this carbon network, carbon atoms with hybridization of SP^2 form a two-dimensional plate with hydroxyl and epoxy groups being located on the carbon plate while carboxylic acid groups locating on the edges [40]. The presence of COOH and OH functional groups on GO sheet causes the contaminants to bond to the surface of the sheet by forming Van der Waals or electrostatic forces. However, in surface adsorption

applications, separation of the GO after the binding of the contaminants is difficult. In this study, two-dimensional GO sheets were incorporated into the carbon composite matrix through the sol-gel process, which allows it to be separated from the solution by filtration using Whatman 42D filter paper.
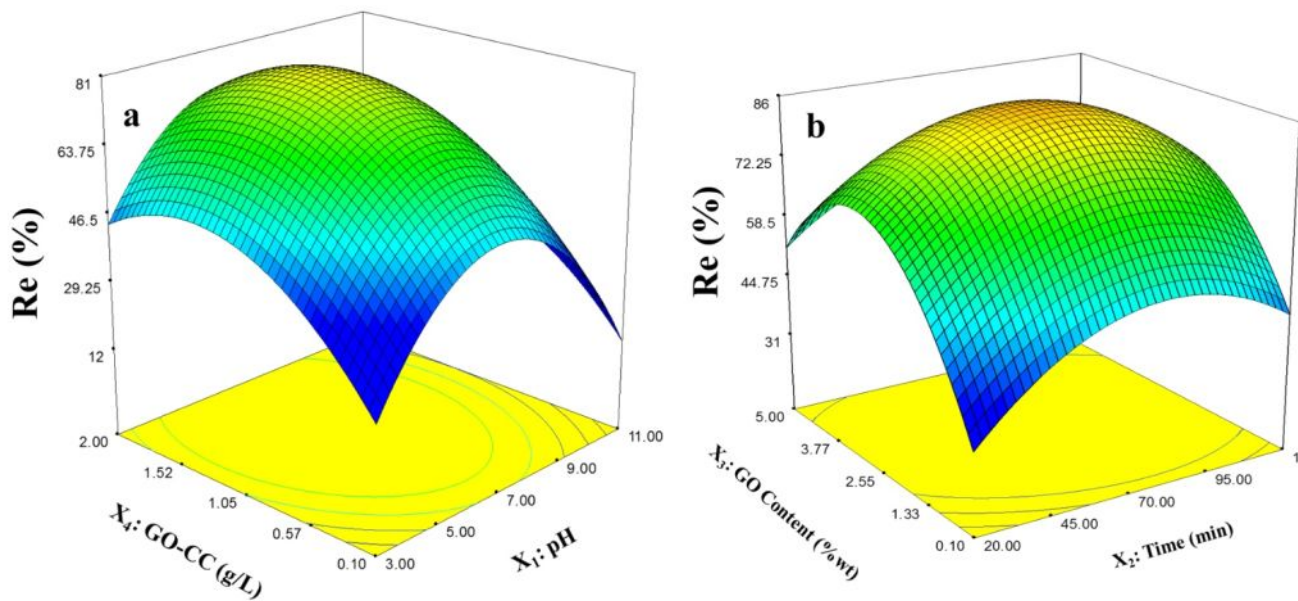

Figure 7- 3D surface plot for interaction effect of a) the pH and the adsorbent dose at constant adsorption time of 65 min and GO content of 4. 0 wt %. B) GO content and adsorption time at of pH 5.8 and adsorbent dose of 1.3 g/L.

Figure 7b shows that augmentation of GO content in the carbon composite improves the dye removal efficiency. This can be attributed to the increase in the available surface area, porosity, and the carbon composite pores due to the presence of GO, which was already mentioned in the study of the textural properties of the composite. Increment in the GO content can raise the pore diameter, increase the pore volume and improve the adsorbent surface area.

3.2.3 Optimization of the dye removal by GO-CC

The objective of optimization is to find a combination of variables that maximize removal. The RSM determines the best values for the process of variables, including pH, adsorption time, GO content and adsorbent dose. It is expected that this situation is considered as the best available conditions.

In DOE software, the desirability coefficient was chosen equal to 1 for maximum removal efficiency. As a result, 97% efficiency for RR241 removal was predicted by the model under optimal conditions as: pH of 5.0, adsorption time of 75 min, GO content of 4.15 wt. % and the adsorbent dose of 1.47 g/L.

3.3 Adsorption Kinetics

A study of the adsorption kinetics is suitable for the prediction of the adsorption rate and demonstration of the adsorption capacity over time and the type of adsorption mechanism. Hence, kinetic equations are used to describe the transfer behavior of the molecules adsorbed per unit time as well as to investigate the variables affecting the reaction rate. Two kinetic models of pseudo-first and second-order kinetic models were used to evaluate the kinetics of the dye adsorption. The pseudo-first-order kinetic model states that the diffusion process controls the reaction rate, while the pseudo-second-order kinetics states that the chemical absorption is the deceleration step of the reaction. Equations 7 and 8 give the pseudo-first-order and second-order kinetics, respectively:

$$\log(q_e - q_t) = \log q_e - \frac{k_1}{2.303} t \qquad \text{(Eq. 7)}$$

$$\frac{t}{q_t} = \frac{1}{k_2 q_e^2} + \frac{1}{q_e} t \qquad \text{(Eq. 8)}$$

In the above equations, q_e, q_t, k_1, and k_2 represent the equilibrium adsorption capacity (mg /g), the adsorption capacity (mg/g) at time t, the pseudo-first-rate constant, and the pseudo-second-order constant, respectively. Figure 8 shows the curves for the pseudo-first and second-order kinetics of RR241 adsorption. The obtained kinetic data are also summarized in Table 5.
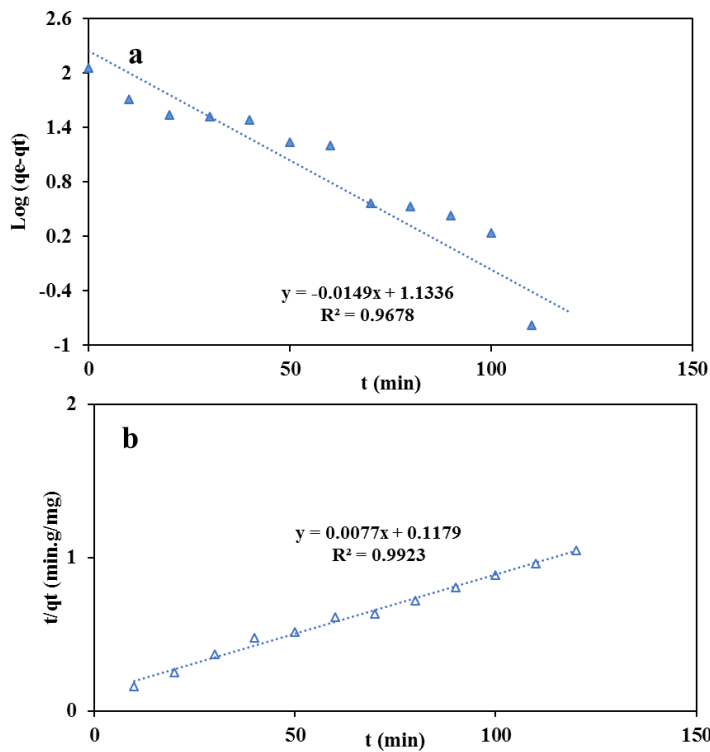

Figure 8. Kinetic plots for RR241 adsorption on GO-CC according to a) Pseudo-First-order and b) Pseudo-second-order models.

Table 5. Kinetic parameters for RR241 adsorption from aqueous using GO-CC at initial concentration of 100 mg/L.

Kinetic Model					
Pseudo-First-order			Pseudo-second-order		
K_1 (min^{-1})	q_e	R^2	K_2 (min^{-1})	q_e	R^2
0.034	21.67	0.9678	5.03	129.8	0.9923

A comparison of the coefficients shows that the pseudo-second-order kinetic model ($R^2 = 0.9923$) is more consistent and better suited to describe RR241 adsorption than the pseudo-first model ($R^2 = 0.9678$). The pseudo-second kinetics model shows that the adsorption rate is controlled by chemical bonding and the adsorption capacity is proportional to the active sites of the adsorbent [41]. In other words, the equation of the pseudo-second-order kinetics is chemical adsorption, and the adsorption process is slowed down because chemical adsorption is based on the adsorption of the solid phase. The pseudo-first-order kinetic equation is based on the adsorption capacity. If the adsorption process is restricted as a reversible process through the adsorbent boundary layer, the process follows the pseudo-first-order kinetic model. However, different mechanisms are involved in the adsorption process, including electrostatic and chemical interactions between active adsorption sites and pollutants [41]. The pseudo-first-order kinetic model indicates that the bonds depend on the reaction rate at concentrations or different pressures between the contaminant and the adsorbent surface. Wang et al. developed a GO doped with porous chitosan as an adsorbent to remove the methyl orange. The results showed that the adsorption process is well suited to pseudo-quadratic kinetics [42].

3.4 adsorption isotherm

Adsorption isotherms are equations to describe the equilibrium between the adsorbent and the pollutant. The most common models describing surface adsorption are the Langmuir and Freundlich models. The linear form of Freundlich and Langmuir isothermal models are expressed by Equations 9 and 10, respectively [43].

$$\ln q_e = \frac{1}{n} \ln C_e + \ln K_F \qquad \text{(Eq. 9)}$$

$$\frac{1}{q_e} = \frac{1}{C_e K_L q_m} + \frac{1}{q_m} \qquad \text{(Eq. 10)}$$

Where, q_e refers to amount of dye absorbed per unit mass of adsorbent at equilibrium (mg/g), C_e is dye equilibrium concentration (mg/L), K_F and n, reflect the intensity and capacity of adsorption, respectively. Also, in Langmuir equation, the q_m, adsorption capacity (mg/g), and b as the Langmuir constant represent the adsorption energy.

The isotherms diagram of Langmuir and Freundlich for the adsorption of RR241 using GO-CC is shown in Fig. 9. The values of the constants of Langmuir and Freundlich models with their correlation coefficients are presented in Table 7. Assessing the adsorption isotherms diagrams and comparison of correlation coefficients obtained from the two models express that the adsorption of RR241 on the modified carbon composite well fitted by the Langmuir model. Therefore, it can be said that the adsorption process of RR241 on the composite is monolayer and the maximum adsorption capacity is 160 mg/g.
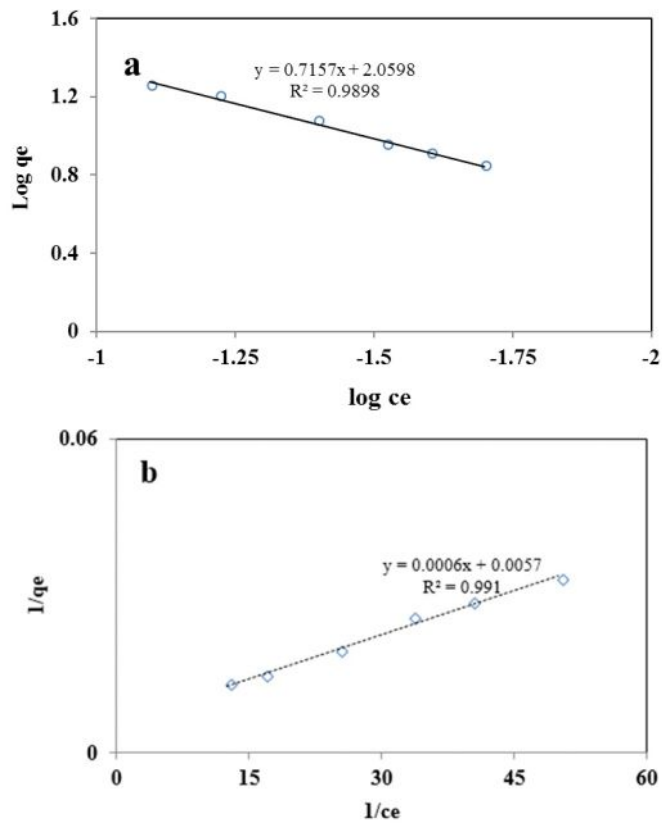
Figure 9- Fitting of RR241 adsorption on GO- carbon composite with a) Freundlich and b) Langmuir isotherm.

Table 7 - Freundlich and Langmuir constants for adsorption of RR241 onto GO-CC.

Isotherm model	Parameters	
Freundlich	K_F	7.85
	$1/n$	0.716
	R^2	0.9898
Langmuir	q_{max}	160
	K_L	9.52
	R^2	0.991

In the Freundlich isotherm, as K_F increases, the adsorption capacity for the adsorbent for adsorbing the adsorbed material increases, and so *n* value between 1 and 10 represents the appropriate adsorption process. If the value of n is close to 1, the heterogeneity of the surface becomes less important and if it is close to 10, it becomes more important. The relevant parameters and coefficients are summarized in Table 7. In this study the

calculated value of K_F is 7.85, and the numerical value of n is 1.40, which is between the specified intervals. Therefore, the adsorption process of RR241 dye on the adsorbent is suitable.

3.5 Thermodynamics of the adsorption

Thermodynamic parameters comprising enthalpy change ($\Delta H°$), entropy change ($\Delta S°$), and Gibbs free energy change ($\Delta G°$) of RR241 adsorption are dependent on the coefficient of distribution of the adsorbed material between the solid and liquid phases. The thermodynamic parameters are expressed using Equations 11-13 [44-45]:

$$K_d = \frac{q_e}{C_e} \qquad \text{(Eq. 11)}$$

$$\Delta G^0 = -RT \, Ln \, K_d \qquad \text{(Eq. 12)}$$

$$Ln \, K_d = \left(\frac{\Delta S^0}{R}\right) - \left(\frac{\Delta H^0}{RT}\right) \qquad \text{(Eq. 13)}$$

In these equations, K_d, R, and T are the distribution coefficients, the universal gas constant (8.314 J/molK), and the absolute temperature in K, respectively. The values of $\Delta H°$ and $\Delta S°$ are obtained from the slope and intercept of the linear plot of $Ln K_d$ versus $1/T$.

The results of the effect of temperature on the removal process of RR241 are illustrated in Table 8 and Figure 10. The negative values of the $\Delta H°$ indicates that the adsorption process is exothermic and the dye removal rate decreases with increasing ambient temperature. The negative value of $\Delta G°$ also indicates the feasibility and spontaneity of the process. The negative $\Delta S°$ values also indicate that the adsorption rate on the solid-liquid interface decrease during the adsorption process.

Table 8 - Thermodynamic parameters for the adsorption of RR241 by GO-CC.

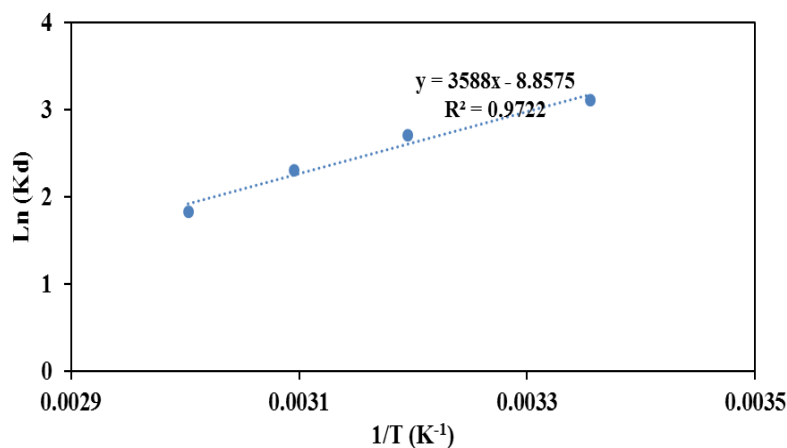| C_e (ppm)	$\Delta H°$	$\Delta S°$	$\Delta G°$ (kJ/mol)			
	(kJ/mol)	(kJ/molK)	298	308	318	328
200	- 29.830	- 0.0736	-7.714	-7.047	-6.183	-5.073

Figure 10- Thermodynamic Model of RR241 Adsorption on GO-CC.

4. Conclusion

The modified carbon composites with GO (GO-CC) were synthesized using sol-gel method. The structure and morphology properties of the prepared composites were investigated by BET, FTIR and SEM techniques. The prepared composites were used as an effective adsorbent for the removal of RR241 dye from aqueous solutions. The effect of different operational factors including pH, amount of GO in fabrication of the composite, amount of composite as adsorbent and the contact time were investigated by the response surface methodology. The removal experiments showed that the amount of the adsorbent, GO content and pH had a significant effect on RR241 removal. BET analysis indicated that the addition of GO to the carbon composite structure improved the pore size, total pore volume, and effective surface area of the composite. Also, isotherms, kinetics, and thermodynamic studies of adsorption were depicted that Langmuir isotherm model, pseudo-second-order kinetic model and self-adsorption are suitable models for RR241dye adsorption.

Acknowledgements

References

[1] Ma, B., Hauer, R. J., & Xu, C. (2020). Effects of design proportion and distribution of color in urban and suburban green space planning to visual aesthetics quality. Forests, 11(3), 278.

[2] Tamburini, D., Cartwright, C. R., Di Crescenzo, M. M., & Rayner, G. (2019). Scientific characterization of the dyes, pigments, fibres and wood used in the production of bark cloth from Pacific islands. Archaeological and Anthropological Sciences, 11(7), 3121-3141.

[3] Haji, A., & Naebe, M. (2020). Cleaner dyeing of textiles using plasma treatment and natural dyes: A review. Journal of Cleaner Production, 121866.

[4] Kabir, S. M. M., & Koh, J. (2018). Dyeing Chemicals. In Chemistry and Technology of Natural and Synthetic Dyes and Pigments. IntechOpen.

[5] Nambela, L., Haule, L. V., Mgani, Q. (2020). A review on source, chemistry, green synthesis and application of textile colorants. Journal of Cleaner Production, 246, 119036.

[6] Abdou, M. M. (2013). Thiophene-based azo dyes and their applications in dyes chemistry. American Journal of Chemistry, 3(5), 126-135.

[7] Ilyas, M., Ahmad, W., Khan, H., Yousaf, S., Yasir, M., & Khan, A. (2019). Environmental and health impacts of industrial wastewater effluents in Pakistan: a review. Reviews on environmental health, 34(2), 171-186.

[8] Colombetti, P., Calderon, M., Tello, J., González, P., & Jofré, M. (2020). Relationships between aquatic invertebrate assemblages and environmental quality on saline wetlands of an arid environment. Journal of Arid Environments, 181, 104245.

[9] Guadie, A., Yesigat, A., Gatew, S., Worku, A., Liu, W., Minale, M., & Wang, A. (2021). Effluent quality and reuse potential of urban wastewater treated with aerobic-anoxic system: A practical illustration for

environmental contamination and human health risk assessment. Journal of Water Process Engineering, 40, 101891.

[10] Lin J, Su T, Chen J, Xue T, Yang S, Guo P, Lin H, Wang H, Hong Y, Su Y, Peng L, Li J. Efficient adsorption removal of anionic dyes by an imidazolium-based mesoporous poly(ionic liquid) including the continuous column adsorption-desorption process, Chemosphere 2021; 272.

[11] Pai S, Kini MS, Selvaraj R. A review on adsorptive removal of dyes from wastewater by hydroxyapatite nanocomposites. Environ Sci Pollut Res 2021; 28: 11835–11849.

[12] Guo J, Yang Q, Meng QW, Lau C H, Ge Q. Membrane Surface Functionalization with Imidazole Derivatives to Benefit Dye Removal and Fouling Resistance in Forward Osmosis. ACS Appl Mater Interfaces 2021; 13 (5): 6710–6719.

[13] Moradihamedani P. Recent advances in dye removal from wastewater by membrane technology: a review. Polym Bull 2021.

[14] Mcyotto F, Wei Q, Macharia DK., Huang M, Shen C, Chow CWK. Effect of dye structure on color removal efficiency by coagulation. Chem Eng J 2021; 405: 126674.

[15] Bustos-Terrones Y A, Hermosillo-Nevárez JJ, Ramírez-Pereda B, Vaca M, Rangel-Peraza J G, Bustos-Terrones V, Rojas-Valencia MN. Removal of BB9 textile dye by biological, physical, chemical, and electrochemical treatments. J Taiwan Inst Chem E 2021; 121: 29-37.

[16] Kubra K T, Salman MSH, M Nazmul. Enhanced toxic dye removal from wastewater using biodegradable polymeric natural adsorbent. J Mol Liq 2021; 328: 115468

[17] Ata R and Tore GY. Characterization and removal of antibiotic residues by NFC-doped photocatalytic oxidation from domestic and industrial secondary treated wastewaters in Meric-Ergene Basin and reuse assessment for irrigation. J Environ Manage 233: 673-80 (2019).

[18] Kumari S, Khan AA, Chowdhury A, Bhakta AK, Mekhalif Z and Hussain S. Efficient and highly selective adsorption of cationic dyes and removal of ciprofloxacin antibiotic by surface modified nickel sulfide nanomaterials: Kinetics, isotherm and adsorption mechanism. Colloids Surf A Physicochem Eng Asp 586: 124264 (2020).

[19] Peng W, Li H, Liu Y and Song S. A review on heavy metal ions adsorption from water by graphene oxide and its composites. J Mol Liq 230: 496-504 (2017).

[20] Ahmad H, Fan M and Hui D. Graphene oxide incorporated functional materials: A review. Compos B Eng 145:270-280 (2018).

[21] Katsnelson MI. Graphene: carbon in two dimensions. Mater Today 10 (1–2): 20-27(2007).

[22] Cao G. Atomistic Studies of Mechanical Properties of Graphene. Polymers 6: 2404-2432 (2014).

[23] Sherlala AIA, Raman AAA, Bello MM and Asghar A. A review of the applications of organo-functionalized magnetic GO nanocomposites for heavy metal adsorption, Chemosphere 193: 1004-1017 (2018).

[24] Fraga TJ, Carvalho MN, Ghislandi MG and Motta Sobrinho MA. Functionalized graphene-based materials as innovative adsorbents of organic pollutants: A concise overview. Braz J Chem Eng 36(1): 1-31 (2019).

[25] Bhattacharyya A, Ghorai S, Rana D, Roy I, Sarkar G, Saha NR, Orasugh JT, De S, Sadhukhan S, Chattopadhyay D. Design of an efficient and selective adsorbent of cationic dye through activated carbon - graphene oxide nanocomposite: Study on mechanism and synergy. Mater Chem Phys 260: 1-10 (2021).

[26] Martins JT, Guimaraes CH, Silva PM, Oliveira RL, Prediger P. Enhanced removal of basic dye using carbon nitride/graphene oxide nanocomposites as adsorbents: high performance, recycling, and mechanism. Environ Sci Pollut Res 28, 3386–3405 (2021).

[27] Cao M, Shen Y, Yan Z, Wei Q, Jiao T, Shen Y, Han Y, Wang Y, Wang S, Xia Y, Yue T. Extraction-like removal of organic dyes from polluted water by the graphene oxide/PNIPAM composite system, Chem Eng J 405: 126647 (2021)

[28] Rostamian M, Hosseini H, Fakhri V, Yousefi Talouki P, Farahani M, Jalali Gharehtzpeh A, Goodarzi V, Su CH. Introducing a bio sorbent for removal of methylene blue dye based on flexible poly (glycerol sebacate)/chitosan/graphene oxide ecofriendly nanocomposites. Chemosphere 289:133219 (2022).

[29] Jafari S, Dehghani M, Nasirizadeh N and Azimzadeh M. An azithromycin electrochemical sensor based on an aniline MIP film electropolymerized on a gold nanourchins/graphene oxide modified glassy carbon electrode. J Electroanal Chem 829: 27-34 (2018).

[30] Aghili Z, Nasirizadeh N, Divsalar A, Shoeibi S and Yaghmaei P. A nanobiosensor composed of exfoliated graphene oxide and gold nano-urchins, for detection of GMO products. Biosens Bioelectron 95:72-80 (2017).

[31] Dehghani M, Nasirizadeh N and Yazdanshenas ME. Determination of cefixime using a novel electrochemical sensor produced with gold nanowires/graphene oxide/electropolymerized molecular imprinted polymer. Mater Sci Eng C 96:654-660 (2019).

[32] Seifati SM, Nasirizadeh N and Azimzadeh M. Nano-biosensor based on reduced graphene oxide and gold nanoparticles, for detection of phenylketonuria-associated DNA mutation. IET Nanobiotechnol. 12(4):417-422 (2017).

[33] Jafari S, Dehghani M, Nasirizadeh N, Baghersad MH and Azimzadeh M. Label-free electrochemical detection of Cloxacillin antibiotic in milk samples based on molecularly imprinted polymer and graphene oxide-gold nanocomposite. Measurement. 145:22-29 (2019).

[34] Rahman M, Cui D, Zhou S, Zhang A and Chen D. A GO coated gold nanostar based sensing platform for ultrasensitive electrochemical detection of circulating tumor DNA, Anal Methods 12 (2020) 440-447.

[35] Azimzadeh M, Nasirizadeh N, Rahaie M and Naderi-Manesh H. Early detection of Alzheimer's disease using a biosensor based on electrochemically-reduced graphene oxide and gold nanowires for the quantification of serum microRNA-137. RSC Adv 7(88):55709-55719 (2017).

[36] Wang Z, Pakoulev A, Pang Y and Dlott DD. Vibrational substructure in the OH stretching transition of water and HOD. J Physic Chem A 108(42):9054-9063 (2004).

[37] Hosseinzadeh M. sorption of lead ion from aqueous solution by carboxylic acid groups containing adsorbent polymer. J Chil Chem Soc 64(2): 4466-4470 (2019).

[38] Monji P, Jahanmardi R and Mehranpour M. Preparation of melamine-grafted graphene oxide and evaluation of its efficacy as a flame retardant additive for polypropylene. Carbon Lett 27:81-89 (2018).

[39] Sangster J. Octanol-water partition coefficients of simple organic compounds. J Phys Chem Ref Data 18(3): 1111-1229 (1989).

[40] Chavoshi N and Jahanmardi R. Chemical functionalization of graphene oxide by a hindered amine stabilizer and evaluation of the product as a UV-stabilizer for polypropylene. Fuller Nanotub Car N 27(1):1-9 (2019).

[41] Tabasideh S, Maleki A, Shahmoradi B, Ghahremani E and McKay G. Sonophotocatalytic degradation of diazinon in aqueous solution using iron-doped TiO2 nanoparticles. Sep Purif Technol 189:186-192 (2017).

[42] Wang Y, Xia G, Wu C, Sun J, Song R and Huang W. Porous chitosan doped with graphene oxide as highly effective adsorbent for methyl orange and amido black 10B. Carbohydr polym 115: 686-693 (2015).

[43] Esfandiyari T, Nasirizadeh N, Dehghani M and Ehrampoosh MH. Graphene oxide based carbon composite as adsorbent for Hg removal: Preparation, characterization, kinetics and isotherm studies. Chin J Chem Eng 25(9):1170-1175 (2017).

[44] Esfandiyari T, Nasirizadeh N, Ehrampoosh MH and Tabatabaee M. Characterization and absorption studies of cationic dye on multi walled carbon nanotube–carbon ceramic composite. J Ind Eng Chem 46:35-43 (2017).

[45] Boukhelkhal A, Benkortbi O and Hamadache M. Use of an anionic surfactant for the sorption of a binary mixture of antibiotics from aqueous solutions. Environ Technol 40(25): 3328-3336 (2019).

Free Chemicals - Sonoelectrochemical Treatment as a Biocompatible Procedure for Decolourization of Anthraquinone Dyes

Atefeh-sadat Rezaei Tousi[a], Mohamad Hasan Ehrampoosh[a][*], M. D. AhmadAbadi[b]

[a] Department of Environmental Health Engineering, Shahid Sadoughi University of Medical Sciences, Yazd, Iran.

[b] Research and Development Centre, Nano Kimia Kavir Yazd Company, Yazd, Iran.

Abstract

Dye compounds are known as one of the most important environmental pollutants. Up to now, several methods have been offered to eliminate these pollutants from industrial wastes, especially in the textile industry. A method that has received a great deal of attention in recent years is the sono-electro-chemical method. In this study, using the Central Composite Design, the interactive effects of four essential variables such as pH, initial dye concentration, time, and applied potential on sonoelectrochemical decolorization of Basic Blue 47 were optimized and investigated. Based on the obtained results in the absence of oxidant agents, the best index for decolorization in optimal conditions includes pH of 9.0, initial dye concentration of 303.3 μM, time of 93 min, and potential of 0.81 V corresponding to the design by the CCD was 98%. It was experimentally found to be 96.0 %, and the Chemical Oxygen Demand (COD) was 97 %.

Keywords: Sonoelectrochemical, Basic Blue 47, Free Chemicals, Degradation.

———————

[*]* Corresponding author. Tel: +9836281788
 *E-mail address: Ehrampoosh@ssu.ac.ir*

1. INTRODUCTION

Textile industries are growing in developing countries. Textile industries are among the largest water-consuming and waste-producing industries [1-2]. In different stages of the textile industry, the dyeing process uses a large amount of water for dyeing, repairing, and washing purposes. The waste produced in textile industries originate from dyeing and supplementary processes and can be a significant threat to the environment. The wastewater with a COD above 1600 mg/L and a high dye concentration is classified as a very potential wastewater [3-4]. Around one million tons of dye are annually produced worldwide, while Azo and Anthraquinone dyes account for 65-75% of the total textile dyes. [5]. In addition, this wastewater contains a complex mixture of pollutants like heavy metals, additives, detergents, and surfactants. The release of these agents in wastewater makes the treatment process more difficult. The discharge of dye wastewater into the environment results in carcinogenicity and mutation due to the presence of toxic elements such as benzidine, naphthalene, and other undesirable aromatic compounds [6-8]. The removal of textile dyes from industry's wastewater before they are discharged into hydrologic systems is of paramount importance because of the complex structure, artificial origin, and the resistant nature of textile dyes [9-10]. There are various processes such as physical [11-12], chemical [13-14], and biological [15-16] methods for decolorizing the textile industry's wastewater. These methods face several limitations because of the presence of resistant organic chemicals in wastewater as well as problems related to costs, productivity, and sludge production. These restrictions can be overcome by advanced oxidation processes [17-21]. One of the most advanced oxidation processes is provided by sonoelectrochemical technology, which is used to decompose and treat dye solutions. In this process, hydroxyl radicals are released as a result of the cavitation phenomenon caused by ultrasonic vibrations inside the liquid at a high temperature and pressure and by the decomposition of compounds [22-23]. This attractive combinatory technology has received lots of attention owing to such advantages as adaptability to the environment, use of clean energy, recovery of heavy metals, treatment of highly toxic wastes, no generation of secondary pollution in the environment, and being more economical [24-25]. Therefore, the sonoelectrochemical decomposition of pollutants is a favorable method for treating industrial wastes particularly the wastes of textile industries [26, 27]. The aim of this study is to evaluate the efficiency of the sonoelectrochemical process in the decomposition of C.I. Basic Blue 47 from aqueous environments without hydrogen peroxide. In this research, the independent variables are solution pH, initial dye concentration, applied potential, and optimized time using the CCD method.
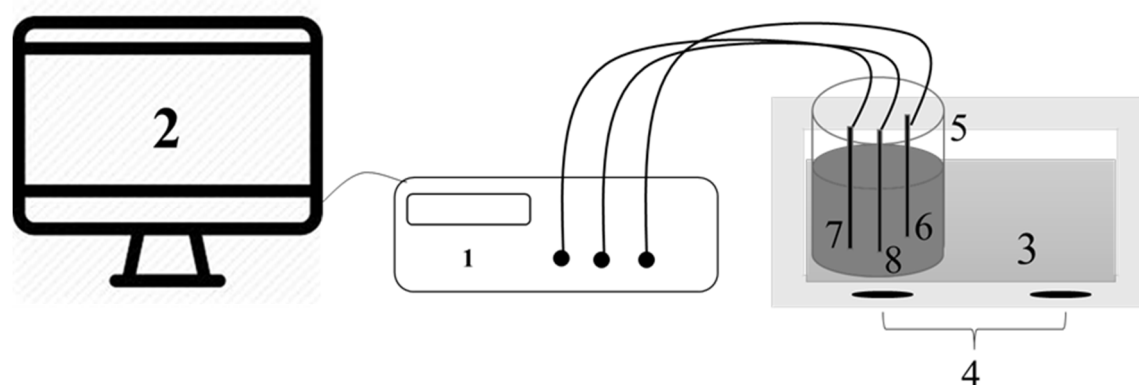
2. EXPERIMENTAL

2.1 Materials and Methods

The C.I. Basic Blue 47 (BB47) dye (Scheme 1) was supplied by the Ciba Company and put to use with no purification. The dye has maximum absorbance (λ_{max}) at 617 nm. The instruments used in this study included a spectrophotometer (UV-Vis- Carry 100 made in Japan), a pH meter of model 876 made by Metrohm, Switzerland, a galvanostat-potentiostat device, a microAutolab from the Netherlands, three-electrode cells including carbon, platinum, and calomel electrodes made by Azar Electrode, Iran, and Euronda S.P.A model 4D (i.e. an ultrasonic generator) made by Vicenza, Italy.

The sonoelectrochemical tests were done in a non-separated electrolyte cell made from a Perix sheet. The working and auxiliary electrodes were placed in the cell vertically and parallel to each other at a distance of 2.5 cm. Carbon electrodes and platinum electrodes were used as working electrodes (anode) and counter electrodes (cathode) respectively. The saturated calomel electrode was used as a reference electrode. (See the setup used for decolorization experiments in Scheme 2).
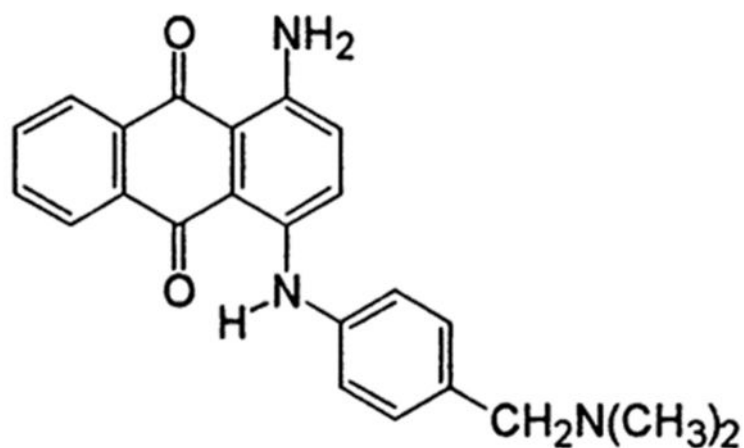
Scheme 1. The Chemical structure of Basic Blue 47.

Scheme 2. Experimental sonoelectrochemical setup used for decolorization. (1) Electro analyzer apparatus; (2) Personal Computer (3) ultrasonic bath; (4) ultrasound Transducer; (5) Pyrex vessel; (6) working electrode (carbon); (7) reference electrode (saturated calomel); (8) auxiliary electrode (platinum plate).

In each experiment 100 mL of a BB47 solution was prepared with different initial concentrations. Various parameters such as the initial pH of the solution, the applied potential, the decolorization time, and the dye solution concentration were optimized simultaneously by the CCD method. At first, using the CCD software, as many as 30 tests were designed based on the four mentioned variables. Table 2 provides the corresponding data. Based on the conditions in Table 2, the decolorization tests were repeated four times, and then the averages from the dye solutions were determined without the presence of oxidants. Thereafter, the value of decolorization was calculated using Eq. (1):

$$\text{Decolorization} = \frac{C_0 - C_t}{C_0} \times 100 \qquad (1)$$

where C_t and C_0 are the concentrations of the dye at the time t and 0 (μM) respectively. It should be noted that the concentration of the remaining dye was calculated through measuring the absorption value at the maximum wavelength (λ_{max}=617 nm) using the spectrophotometer device and a calibration curve. The COD value was determined by the dichromate closed reflux method.

$$\% \text{ COD removal} = \frac{COD_0 - COD_t}{COD_0} \times 100 \qquad (2)$$

where COD_0 and COD_t (in ppm) are the chemical oxygen demand at 0 (the initial time) and t (the reaction time) respectively.

Table 1. The conditions designed for achieving the optimal conditions using the CCD method

Run	pH	[Dye] /μM	Time / min	Applied Potential / V	Decolorization%
1	4.25	752.5	91.25	0.7125	42
2	8.75	752.5	91.25	0.3375	46.46
3	4.25	257.5	33.75	0.7125	40
4	6.5	505	62.5	0.525	58
5	6.5	505	120	0.525	62
6	8.75	257.5	91.25	0.7125	63.06
7	6.5	505	62.5	0.525	54.2
8	6.5	505	62.5	0.525	53.6
9	8.75	752.5	33.75	0.3375	38.99
10	6.5	505	62.5	0.9	59.5
11	6.5	10	62.5	0.525	56.92
12	4.25	752.5	91.25	0.3375	40.12
13	6.5	505	62.5	0.525	52
14	8.75	257.5	33.75	0.7125	51.6
15	4.25	257.5	91.25	0.3375	60
16	4.25	752.5	33.75	0.7125	41.93
17	8.75	752.5	33.75	0.7125	40.33
18	8.75	257.5	33.75	0.3375	50.33
19	4.25	257.5	33.75	0.3375	38.8
20	2	505	62.5	0.525	35.21
21	6.5	505	62.5	0.525	52.65
22	6.5	505	62.5	0.15	53.14
23	8.75	257.5	91.25	0.3375	53.15
24	4.25	752.5	33.75	0.3375	32
25	8.75	752.5	91.25	0.7125	59.21
26	6.5	1000	62.5	0.525	54.95
27	11	505	62.5	0.525	75
28	6.5	505	62.5	0.525	51
29	4.25	257.5	91.25	0.7125	73
30	6.50	505.0	5.0	0.53	35

2.2 Design of the Experiment

With regard to the design of the experiment and the optimization of the dye construction conditions using the sonoelectrochemical system, the simultaneous effects of different factors such as pH, the initial dye concentration, time and the applied potential on the decolorization of BB47 by the CCD and with the help of Design Expert 8.0.2 Software were analyzed. The range and levels of variables are provided in Table 1. Each of the four factors was calculated as 11 according to the alpha value. For this design and based on these four factors, 30 tests were designed. Table 1 provides the conditions of each test. To minimize the variables that were uncontrollable for any reason, the sequence of tests was chosen randomly.

Indeed, to resolve the problem of interaction of different variables and to reduce the cost required for the optimization of conditions for the dye removal, the CCD method was selected. In general, the overall aim of the test design was to determine the effective factors influencing the reaction and their interactions with the minimum number of tests, thereby reporting the best result for achieving the maximum impact factor corresponding with statistical procedures [28].

Table 2. ANOVA results of RSM models provided for decolorization of BB47

Source	Sum of squares	Df	Means square	F value	p-value Prob>F
Model	3802.64	14	271.62	17.58	<0.0001*
A-pH	1.13	1	1.13	0.073	0.073
B-Dye	1.94	1	1.94	0.13	0.7280
C-time	861.13	1	861.13	55.37	<0.0001
D-Potential	170.67	1	170.67	11.04	0.0046
AB	31.92	1	31.92	2.07	0.1712
AC	29.59	1	29.59	1.92	0.1866
BC	72.00	1	72.00	4.66	0.0475
A^2	2.23	1	2.23	0.14	70.94
B^2	0.16	1	0.16	0.010	0.9213
C^2	392.58	1	392.58	25.42	0.0001
ABC	210.83	1	210.83	13.64	0.0022
A^2B	136.76	1	136.76	8.85	0.0094
B^2C	82.64	1	82.64	5.35	0.0354
A^3	319.71	1	319.71	20.69	0.0004
Residual	231.79	15	15.45		
Lack of fit	201.85	10	20.19	3.37	0.0960**
Pure error	29.94	5	5.45		
Cor total	4034.43	29			

* Significant and ** Not significant. The model F-VALUE of 17.58 implies the model is significant. There is only a 0.01% chance that the "model F-VALUE" this large could occur due to noise.

3. RESULTS AND DISCUSSION

3.1. Mathematical Model for Prediction of Decomposition of BB47

The regression model of the coded factors for the performance of the decomposition of BB47 is indicated in Eq. (3), obtained by the CCD method where the coded values of A, B, C, and D are the variables of pH, the dye solution concentration, the time, and the applied potential respectively.

Decolorization % $= +53.26 - 0.38A - 0.49\,B + 10.37\,C + 2.67\,D + 1.41\,AB - 1.36\,AC - 2.12\,AD - 0.28\,A^2 - 0.75\,B^2 - 3.75\,C^2 + 3.63\,ABC - 5.06\,A^2B - 3.94\,B^2C + 2.58\,A^3$ (3)

ANOVA is required for the significance test and the validity of the model provided in Table 1. For ANOVA, an F-value lower than 0.0001 implies significance. According to Table 1, an F-value equal to 17.58 demonstrates that the model is significant. The ability of this model was evaluated by the correlation coefficient of $R^2=0.999$, suggesting that over 99.9% of the sample change was in accordance with the presented model and had an only 0.1% deviation from the total. A value lower than the coefficient of variation (CV%=7.81) implies that the tests are accurate and reliable. "Adeq Precision" measures the signal-to-noise ratio. A ratio larger than 19.607 is desirable.

3.2. The Effect of Independent Variables

Figure 1 illustrates the simultaneous effect of pH and the applied potentials on the decomposition of BB47, using 384.4 µM BB47 and within 71.8 minutes. As it can be seen, as the pH increases from 2.0 to 11.0, the decolorization percentage also improves. Based on the result, it can be suggested that as the solution pH increases, the hydroxyl group (OH⁻) concentration grows gradually. In an alkaline pH, the main anion is OH⁻ which converts into OH• radicals by losing an electron at the anode surface. On the other hand, the presence of ultrasonic waves enhances the migration of hydroxyl anions towards the anode [29]. Therefore, once the pH rises, the number of hydroxyl radicals is increased as the main factor in the dye decomposition.

Figure 1 also shows that when the applied potential increases from 0.15 to 0.71 V, the decolorization rises with fast slope and then continues by gentle slope. It seems that an increase in the voltage is directly related to the further production of hydroxyl radicals. Indeed, the potential and the number of free radicals are tightly correlated [29].
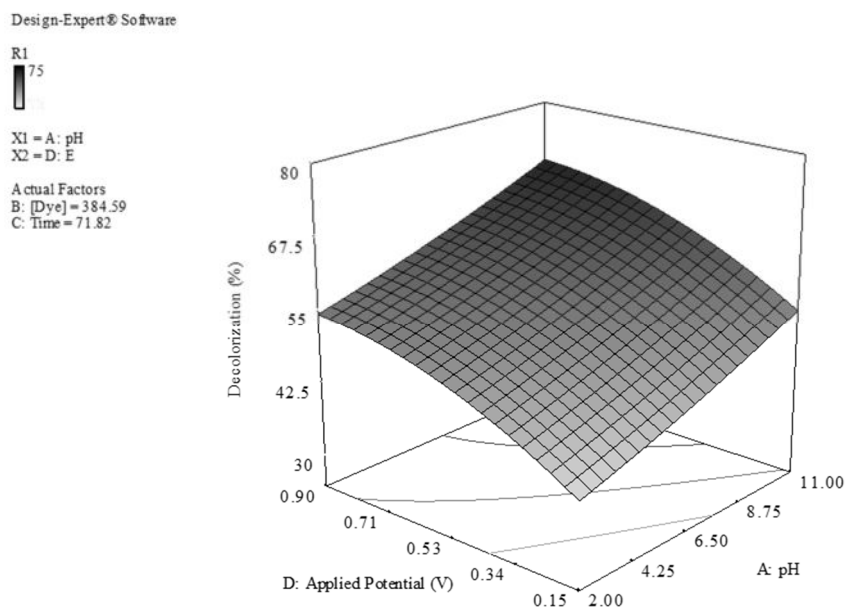
Fig. 1. The 3D ₗ₁ₐgrₐₘ showing the effect of pH and various potentials on decolorization value at the constant
dye concentration of 505 μM and the contact time of 62.5 minutes

Figure 2 shows the simultaneous effect of initial BB47 concentration and time on the decolorization percentage. As it can be observed, within the constant pH of 8.0 and the applied potential of 0.8 V, when dye concentration decreases from 10.0 μM to 675.0 μM, the decolorization percentage shows a rising trend and decreases in higher dye concentration. Based on the literature, it is evident due to the rise of the dye solution concentration, the number of effective contacts between dye molecules and electrode surface as well as exploded bubbles, which due to contact of water with the ultrasonic waves are generated and grew. On the other hand, when the number of dye molecules further increases, the consumption of hydroxyl radicals by dye molecules becomes more than free radical production. The reduction in the number of free radicals in proportion to the number of dye molecules diminishes the system efficiency for dye decomposition purposes [29, 30].

As Figure 2 illustrates, once time increases from 5.0 to 120.0 min, the decolorization percentage is also enhanced. It seems that with an increase in time, free radicals such as •OH and HOO• will be increased, which promotes the discoloration rate [22, 29]. Also, in our case, more dye molecules can move to the electrode surface and oxidize on it.
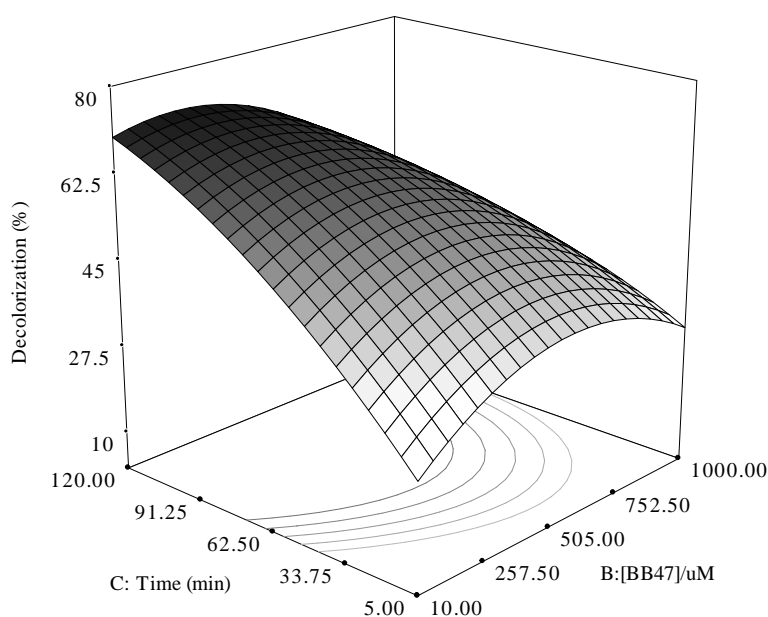

Fig. 2. The three-dimensional diagram showing the effect of time and dye concentration on decolorization
value at pH=8.0 and at the voltage of 0.81 V

3.3. UV/Visible Absorption Spectra OF BB47 Solution

The change in the UV/Visible absorption spectra for BB47, as a function of the time of the sonoelectrochemical degradation, was recorded (Fig. 3), using the applied potential of 0.81 V, and pH of 9.0 for 90 minutes at intervals of 10 minutes.

As it can be seen, one main peak in the UV region (260 nm) and a band in the visible region (650 nm) were observed at the absorption spectra of BB47 (Fig. 3). The disappearance of the visible band was probably due to the fragmentation of the anthraquinone structure by oxidation, and the change of absorbance in the UV region was considered evidence of aromatic fragment degradation in dye molecules.
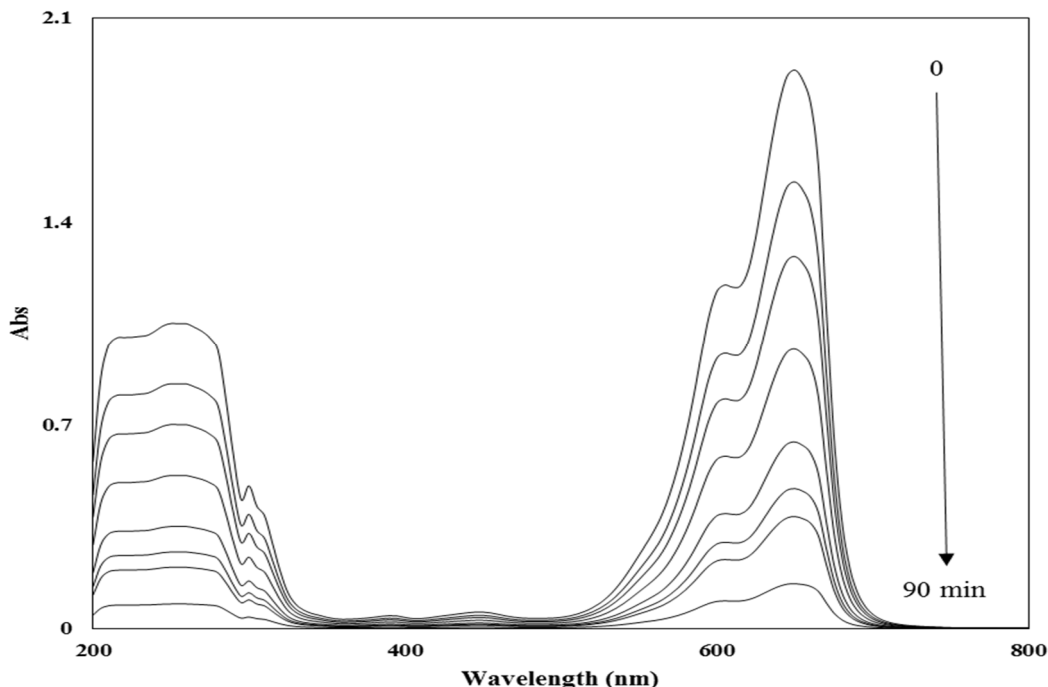

Fig. 3. UV−vis spectra of aqueous solution containing BB47 during sonoelectrochemical process (pH = 9.0, 303.0 μM BB47, applied potential = 0.81 V).

3.4. Decolorization of BB47 with Different Systems

A specific series of experiments was designed under optimum conditions for the decolorization of BB47 using different methods. The experiments were performed using sonoelectrochemistry, electrochemistry, and sonochemistry process. Table 3 shows the decolorization efficiency of BB47 in the mentioned processes. As compared to other techniques, the sonoelectrochemical process resulted in a higher removal percentage (96 %).

Sonoelectrochemical oxidation for decolorization of BB47 (96 %) was more efficient than electrochemical oxidation (23 %) and sonochemical oxidation (46.6 %) after 93 min. This may be due to the general improvement in the hydrodynamics and movement of species toward the surface of electrodes [9, 22].

The results also indicate that decolorization of BB47 occurs at a higher rate through the sonoelectrochemical method in comparison to other methods. In the first case, a decolorization efficiency of 96% was observed in 93 minutes under optimum conditions, whereas in the electrochemistry during the same time, only a decolorization efficiency of 23 % was recorded. However, a decolorization efficiency of 46.6 % was achieved by sonochemistry. This decolorization can be due to the synergetic effect of ultrasound in electrochemical treatment. Similar results were gained by Radi *et al*. (2015) in the decolorization of Reactive Blue 49 using ultrasound-assisted electrochemical oxidation. Their results confirmed that ultrasound improves the production of free radicals, resulting in the generation of additional hydroxyl radicals to react with the substrate. In addition, ultrasonic wave irradiation can eliminate the impurity layer at the surface of the electrode and increase its activity, as well as increase the reaction rates for mass transfer [22].

It should be noted that in these experiments has not been used for decolorization of any oxidant chemical and only is used from electric power as a renewable and biocompatible resource. Finally, sonoelectrochemical degradation was found to be efficient in decolorizing simulated textile effluents. The results show that ultrasound was significantly enhanced in the electrochemical oxidation.

3.5. Energy Consumption

The consumption of Energy (EC (kW h m−3)) is an essential factor for estimating the feasibility of the electrochemical process for the removal of pollutants. It should be clear that the energy consumption was considered for the particular setup used, without any concerns about a design that can lead to low operational cost. It is defined as the required energy of electrochemical oxidation for the removal of 1.0 g of BB47 and can be calculated from EC=UIt/1000V. Here, U is the applied potential (V), I is the applied current (A), t is the time of electro-oxidation (h), and V is the volume of the working solution (m^3). In general, the best results were found for the ultrasound-assisted electrochemical process, considering the constant current density (15 mA cm−2) and applied voltage (0.81 V). The longer the time, the higher will be EC for decolorization treatment.

3.6. The Combination *of Ultrasound-Electrochemical Process in COD Removal*

An optimal formulation for decolorization of BB47 was determined to minimize the chemical oxygen demand (COD). To determine the reduction of COD of the solution containing BB47, COD (before treatment) and final COD (after sonoelectrochemical oxidation) of the aqueous dye solutions were measured. Thus, a considerable percentage of COD removal proved to have occurred. Under optimum operating conditions, a COD reduction of 96% was achieved. The above combination is considered to have an important role in reducing and eliminating COD. The optimization results are shown in Table 3 in the order of desirability.

Table 3. The comparison of different methods for decolorization of BB47 under optimal conditions.

Method	[Dye] (µM)	Time (min)	pH	Applied Voltage (V)	Decolorization (%)	EC (kW h m^3)
Sonoelectrochemistry	303.3	93	9.0	0.81	96	0.25

Electrochemistry	303.3	93	9.0	0.81	23	8.28*
Sonochemistry	303.3	93	9.0	-	46.6	-

* A long time requires for only 75 % decolorization of BB47.

4. CONCLUSION

The results of the present study show that sonoelectrochemical and optimized use of CCD can be efficiently made to decolorize and degrade BB47. Based on the achieved model, each of the parameters is altered within an allowable range so that the optimal response, i.e. the maximum value of decolorization, is achieved. It was observed that an increase in the initial pH, the applied potential, and the duration of the sonoelectrochemical process would enhance the percentage of dye degradation. It is concluded that the percentage of dye degradation decreases with an increase in the initial concentration of the dye molecules. It was found that optimal conditions would include a pH of 9.0, dye concentration of 303.3 μM, duration of 93 minutes, and potential of 0.81 V. The decolorization percentage predicted by the model was 92.8% in these conditions, while it was found to be 92.34% after the experimental test. A high decolorization efficiency of more than 92% was also achieved without an oxidizing agent, which would damage the environment. The closeness of these responses is indicative of the appropriacy of the presented model. According to these results, the sonoelectrochemical process can serve as a valuable alternative to conventional physicochemical methods for the treatment of wastewater.

REFERENCES

1. Eslami, A., Moradi, M., Ghanbari, F., Mehdipour, F., Decolorization and COD removal from real textile wastewater by chemical and electrochemical Fenton processes: a comparative study, J. Environ. Health. Sci. Eng., 2013, vol, 11, p. 1-8.

2. Saggioro, E., Oliveira, A., Buss, D., Magalhaes, D., Pavesi, T., Jimenez, M., Maldonado, M., Ferreira, L., Moreira, J., Photo-decolorization and ecotoxicological effects of solar compound parabolic collector pilot plant and artificial light photocatalysis of indigo carmine dye, Dyes. Pigments., 2015, vol. 113, p. 571-80.

3. Demir, N., Gunduz, G., Dukkancı, M., Degradation of a textile dye, Rhodamine 6G (Rh6G), by heterogeneous sonophotoFenton process in the presence of Fe-containing TiO2 catalysts Environ. Sci. Pollut. R. 2015, vol. 22, p. 3193-3201.

4. Yang, B., Zuo, J., Tang, X., Liu, F., Yu, X., Tang, X., Effective ultrasound electrochemical degradation of methylene blue wastewater using a nanocoated electrode, Ultrason. Sonochem., 2014, vol. 21, p. 1310-1317.

5. Haque, M., Smith, W. T., Wong, D.K.Y., Conducting polypyrrole films as a potential tool for electrochemical treatment of azo dyes in textile wastewaters, J. Hazard. Mater., 2015, vol. 283, p. 164-170.

6. Nava, L. J., Sires, I., Brillas, E., Electrochemical incineration of indigo. A comparative study between 2D (plate) and 3D (mesh) BDD anodes fitted into a filter-press reactor, Environ. Sci. Pollut. R., 2014, vol. 21, p. 8485-8492.

7. Tzikalos, N., Belessi, V., Lambropoulou, D., Photocatalytic degradation of Reactive Red 195 using anatase/brookite TiO2 mesoporous nanoparticles: Optimization using response surface methodology (RSM) and kinetics studies, Environ. Sci. Pollut. R., 2013, vol. 20, p. 2305-2320.

8. Thiam, A., Sires, I., Garrido, J. A., Rodriguez, R. M., Brillas, E., Decolorization and mineralization of Allura Red AC aqueous solutions by electrochemical advanced oxidation processes, J. Hazard. Mater., 2015, vol. 290, p. 34-42.

9. Saez, V., Esclapez, M. D., Tudela, I., Bonete, P., Louisnard, O., Gonzalez-Garcia, J., 20 kHz sonoelectrochemical degradation of perchloroethylene in sodium sulfate aqueous media: Influence of the operational variables in batch mode, J. Hazard. Mater., 2010, vol. 183, p. 648-654.

10. Araujo, C.K., Oliveira, G.R., Fernandes, N., Zanta, C.L.P.S., Castro, S., da Silva, D., Martinez-Huitle, C., Electrochemical removal of synthetic textile dyes from aqueous solutions using Ti/Pt anode: role of dye structure, Environ. Sci. Pollut. R., 2014, vol. 21, p. 9777-9784.

11. Gu, L., Zhu, N., Guo, H., Huang, S., Lou, Z., Yuan, H., Adsorption and Fenton-like degradation of naphthalene dye intermediate on sewage sludge derived porous carbon, J. Hazard. Mater., 2013, vol. 247, p. 145-153.

12. Diriba, D., Hussen, A., Rao, V.M., Removal of Nitrite from Aqueous Solution Using Sugarcane Bagasse and Wheat Straw, B. Environ. Contam. Tox., 2014, vol. 93, p. 126-131.

13. Chen, T.S., Huang, K.L., Chen, J.L., Electrochemical Approach to Simultaneous Determination of Acetaminophen and Ofloxacin, B. Environ. Contam. Tox., 2012, vol. 89, p. 1284-1288.

14. Bagastyo, A.Y., Batstone, D.J., Kristiana, I., Escher, B.I., Joll, C., Radjenovic, J., Electrochemical treatment of reverse osmosis concentrate on boron-doped electrodes in undivided and divided cell configurations, J. Hazard. Mater., 2014, vol. 279, p. 111-116.

15. Kiran, S., Ali, S., Asgher, M., Degradation and Mineralization of Azo Dye Reactive Blue 222 by Sequential Photo-Fenton's Oxidation Followed by Aerobic Biological Treatment Using White Rot Fungi, B. Environ. Contam. Tox., 2013, vol. 90, p. 208-215.

16. Stadler, L.B., Su, L., Moline, C.J., Ernstoff, A.S., Aga, D.S., Love, N.G., Effect of redox conditions on pharmaceutical loss during biological wastewater treatment using sequencing batch reactors, J. Hazard. Mater., 2015, vol. 282, p. 106-115.

17. Wei, S., Hu, X., Liu, H., Wang, Q., He, C., Rapid degradation of Congo red by molecularly imprinted polypyrrole-coated magnetic TiO2 nanoparticles in dark at ambient conditions, J. Hazard. Mater. 2015, vol. 294, p. 168-176.

18. Iglesias, O., de Dios, M. A. F., Rosales, E., Pazos, M., Sanroman, M. A., Optimisation of decolourisation and degradation of Reactive Black 5 dye under electro-Fenton process using Fe alginate gel beads, Environ. Sci. Pollut. R., 2013, vol. 20, p. 2172-2183.

19. Rivera, M., Pazos, M., Sanroman, M., Improvement of dye electrochemical treatment by combination with ultrasound technique, J. Chem. Technol. Biot. 2009, vol. 84, p. 1118-1124.

20. Arat, C., Biçer, E., Electrochemical monitoring of decolorization of diazo dye Evans blue by Fenton process under anaerobic conditions: Kinetics and optimization, Russ. J. Electrochem., 2015, vol. 51, p. 730.

21. Mao, X., Tian, F., Gan, F., Lin, A., Zhang, X., Comparison of the performances of Ti/SnO2-Sb, Ti/SnO2-Sb/PbO2, and Nb/BDD anodes on electrochemical degradation of azo dye, Russ. J. Electrochem., 2008, vol. 44, p. 802.

22. Radi, M.A., Nasirizadeh, N., Rohani-Moghadam, M., Dehghani, M., The comparison of sonochemistry, electrochemistry and sonoelectrochemistry techniques on decolorization of C.I Reactive Blue 49, Ultrason. Sonochem. 2015, vol. 27, p. 609-615.

23. Weng, M., Zhou, Z., Zhang, Q., Electrochemical degradation of typical dyeing wastewater in aqueous solution: performance and mechanism, Int. J. Electrochem. Sci., 2013, vol. 8, p. 290-296.

24. Labiadh, L., Oturan, M.A., Panizza, M., Hamadi, N.B., Ammar, S., Complete removal of AHPS synthetic dye from water using new electro-fenton oxidation catalyzed by natural pyrite as heterogeneous catalyst, J. Hazard. Mater. 2015, vol. 297, p. 34-41.

25. Siddique, M., Farooq, R., Khan, Z.M., Khan, Z., Shaukat, S., Enhanced decomposition of reactive blue 19 dye in ultrasound assisted electrochemical reactor, Ultrason. Sonochem. 2011, vol. 18, p. 190-196.

26. Yaqub, A., Ajab, H., Applications of sonoelectrochemistry in wastewater treatment system, Rev. Chem. Eng., 2013, vol. 19, p. 123-130.

27. Thokchom, B., Kim, K., Park, J., Khim, Ultrasonically enhanced electrochemical oxidation of ibuprofen, J., Ultrason. Sonochem., 2015, vol. 22, p. 429-436.

28. Nasirizadeh, N., Dehghanizadeh, H., Yazdanshenas, M.E., Moghadam, M.R., Karimi, A., Optimization of wool dyeing with rutin as natural dye by central composite design method, Ind. Crop. Prod., 2012, vol. 40, p. 361-366.

29. Guimaraes, J.R., Maniero, M.G., de Araujo, R.N., A comparative study on the degradation of RB-19 dye in an aqueous medium by advanced oxidation processes, J. Environ. Manage., 2012, vol. 110, p. 33-39.

30. He, Z., Song, S., Zhou, H., Ying, H., Chen, J., CI Reactive Black 5 decolorization by combined sonolysis and ozonation, Ultrason. Sonochem., 2007, vol. 14, p. 298-304.

Self-assembly of ZnO nanoparticles on Low-Density Polyethylene Film with sol- gel and its Application for Milk Active Packaging

Mohammadali Shayegh[a*], Sayedeh mona Alavinassab[b], Sommayeh Shahedi[c], Saeid Jafari[c]

[a] Department of Food Science and Technology, Science and Research Branch, Islamic Azad University, Tehran, Iran.
[b] Nabandishan Saynar Sanaat isatis Co., Yazd Science and Technology Park, Yazd, Iran.
[c] Nanokimiakavir Yazd Co., Yazd Science and Technology Park, Yazd, Iran

Abstract

This study reports the antibacterial capability of low-density polyethylene (LDPE) modified with ZnO nanoparticles using a Sol-Gel technique. Antibacterial activity of prepared films against Escherichia coli (E. coli) and Staphylococcus aureus (S. aureus) was examined. The operational conditions such as pH, time, amount of ZnO nanoparticles, and silanol concentration were optimized using the response surface methodology (RSM). The proposed film under optimum conditions was applied for the packaging of the milk sample. The highest antibacterial activity of ZnO/LPDE were pH (6.0), time (103 min), amount of ZnO nanoparticles (0.68 % w/v) and silanol agent concentration (4.81 % v/v). The antibacterial properties of ZnO/LDPE films were assessed based on the diameter of the inhibition zone in a disk diffusion test against E. coli and S. aureus. These films have significantly reduced the growth of mentioned bacteria. Overall, antimicrobial packaging shows promise as an effective method to inhibit the growth of certain bacteria like E. coli and S. aureus in milk. The resulting ZnO/LDPE package films containing milk samples exhibit superior and prolonged antibacterial activity against E. coli and S. aureus in 7 and 14 days.

Keywords: Antibacterial Package, Zinc Oxide, Sol-Gel, E. coli, S. aureus.

---

[*]* Corresponding author. Tel:.+98-9133550583
  E-mail address: m.a.shayegh67@gmail.com

1. Introduction

The demand for minimally processed, easily prepared and ready-to-eat 'fresh' food products, globalization of food trade, and distribution from centralized processing pose most important concern s for food safety and quality [1-2]. In recent years, interest has been growing in using smart or active packaging that meets producers' and consumers' demands for products with longer shelf lives [3]. Food packaging systems are designed to act as passive barriers, protecting food from the surrounding environment. On the other hand, active food packaging systems are supposed to perform some role other than providing an inert barrier to external conditions [4]. Antimicrobial packaging is a kind of active packaging [5]. Antimicrobial food packaging materials have to extend the lag phase and reduce the growth rate of microorganisms to extend shelf life and maintain product quality and safety [6]. Nano food packaging with antimicrobial properties represents a new generation of active packaging based on nanocomposites [7]. Inorganic materials such as metals and metal oxides have been the focus of nanotechnology research [8]. Because of the high surface area-to-volume ratio and enhanced surface reactivity of nanosized antimicrobials, these systems can inactivate more microbial cells when compared to higher-scale counterparts. Nanoscale materials have been investigated for antimicrobial activity as growth inhibitors, killing agents, or antimicrobial [9- 10].

Nevertheless, of the variety of antimicrobial agents, the search for effective biocidal agents has focused on the development of nanostructures of certain metals such as Ag, Cu, Zn, and Au [11, 12]. Metal oxide materials such as titanium dioxide (TiO2), zinc oxide (ZnO), and magnesium oxide (MgO) have been shown antibacterial activity, which may be attributed to the generation of ROS [13-14]. The great advantage of metal oxides over organic antimicrobial agents is their higher stability. However, given their reduced cost, recent research efforts have focused on using ZnO nanoparticles [15]. The Zinc Oxide particles are particularly interesting since they appear to cause no harm to either animals or humans [16] but have a strong antimicrobial effect on a broad spectrum of microorganisms [17, 18, 19]. Nano-sized ZnO particles present biocidal activity and have some advantages compared to AgNPs, such as their lower cost, white appearance, and UV blocking properties [8]. They also present high versatility, and inorganic carriers, such as hydroxyapatite, can also be doped with zinc oxide providing novel structures with antimicrobial activity against E. coli, S. aureus, and Candida albicans [17, 20, 15]. The feasibility of ZnO incorporated in polymer nanocomposites intended for food packaging has been examined in many studies. For example, Li et al. [21] reported antimicrobial activities of the poly (vinyl chloride) films coated with ZnO nanoparticles. In another study, Li et al. [22] confirmed the potential of the nano-packaging modified ZnO nanoparticles during the storage of Fuji apple cuts, observing better preservation of quality indicators such as ascorbic acid and polyphenol content, and lower counts of typical altering microorganisms. Emamifar et al. [23] evaluated the antimicrobial activity of nanocomposites of low-density polyethylene (LDPE) containing Ag, NPs, and ZnO showing a significant impact of the proposed nano-packaging on the shelf-life of orange juice. Additionally, jin and Gurtler [24] reported that glass jars coated with allyl isothiocyanate, nisin, and ZnO nanocomposite could inactivate effectively Salmonella in liquid egg albumen.

In antimicrobial packaging, antibacterial particles may be deposited [25], incorporated [26], immobilized [27], or surface modified into packaging materials [28]. There are only a few approaches describing the surface coatings of ZnO nanoparticles such as the "pad-dry-cure" method, radiation, and thermal treatments. [29-30].

The use of appropriate coatings can impart antimicrobial effectiveness to a substrate. A sol-gel-based solution coating would be the most appropriate method in terms of stability and adhesiveness of attaching an antibacterial agent to a polymeric film [31 -32]. In this study, low-density polyethylene (LDPE) film was successfully coated with nano-sized ZnO using the Sol-Gel technique. Additionally, the antibacterial properties of modified films were evaluated versus gram-negative and gram-positive bacteria.

2. Experimental

2.1. Material *and apparatus*

Potassium trimethoxy silane (PTMS) (purity 95%) was supplied from Merck (Germany). ZnO nanoparticles (average diameter 10 -30 nm, surface area 20-60 m2 /g) were purchased from US Research Nanomaterial Co. (USA). Hydrochloric acid and methanol (with a purity grade 98%) were purchased from Sigma -Aldrich Co. (U.K). The pH measurement was made with a Metrohm model 827 pH/mV meter. The X-pert-Philips X-ray diffractometer (PW1930 generator, PW 1820 goniometer) with CuK radiation source ($\lambda = 0.15418$ nm) was used to compare the chemical structure of the blank and modified films with ZnO.

2.2. Preparation *of Antibacterial Film*

A response surface method (RSM) was employed to determine the optimal conditions for preparing the antibacterial film using Sol-Gel. The experimental results were analyzed using Design-Expert Version: 7.0.1, and the regression model was proposed. The pH solution, time (min), amount of ZnO nanoparticles (w/v %), and PTMS concentration (v/v %) were selected as four independent variables in the deactivation of E. coli and S. Aureus. The experimental ranges and the levels of the independent variables for antibacterial response are given in Table 1. It should be noted that initial experiments were accomplished to determine the extreme values of the variables. Accordingly, the CCD matrixes of 30 experiments covering the design of four process parameters were selected to study, names and results are shown in Table 2. Generally, the antibacterial film was prepared as follows: 0.48 mL PTMS was added to 10.0 mL methanol/de-ionized water solution with a ratio of 9:1. Before adding PTMS, the solution pH was adjusted by adding several drops of the 0.1 M HCl until solution pH equal to 6.5. Then, 0.068 g ZnO nanoparticles were added to this mixture. The mixture was placed on a magnetic stirrer and stirred with moderate speed for 95.0 min. Subsequently, a 2.0 cm × 2.0 cm LDPE film is immersed in the prepared solution and dried at ambient temperature for 60.0 min.

Table 1: Experimental range and levels of independent variables.

Factors	+α	+1	0	-1	-α
pH	1.0	3.5	6	8.5	11
Time (min)	1.0	30.75	60.5	90.25	120.0
ZnO (w/v %)	0.5	1.63	2.75	3.88	5
PTMS (v/v %)	0.25	1.44	2.63	3.81	5

2.3. Antibacterial *activity test*

The antibacterial response of the prepared films against E. coli and S. Aureus was studied utilizing the Kirby–Bauer technique. Accordingly, the bacterial inhibition zone around the circumference of a prepared film was employed to qualitatively assess whether or not the modified film possesses antibacterial properties [33 – 34] (Mahendran et al., 2016; Shemesh et al., 2015). Square pieces (of 12 mm in diameter) were cut out of modified films and placed into the surface of a full concentration of Nutrient Broth (NB) agar in 9.0 cm Petri plates inoculated with 0.1 ml of 108 colony forming units (CFU)/mL of bacterial culture The plates were incubated at 37 °C for 24 h. Then, the antibacterial activity was recorded by observing the presence or absence of an inhibition zone diameter (IZD) around the prepared films. Unmodified films were assayed as a negative control. The inhibition zone tests were performed in triplicates and reported the average values. Schematic of antibacterial test stages of the prepared films are shown in Figure. 1.
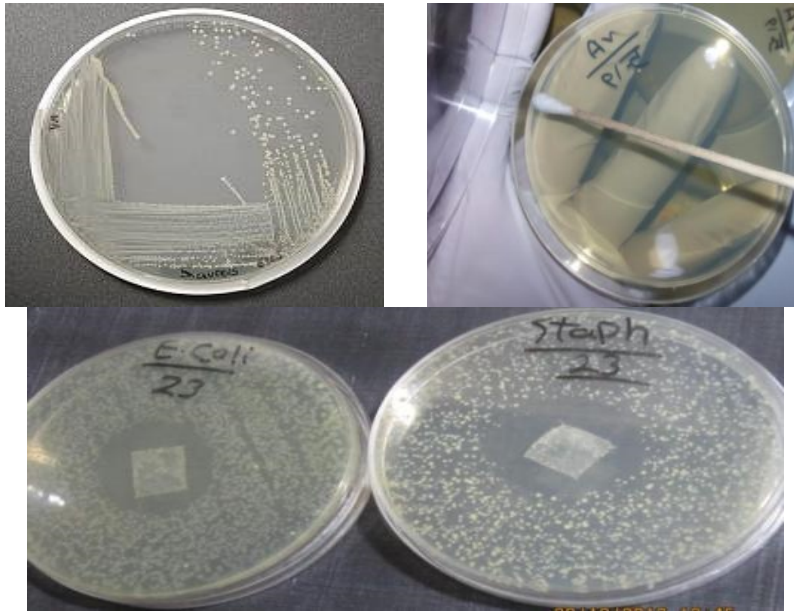
Fig 1. The antibacterial experiment processes of films

3. 3. Results and discussion
3.1. XRD

The structural characteristics of the nano-ZnO/LDPE film were determined by X-ray diffraction (XRD). Figure 2 shows the XRD patterns of the nano-ZnO/LDPE film, for which five main peaks were detected in the XRD spectrum, at 2θ of 26.5 °, 33.8 °, 37.9 °, 51.7 °, and 54.6 °, respectively, corresponding to the crystal structure of nano-ZnO. The peaks at 26.5 °, 33.8 °, 37.9 °, 51.7 °, and 54.6 °, belong to the (110), (101), (200), (211) and (220) planes of ZnO nanoparticles. Liang et al. [35] also found similar results.
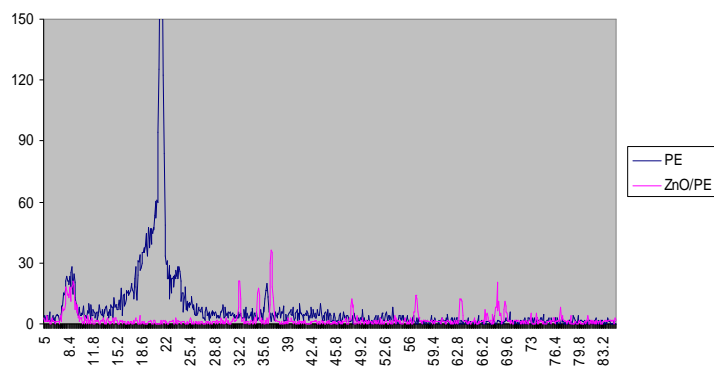

Fig 2. XRD patterns of LDPE and ZnO modified LDPE film

Table 2: Experimental design based on Central Composite design (CCD) used in present study

Order Test	pH	Time (min)	ZnO (w/v %)	PTMS (v/v %)	IZD (mm) for E coli	IZD (mm) for S. aureus
1	8.5	90.25	1.63	3.81	0	6
2	8.5	30.75	3.88	1.44	1.5	1.25
3	3.5	90.25	1.63	1.44	3	0
4	8.5	90.25	3.88	3.81	3.5	4
5	6	60.5	2.75	2.63	3.7	7.5
6	6	60.5	2.75	2.63	7	6
7	8.5	30.75	3.88	3.81	5	3
8	6	60.5	0.5	2.63	5	5
9	11	60.5	2.75	2.63	2	1
10	6	60.5	2.75	5	9	8
11	3.5	90.25	3.88	3.81	11	7.5
12	8.5	30.75	1.63	3.81	0.5	2
13	6	60.5	2.75	2.63	6	6.5
14	6	60.5	2.75	0.25	11	9
15	3.5	30.75	1.63	3.81	0	3.5
16	1	60.5	2.75	2.63	7	10
17	8.5	90.25	3.88	1.44	4	6
18	3.5	90.25	1.63	3.81	8.5	15
19	3.5	30.75	3.88	3.81	10	9
20	3.5	90.25	3.88	1.44	5	5
21	6	60.5	2.75	2.63	4.8	5.5
22	6	60.5	2.75	2.63	5.5	5.75
23	6	1	2.75	2.63	6.5	10
24	3.5	30.75	3.88	1.44	7	9
25	6	120	2.75	2.63	9	9
26	6	60.5	2.75	2.63	7	7
27	6	60.5	5	2.63	4	1.5
28	8.5	30.75	1.63	1.44	4	5
29	8.5	90.25	1.63	1.44	0	0
30	3.5	30.75	1.63	1.44	9	4

3.2. Effect *of Variables as Response Surface and Counter Plots*

In Figure. 3a, the effect of reaction time and pH on deactivation of E. Coli (as inhibition zone diameter (mm)) is shown at ZnO and PTMS concentration of 2.75 (w/v %) and 2.63 (v/v %), respectively. Figure 3a shows that as the PH of the solution increases from 5.5 to 11.0, the IZD value decreases. Figure 3a, also, illustrates that by increasing the reaction time to 95 min, the IZD value increases. The pH effect on IZD was significantly higher than the process variable of reaction time. On the other hand, when a lower pH was available, IZD increased with increasing the reaction time.

In Figure.3b, the change of IZD for E. Coli with ZnO and PTMS dosage is depicted at a time of 70 min and pH = 4.7. As the amount of nano-sized-ZnO increased, the IZD increased. Given the antibacterial properties of zinc oxide nanoparticles, it can be expected that as the amount of nanoparticles increases, more bacteria will be killed, and thus deactivation efficiency is higher. Several researchers [21, 22, 29, 30] also stated the effect of antimicrobial activity of ZnO nanoparticles on Listeria monocytogenes, Salmonella enteritidis, and E. coli. The results of their studies revealed that antibacterial efficiencies were related to the interaction or penetration of ZnO nanoparticles into microbial cells, which may be bactericidal or bacteriostatic, depending on the ZnO concentrations. The ZnO nanoparticles, which have positive zeta potential, easily disrupt the cell membrane of E. coli (gram negative) on contact and discharge Zn^{2+} ions, which cause lysosomal and mitochondrial destructions. In conclusion, this leads to the death of bacterial cells [33, 34].

On the other hand, when the concentration of PTMS is increment, the IZD will be reduced gradually. Figure. 3c shows the response surface of the deactivation efficiency of S. Aureus (in IZD (mm)) as a function of pH and reaction time. As Figure 3 c shows, IZD increased with the increase of pH at 1.0 to 4.8 range, and then decreased. This can be related to the dehydration PTMS and formation of the 3D networks of SiO_2. The PTMS is a silanol compound, which is hydrolyzed in the pH range of 4.5-5.0, and through its hydrolysis, a three-dimensional network of SiO2 will be formed. Only in this range PTMS was hydrolyzed and formed a three-dimensional network. It can be expected that nanoparticles are fixed on the surface of the film by the formation of the SiO_2 layer. These findings are in agreement with those observed in our previous study [32].

The effect of PTMS and ZnO values on deactivation efficiency of the S. Aureus are shown in Figure.3d. Figure 3d shows that IZD increased with the increase in nano-sized ZnO values from 0.1 to 4.0 w/v % and then plateaued. This observation implies that due to the higher concentration of nanoparticles on film, the inhibition zone surrounding the film will be larger [35, 36]. These studies revealed that increasing the concentration of nanosized- ZnO resulted in higher antibacterial activity.
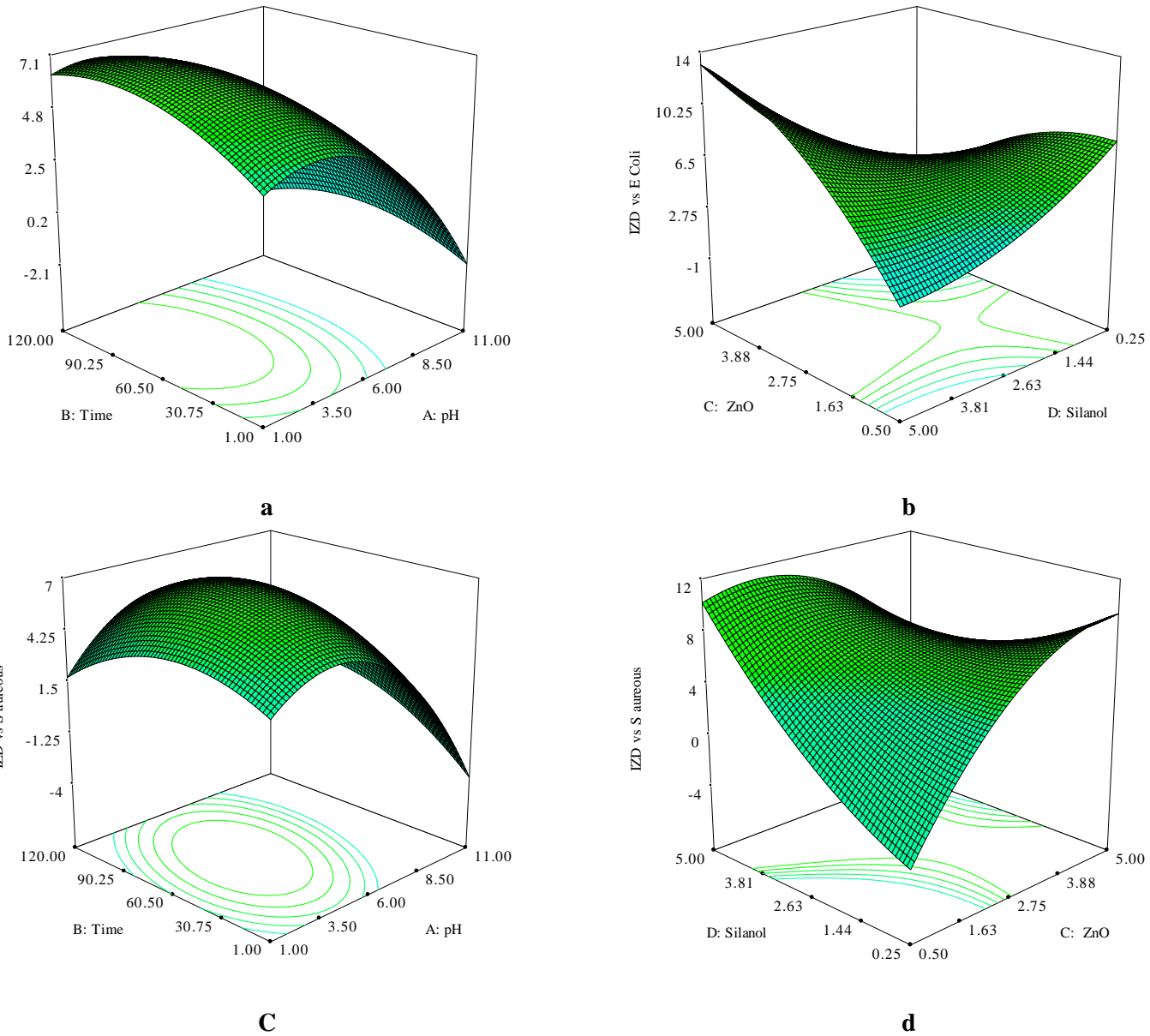
Fig. 3. The effect of operational parameters on inhibition growth E. Coli (a,b) and S. Aureus (c, d)

3.3. Statistical *analysis*

To find the optimum conditions for the preparation of the antibacterial packaging film, the experimental design as a function of the selected main factors has to be determined. The total number of experiments was 30 determined by the expression: 2n (24 = 16: factor points) +2n (2 *4=8: axial points) + 6 (center points: six

replications), as shown in Table 2. A full second-order polynomial model found by multiple regression method for four factors using the design of the expert 7.0.1 package was approved to describe the response surface.

The behavior of the system can be defined by the resulting quadratic equation:

$$Y = b_0 + \sum b_i x_i + \sum b_{ii} x_i^2 + \sum b_{ij} x_i x_j$$

where Y is the predicted response, b0 is the constant, bi is the linear effect of factor xi, bij is the linear interaction effect between the input factors xi and xj and bij is the quadratic effect of factor xi. Results attained for deactivation efficiencies of the E. coli and S. aureus are given in Table 2. Based on these results, an experiential model (for each bacterium) was generated in terms of coded factors (standardized equation) and stated by the following second-order polynomial equation (Eqs. (2) and (3)):

$$\text{IZD vs E Coli} = +5.38 - 2.41\,A - 0.26\,B + 0.44\,C + 0.51\,D - 0.51\,AD + 0.56\,BD + 1.24\,CD \quad \text{eq. (2)}$$

$$\text{IZD vs S aureous} = +5.61 - 1.64\,A + 0.079\,B + 0.27\,C + 0.93\,D + 0.32\,AB - 0.094\,AC - 1.22\,AD - 0.26\,BC + 1.29\,BD - 1.27\,CD \quad \text{eq. (3)}$$

The achieved results were then examined by ANOVA to evaluate the "goodness of fit" and the significance and adequacy of the model [37-38]. As can be seen from Table 3 and 4, the model had a high value of coefficient of determination the $R^2 = 88$ % and $R'^2 = 91$ % for E coli and S aureus, respectively. A desirable R^2 value is close to 1 and a reasonable agreement with adjusted R2 is essential. A high correlation coefficient (R2) provides a suitable adjustment of the quadratic model to the experimental data [38]. This high R^2 value implies that 88 and 91 % of the deviations for antibacterial efficiency are clarified by the independent variables which means that the model does not demonstrate only about 12 and 9 % of variation. The value of the adjusted R^2 of 0.845 and 0.851 was also high to advocate the high significance of the models for the killing of E coli and S aureus. Therefore, the response surface model is precisely applied for forecasting variation of antibacterial efficiency.

The F values were used as a tool to check the significance of each of the interactions among the variables, which, in turn, may show the patterns of the mutual interactions between the experiment variables. Overall, the larger the magnitude of the F-value and the smaller the p-value, the more significant the corresponding coefficient term is pH. Here, the pH parameter was a more effective factor for two bacterium (F- value = 124.26 for E coli and 17.68 for S. aureus). Also, D (5.69), AD (6.53), BD (7.36), and CD (7.07) for S aureus, and D 2 (8.49) and BCD (5.17) for E coli were the next effective factors.

3.4. Determination of optimal conditions

The key objective of the optimization is to define the optimal values of variables for the preparation of antibacterial LDPE with ZnO nanoparticles from the model obtained using experimental data.

Concerning storage conditions of Milk in the range in neutral pH, best conditions in terms of pH of Milk storage i.e. pH= 6.0 were chosen. The optimization results which was selected included pH= 6.0, time= 103 min, 0.68 % w/v ZnO nanoparticles and 4.81 % v/v silanol agent. Then a specific experiment was performed under these optimum conditions to confirm the agreement of the result attained from the model and experiment. The results revealed that the killing efficiency of the E. coli and S. aureus for response parameter obtained from the experiment and as estimated by the model was satisfactory.

Table 3. ANOVA analysis of data for growth inhibition of E. Coli

Source	Sum of Squares	Df	Mean Square	F Value	p-value Prob > F	
Model	186.257	10	18.62570542	14.49104684	< 0.0001	significant
A-pH	139.6355	1	139.6355042	108.6382817	< 0.0001	
B-Time	1.6485	1	1.648504167	1.282558194	0.2715	
C- ZnO	4.6025	1	4.602504167	3.58080953	0.0738	
D-Silanol	6.2935	1	6.293504167	4.896430048	0.0394	
AB	0.2232	1	0.22325625	0.173696335	0.6815	
AC	0.0770	1	0.07700625	0.059911888	0.8093	
AD	4.1107	1	4.11075625	3.198223103	0.0897	
BC	0.00075	1	0.00075625	0.000588373	0.9809	
BD	4.9395	1	4.93950625	3.843001639	0.0648	
CD	24.7257	1	24.72575625	19.23696762	0.0003	
Residual	24.4211	19	1.285325044			
Lack of Fit	16.1078	14	1.150560179	0.6919969	0.7312	not significant
Pure Error	8.3133	5	1.662666667			
Cor Total	210.67823	29				

R-Squared= 0.8841 and Adj R-Squared= 0.845

Table 4. ANOVA analysis of data for growth inhibition of S aureus

| Source	Sum of Squares	Df	Mean Square	F Value	p-value Prob > F	
Model	166.1038	10	16.61038	4.562322	0.0022	significant
A-pH	64.35375	1	64.35375	17.67585	0.0005	
B-Time	0.150417	1	0.150417	0.041314	0.8411	
C- ZnO	1.760417	1	1.760417	0.483528	0.4952	
D-Silanol	20.72042	1	20.72042	5.691215	0.0276	
AB	1.625625	1	1.625625	0.446506	0.5120	
AC	0.140625	1	0.140625	0.038625	0.8463	
AD	23.76563	1	23.76563	6.527634	0.0194	
BC	1.050625	1	1.050625	0.288572	0.5974	
BD	26.78063	1	26.78063	7.355755	0.0138	
CD	25.75563	1	25.75563	7.074221	0.0155	
Residual	69.17467	19	3.640772			
Lack of Fit	66.20592	14	4.728994	7.964622	0.0158	not significant
Pure Error	2.96875	5	0.59375			
Cor Total	235.2784	29				

R-Squared= 0.9104 and Adj R-Squared= 0.851

3.5. Application *of Antibacterial LDPE for packaging of Milk*

 The application of such packaging materials is not meant to be a substitute for good sanitation practices, but it should enhance the safety of food as an additional hurdle for the growth of pathogenic and/or spoilage microorganisms. Milk is a good source of vitamins and minerals and a staple food for human beings. So it's no surprise that an appropriate medium for bacterial growth. Bacteria that are randomly entered into milk, can cause health problems for consumers. Therefore, the main objective of this research was established to provide antibacterial polyethylene films for milk packaging [39 -41].

 To prepare antibacterial packaging and study the anti-bacterial properties of the prepared packages on milk, a packaging film according to the size of milk packet available in the market was prepared based on optimum conditions. Some packets of milk using the sewing machine were prepared as antibacterial films. Then, a liter of milk (low-fat milk supplied from KALLEH dairy Co.) was transferred into each prepared packets, and 1.0 mL of a solution containing bacteria E Coli and s. aureus with a concentration of 1.50×10^8 CFU/mL was added to each packet.

 The packets containing milk were gently shaken until a homogeneous solution was made. Packages were placed in an incubator for 48 h at 37 °C. Then, the number of surviving bacteria were counted after 7 and 14 days of culturing. A 1.0 mL sample of each dilution was plated on Count Skim Milk Agar and incubated at 37 °C for 48 h. The number of colony-forming units (CFU) per gram of sample was determined by counting typical colonies. All of these stages were repeated for unmodified polyethylene film. The results are shown in Figure 4. As Figure 4 illustrates, there is no antibacterial activity observed for unmodified LDPE. The ZnO nanoparticles coated LDPE result in better antibacterial activity than LDPE due to the presence of ZnO nanoparticles, which are having inhibition properties of bacteria. Moreover, the number of E. coli colonies in prepared milk packaging from nano-ZnO/LDPE decreased after 7 and 14 days. However, it is clear that the ZnO nanoparticles inhibit the growth of S. aureus in its medium.

Fig 4. Antibacterial activity test of the unmodified and ZnO modified LDPE against S. aureus and E. coli after
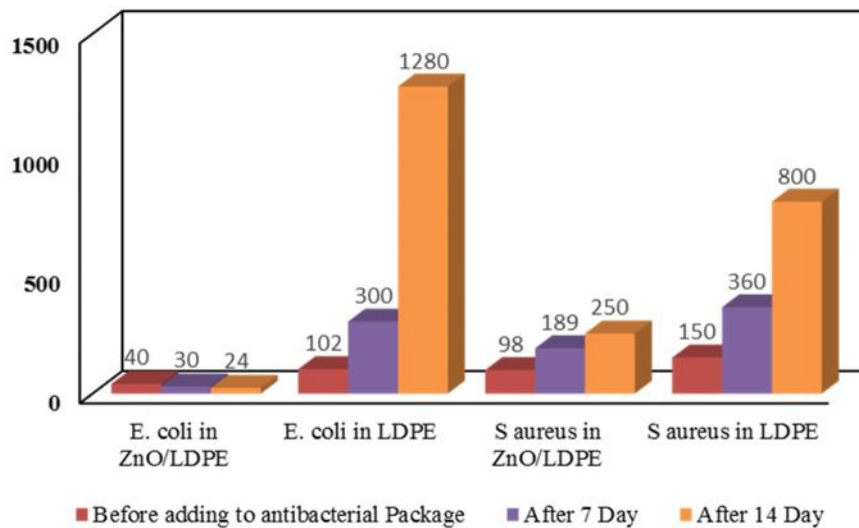
7 and 14 day culturing in Milk.

Figure. 5 a and 5 b illustrate the visual growth of E. coli and S. aureus bacteria after 14 days incubation in prepared milk packaging. It can be seen that milk color in blank LDPE was changed (from white to brown) due to the duplication of bacteria in milk.

Fig. 5. Milk sample contain a) E. Coli and b) S aureus packaged into LDPE and ZnO/LDPE films.

It was also important to evaluate the acidity value of milk samples after packaging in developed packaging film. For this, the acidity value (in terms of D: Dornic acidity degree) of milk samples in LDPE and ZnO/LDPE packages after 14 days was determined for E coli and S aureus inoculated, and its changes were depicted in Figure 6.

Figure 6. illustrates that the amount of milk acidity in samples containing S aureus remained relatively constant after 14 days of inoculation, and the amount of milk acidity in samples inoculated with E. coli bacteria was slightly increased than in sterilized milk. In the control samples, the samples acidity was much higher than those packaged in antibacterial films.
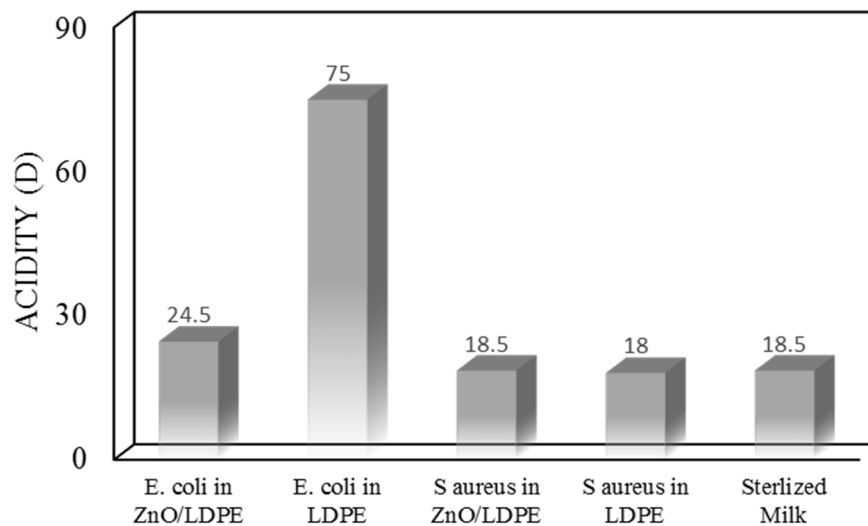

Fig. 6. Acidity changes of MILK packaged in LDPE and ZnO/LDPE films after 14 days inoculation of E coli and S aureus

4. Conclusion

This study has focused on presenting a method for coating LDPE film with ZnO nanoparticles using Sol-gel. The effect of pH solution, time (min), amount of ZnO nanoparticles (w/v %), and silanol agent concentration (v/v %) were investigated on the antibacterial activity of films using response surface methodology (RSM). Characteristics of the prepared films were investigated by FT-IR and XRD. The highest antibacterial activity of ZnO/LPDE were pH (6.0), time (103 min), amount of ZnO nanoparticles (0.68 % w/v) and silanol agent concentration (4.81 % v/v). The antibacterial properties of ZnO/LDPE films were evaluated based on the diameter of the inhibition zone in a disk diffusion test against E. coli and S. aureus. These films have significantly reduced the growth of mentioned bacteria. Overall, antimicrobial packaging shows promise as an effective method to inhibit the growth of certain bacteria like E. coli and S. aureus in milk.

References

[1] de Moura, M.R., Mattoso, L.H.C., Zucolotto, V., 2012. Development of cellulose-based bactericidal nanocomposites containing silver nanoparticles and their use as active food packaging. Journal of Food Engineering 109, 520-524.

[2] Llorens, A., Lloret, E., Picouet, P.A., Trbojevich, R., Fernandez, A., 2012. Metallic-based micro and nanocomposites in food contact materials and active food packaging. Trends in Food Science & Technology 24, 19-29.

[3] Panea, B., Ripoll, G., González, J., Fernández-Cuello, Á., Albertí, P., 2014. Effect of nanocomposite packaging containing different proportions of ZnO and Ag on chicken breast meat quality. Journal of Food Engineering 123, 104-112.

[4] Rotem, S., Maksym, K., Diana, G., Yael, D.-P., Yechezkel, K., Nadav, N., Anita, V., Ester, S., 2015. Antibacterial and antifungal LDPE films for active packaging. Polymer Advanced Technologies 26, 110-116.

[5] Mangalassary, S., 2012. Antimicrobial Food Packaging to Enhance Food Safety: Current Developments and Future Challenges. Food Processing & Technology 3, 5-7.

[6] Appendini, P., Hotchkiss, J.H., 2002. Review of antimicrobial food packaging. Innovative Food Science & Emerging Technologies 3, 113-126.

[7] de Azeredo, H.M.C., 2013. Antimicrobial nanostructures in food packaging. Trends in Food Science & Technology 30, 56-69.

[8] Dastjerdi, R., Montazer, M., 2010. A review on the application of inorganic nano-structured materials in the modification of textiles: Focus on anti-microbial properties. Colloids and Surfaces B: Biointerfaces 79, 5-18.

[9] Duncan, T.V., 2011. Applications of nanotechnology in food packaging and food safety: Barrier materials, antimicrobials and sensors. Journal of Colloid and Interface Science 363, 1-24.

[10] Guo, L., Yuan, W., Lu, Z., Li, C.M., 2013. Polymer/nanosilver composite coatings for antibacterial applications. Colloids and Surfaces A: Physicochemical and Engineering Aspects 439, 69-83.

[11] Longano, D., Ditaranto, N., Cioffi, N., Di Niso, F., Sibillano, T., Ancona, A., Conte, A., Del Nobile, M.A., Sabbatini, L., Torsi, L., 2012. Analytical characterization of laser-generated copper nanoparticles for antibacterial composite food packaging. Analytical and Bioanalytical Chemistry 403, 1179-1186.

[12] Rai, M.K., Deshmukh, S.D., Ingle, A.P., Gade, A.K., 2012. Silver nanoparticles: The powerful nanoweapon against multidrug-resistant bacteria. Journal of Applied Microbiology 112, 841-852.

[13] Barnes, R.J., Molina, R., Xu, J., Dobson, P.J., Thompson, I.P., 2013. Comparison of TiO2 and ZnO nanoparticles for photocatalytic degradation of methylene blue and the correlated inactivation of gram-positive and gram-negative bacteria. Journal of Nanoparticle Research 15, 1432.

[14] Leung, Y.H., Xu, X., Ma, A.P.Y., Liu, F., Ng, A.M.C., Shen, Z., Gethings, L.A., Guo, M.Y., Djurišić, A.B., Lee, P.K.H., Lee, H.K., Chan, W.K., Leung, F.C.C., 2016. Toxicity of ZnO and TiO2 to Escherichia coli cells. Scientific Reports 6, 35243.

[15] Tankhiwale, R., Bajpai, S.K., 2012. Preparation, characterization and antibacterial applications of ZnO-nanoparticles coated polyethylene films for food packaging. Colloids and Surfaces B: Biointerfaces 90, 16-20.

[16] Moezzi, A., McDonagh, A.M., Cortie, M.B., 2012. Zinc oxide particles: Synthesis, properties and applications. Chemical Engineering Journal 185–186, 1-22.

[17] Al-Naamani, L., Dobretsov, S., Dutta, J., 2016. Chitosan-zinc oxide nanoparticle composite coating for active food packaging applications. Innovative Food Science and Emerging Technologies 38, 231-237.

[18] Jafari, A.R., Mosavi, T., Mosavari, N., Majid, A., Movahedzade, F., Tebyaniyan, M., Kamalzadeh, M., Dehgan, M., Jafari, S., Arastoo, S., 2016. Mixed metal oxide nanoparticles inhibit growth of Mycobacterium tuberculosis into THP-1 cells. International Journal of Mycobacteriology 5, S181-S183.

[19] Venkatasubbu, G.D., Baskar, R., Anusuya, T., Seshan, C.A., Chelliah, R., 2016. Toxicity mechanism of titanium dioxide and zinc oxide nanoparticles against food pathogens. Colloids and Surfaces B: Biointerfaces 148, 600-606.

[20] Selvam, S., Sundrarajan, M., 2012. Functionalization of cotton fabric with PVP/ZnO nanoparticles for improved reactive dyeability and antibacterial activity. Carbohydrate Polymers 87, 1419-1424.

[21] Li, X.H., Xing, Y.G., Li, W.L., Jiang, Y.H., Ding, Y.L., 2010. Antibacterial and Physical Properties of Poly(vinyl chloride)-based Film Coated with ZnO Nanoparticles. Revista de Agaroquimica y Tecnologia de Alimentos 16, 225-232.

[22] Li, X., Li, W., Jiang, Y., Ding, Y., Yun, J., Tang, Y., Zhang, P., 2011. Effect of nano-ZnO-coated active packaging on quality of fresh-cut 'Fuji' apple. International Journal of Food Science & Technology 46, 1947-1955.

[23] Emamifar, A., Kadivar, M., Shahedi, M., Solimanian-Zad, S., 2012. Effect Of Nanocomposite Packaging Containing Ag And Zno On Reducing Pasteurization Temperature Of Orange Juice. Journal of Food Processing and Preservation 36, 104-112.

[24] Jin, T., Gurtler, J.B., 2011. Inactivation of Salmonella in liquid egg albumen by antimicrobial bottle coatings infused with allyl isothiocyanate, nisin and zinc oxide nanoparticles. Journal of Applied Microbiology 110, 704-712.

[25] Quadrini, F., Bellisario, D., Santo, L., Tedde, G.M., 2017. Anti-bacterial nanocomposites by silver nano-coating fragmentation, Materials Science Forum, pp. 1540-1545.

[26] Shaaban, H.A., Mahmoud, K.F., Amer, M.M., Amin, A.A., Mohamed, S.S., 2016. Preparation of antibacterial food active package nano-biocomposite edible film containing pectin and cinnamon essential oilnano-emulsion. Research Journal of Pharmaceutical, Biological and Chemical Sciences 7, 2665-2672.

[27] Yuan, G., Chen, X., Li, D., 2016. Chitosan films and coatings containing essential oils: The antioxidant and antimicrobial activity, and application in food systems. Food Research International.

[28] Ebrahimiasl, S., Rajabpour, A., 2015. Synthesis and characterization of novel bactericidal Cu/HPMC BNCs using chemical reduction method for food packaging. Journal of Food Science and Technology 52, 5982-5988.

[29] Li, Y.N., Xu, W.M., Zhang, G.Q., 2015. Effect of coupling agent on nano-ZnO modification and antibacterial activity of ZnO/HDPE nanocomposite films, IOP Conference Series: Materials Science and Engineering, 1 ed.

[30] Mirhosseini, M., Barzegari Firouzabadi, F., 2014. Preparation of ZnO-polystyerne composite films and investigation of antibacterial properties of ZnO-polystyerne composite films. Iranian Journal of Pathology 9, 99-106.

[31] Cotolan, N., Rak, M., Bele, M., Cör, A., Muresan, L.M., Milošev, I., 2016. Sol-gel synthesis, characterization and properties of TiO2 and Ag-TiO2 coatings on titanium substrate. Surface and Coatings Technology 307, 790-799.

[32] Nasirizadeh, N., Dehghani, M., Yazdanshenas, M.E., 2015. Preparation of hydrophobic and conductive cotton fabrics using multi-wall carbon nanotubes by the sol–gel method. Journal of Sol-Gel Science and Technology 73, 14-21.

[33] Halder, S., Yadav, K.K., Sarkar, R., Mukherjee, S., Saha, P., Haldar, S., Karmakar, S., Sen, T., 2015. Alteration of Zeta potential and membrane permeability in bacteria: a study with cationic agents. SpringerPlus 4, 672.

[34] Mahendran, R., Sridharan, D., Arunmozhidevan, C., Selvakumar, T.A., Rajasekar, P., 2016. Fabrication and Antibacterial Effects of Polycarbonate/Leaf Extract Based Thin Films. Journal of Materials 2016, 7.

[35] Seil, J.T., Webster, T.J., 2012. Antimicrobial applications of nanotechnology: methods and literature. International Journal of Nanomedicine 7, 2767-2781.

[36] Shemesh, R., Krepker, M., Goldman, D., Danin-Poleg, Y., Kashi, Y., Nitzan, N., Vaxman, A., Segal, E., 2015. Antibacterial and antifungal LDPE films for active packaging. Polymers for Advanced Technologies 26, 110-116.

[37] Jalal, R., Goharshadi, E.K., Abareshi, M., Moosavi, M., Yousefi, A., Nancarrow, P., 2010. ZnO nanofluids: Green synthesis, characterization, and antibacterial activity. Materials Chemistry and Physics 121, 198-201.

[38] Liang, G.-D., Liu, T.-T., Qin, W.-P., Zhu, F.-M., Wu, Q., 2012. Crystallization of low-density polyethylene embedded inside zinc oxide nanoparticle percolating network. Polymer Engineering & Science 52, 1250-1257.

[39] Radheshkumar, C., Münstedt, H., 2006. Antimicrobial polymers from polypropylene/silver composites—Ag+ release measured by anode stripping voltammetry. Reactive and Functional Polymers 66, 780-788.

[40] Esfandiyari, T., Nasirizadeh, N., Ehrampoosh, M.H., Tabatabaee, M., 2017. Characterization and absorption studies of cationic dye on multi walled carbon nanotube–carbon ceramic composite. Journal of Industrial and Engineering Chemistry 46, 35-43.

[41] Etemadifar, A., Dehghanizadeh, H., Nasirizadeh, N., Rohani-Moghadam, M., 2014. Statistical optimization of wool dyeing with Alizarin Red S as a natural dye via central composite design. Fibers and Polymers 15, 254-260.

[42] Abo-Elnaga, I.G., Hessain, A., Sarhan, H.R., 1985. Bacteria and food poisoning organisms in milk. Food / Nahrung 29, 375-380.

[43] Davoodi, H., Esmaeili, S., Mortazavian, A.M., 2013. Effects of Milk and Milk Products Consumption on Cancer: A Review. Comprehensive Reviews in Food Science and Food Safety 12, 249-264.

[44] Larson, B., 1974. CONTRIBUTORS A2 - LARSON, BRUCE L, in: Smith, V.R. (Ed.), Nutrition and Biochemistry of Milk/maintenance. Academic Press, p. ii.